



Maria Eugénia Marques da Costa Estabelecimento e caracterização de modelos resistentes e metastáticos de osteossarcoma humano *in vitro* e *in vivo*

***In vitro* and *In vivo* establishment and characterization of resistant and metastatic human osteosarcoma models**



Maria Eugénia Marques da Costa **Estabelecimento e caracterização de modelos resistentes e metastáticos de osteossarcoma humano *in vitro* e *in vivo***

***In vitro* and *In vivo* establishment and characterization of resistant and metastatic human osteosarcoma models**

Tese apresentada à Universidade de Aveiro para cumprimento dos requisitos necessários à obtenção do grau de Doutor em Biologia, realizada sob a orientação científica da Doutora Nathalie Gaspar, (Pediatra Oncologista, M.D. PhD no Instituto Gustave-Roussy), da Doutora Birgit Geoerger (Pediatra Médica Oncologista, M.D. PhD no Instituto Gustave-Roussy) e da Doutora Conceição Santos, (Professora Titular do Departamento de Biologia da Faculdade de Ciências da Universidade do Porto e Anteriormente Professor Associado da Universidade de Aveiro).

Apoio financeiro da FCT e do FSE no âmbito do III Quadro Comunitário de Apoio através da atribuição de uma bolsa de doutoramento a Maria Eugénia Marques da Costa com a referência SFRH/BD/89137/2012.

“O que me preocupa não é o grito dos maus. É o silêncio dos bons.”

Martin Luther King Jr.

o júri

Presidente

Prof. Doutor Amadeu Mortágua Velho da Maia Soares,
Professor Catedrático da Universidade de Aveiro

Vogal

Prof. Doutor António José Arsénia Nogueira,
Professor Catedrático da Universidade de Aveiro

Arguente Principal

Doutor José Miguel Pimenta Ferreira de Oliveira
Investigador na Universidade do Porto

Arguente Principal

Doutora Verónica Isabel Correia Bastos
Investigadora na Universidade do Porto

Vogal (Orientadora)

Doutora Elsa Nathalie Gaspar,
Médica Oncologista, M.D. PhD no Instituto Gustave-Roussy

agradecimentos

Gostaria de agradecer, em primeiro lugar, às minhas orientadoras. Em especial à Doutora Nathalie Gaspar por toda a paciência, apoio e ajuda que me deu durante estes 4 anos e por em alguns momentos me ensinar a ser mais paciente. À professora Doutora Conceição Santos por ter acreditado em mim e me ter sugerido concorrer à bolsa de Doutoramento e por todo apoio.

To Dra. Birgit Georger for helping me on the development of this thesis and for her support.

To Estelle Daudigeos-Dubus for helping me and support me during the last years of my thesis in Gustave Roussy.

Quero agradecer a toda a equipa do Laboratório de Biotecnologia e Citómica, bem como a todos os meus colegas do Instituto Gustave Roussy pelo apoio e ajuda no desenvolvimento da tese.

À FCT, ao departamento de Biologia da Universidade de Aveiro e ao Instituto Gustave Roussy por me terem acolhido e por me terem dado esta oportunidade.

To all my friends for the support and friendship in these 4 years, Cláudia Evangelista, Anne Harttrampf and especially Noémie Assoun that supported me in some of the most difficult moments.

Aos meus pais e irmãos que sempre acreditaram em mim e me incentivaram na realização do doutoramento. Por todo o apoio e amizade que me deram.

Ao meu namorado por todo o apoio e partilha nos bons e maus momentos, e por me mostrar que há mais para além do laboratório.

palavras-chave

Resistência, osteossarcoma, humano, *In vitro*, *In vivo*, quimioterapia

resumo

Osteossarcoma é uma doença rara, sendo o tipo mais comum de tumor maligno do osso. O pico de incidência ocorre durante a adolescência e desenvolve-se principalmente nos ossos longos. Os tratamentos atuais incluem quimioterapia antes e após a cirurgia e a ressecção cirúrgica de todos os locais envolvidos (tumor primário e metástases quando presente). As metástases, principalmente nos pulmões, são um grande problema no diagnóstico (20-30% dos pacientes) e durante a história natural do osteossarcoma (cerca de 30% de recaída), afetam uma percentagem considerável de pacientes e são considerados os maiores problemas desta doença. Biologicamente, os osteossarcomas são um dos tumores mais complexos observados nas crianças, no que diz respeito à heterogeneidade, anomalias moleculares e cromossômicas e ao seu microambiente específico. A resistência aos agentes quimioterápicos utilizados no tratamento do osteossarcoma também é um fator prognóstico de alto risco de recaída, independentemente da quimioterapia utilizada. É urgente compreender os mecanismos relacionados a esses fenômenos e desenvolver novos quimioterápicos para superar esses problemas e aumentar a taxa de sobrevivência do paciente.

O desenvolvimento de novos fármacos requer múltiplos modelos pré-clínicos adequados para mimetizar a complexidade genômica do osteossarcoma que se desenvolve-se num microambiente ósseo e metastático nos pulmões, apesar dos tratamentos quimioterápicos habituais. Nesta tese, foram desenvolvidos e caracterizados diferentes modelos pré-clínicos clinicamente relevantes *in vitro* e *in vivo*, incluindo modelos resistentes bioluminescentes, de modo a melhor compreender esta doença e alguns dos mecanismos de resistência relacionados.

Desenvolvemos, em primeiro lugar, dois modelos ortotópicos xenotransplantados derivados de linhas celulares (CDX) bioluminescentes (Luc/mKate2), capazes de desenvolver metástases espontaneamente. As células bioluminescentes foram injetadas ortotopicamente, em diferentes contextos: imune (estirpes de ratinhos de laboratório - nude e NSG) e ósseo (intratibial e paratibial com ativação do periósteo). O sistema IVIS SpectrumCT, combinando tomografia computadorizada longitudinal (TC) e bioluminescência, foi utilizado para acompanhar o crescimento primário do tumor e a disseminação metastática em tempo real. O contexto imune murino, o contexto genético dos dois modelos CDX e o contexto ósseo (intratibial ou paratibial) influenciaram o enxerto tumoral, o crescimento primário do tumor e o comportamento agressivo local (osteocondensação e osteólise), bem como a disseminação metastática para os pulmões, ossos e baço (uma localização incomum em seres humanos).

resumo (cont.)

Observou-se também que a estirpe de ratinhos NSG e a injeção intratibial apresentam melhores características para o desenvolvimento de modelos que a injeção paratibial ou a estirpe de ratinhos nude. Seguidamente, desenvolvemos modelos resistentes bioluminescentes *in vitro*, aos principais medicamentos utilizados no osteossarcoma, nomeadamente metotrexato (5modelos) e doxorrubicina (1modelo), por exposição contínua a esses medicamentos. Realizando o mesmo procedimento, não foi obtida resistência à mafosfamida. Investigamos os mecanismos da resistência adquirida relacionados com estas drogas e observamos comportamentos diferenciais *in vitro* e *in vivo* (com modelos CDX ortotópicos bioluminescentes) das linhas resistentes e respetivas linhas parentais. Um mecanismo de resistência na linha celular resistente à doxorrubicina foi observado, nomeadamente a indução da proteína PgP. Mostramos diferentes mecanismos de resistência adquirida ao metotrexato de acordo com o *background* genético das linhas celulares, que afetam a expressão génica e provocam alterações no número de cópias ao nível dos cromossomas. Foram observados diferentes comportamentos dos modelos resistentes bioluminescentes ortotópicos (CDX) *in vivo* em comparação com as respetivas linhas parentais.

Finalmente, utilizando amostras de osteossarcoma humano provenientes de biópsias de pacientes em recidiva após a quimioterapia habitual, foram desenvolvidos modelos resistentes xenotransplantados derivados do paciente (PDX), quer subcutaneamente quer ortotopicamente (no osso). A caracterização desses modelos está em curso, em particular a comparação das características moleculares destes (sequenciamento completo do exoma e sequenciamento do ARN) com as do tumor do paciente na recaída e do mesmo no diagnóstico.

Todos esses modelos desenvolvidos em diferentes contextos *in vitro* e *in vivo* trazem informações complementares para outros tipos de modelos de osteossarcoma já existentes. Estes modelos são necessários para obter mais informações sobre os diferentes processos que envolvem o desenvolvimento inicial, a progressão e a sensibilidade/resistência ao tratamento no osteossarcoma. Permitem ajudar ainda a avaliação de novos quimioterápicos, de modo a encontrar soluções para a atual falta de terapias eficientes no osteossarcoma.

keywords

Resistance, osteosarcoma, human, *In vitro*, *In vivo*, chemotherapy

abstract

Osteosarcoma is a rare disease and the most common type of malignant bone tumor. The peak incidence occurs during the adolescence and the disease develops mainly in long bones. Current treatments include chemotherapy before and after surgery and surgical resection of all the involved sites (primary tumor and metastasis when present). Metastases mainly in the lungs are a major challenge at diagnosis (20-30% of the patients) and during the natural history of osteosarcoma (around 30% of relapse, most being metastatic), affect a considerable percentage of patients with osteosarcoma, being considered the biggest problem of this disease. Biologically, osteosarcomas are one of the most complex tumours in children in regard to tumour heterogeneity, molecular and chromosomal abnormalities, and their specific microenvironment. Resistance to the chemotherapeutic agents used in osteosarcoma is also a prognostic factor of high risk of relapse, whatever the chemotherapy used. It is urgent to understand the mechanisms related with these phenomena and develop new drugs in order to overcome these challenges and increase patient survival.

New drug development requires suitable multiple pre-clinical models to better mimic the genomic complexity of osteosarcoma which develops in a bone microenvironment and in a metastatic setting in the lungs, despite usual chemotherapeutic treatments. In this thesis, we developed and characterised different and clinically relevant *in vitro* and *in vivo* preclinical models, including bioluminescent resistant models in order to understand better this disease and some of the resistant mechanism related.

First, two bioluminescent (Luc/mKate2) cell line derived xenograft (CDX) models were developed in an orthotopic bone setting able to spontaneously metastasize. Bioluminescent cells were injected orthotopically, in different immune (nude and NSG mouse strains) and bone (intratibial and paratibial with periosteum activation) contexts. IVIS SpectrumCT system, combining longitudinal computed tomography (CT) and bioluminescence, was used to follow primary tumor growth and metastatic spread in real-time. The murine immune context, the genetic background of the two CDX-models, and the bone context (intratibial or paratibial) influenced tumor engraftment, primary tumor growth and local aggressive behavior (osteocondensation and osteolysis) as well as metastatic spread to lungs, bone, and spleen (an unusual localization in humans). It was also observed that intratibial injection in NSG mice showed better characteristics for model development than paratibial injection or nude mice recipient. We further developed *in vitro* bioluminescent models that were resistant to the main drugs used in osteosarcoma, methotrexate (5 models) and doxorubicin (one model), by continuous exposure to these drugs.

**abstract
(cont.)**

With the same technique no resistance was obtained for mafosfamide. We explored the mechanism of the acquired resistance to these drugs and observed the differential *in vitro* and *in vivo* behaviors (with CDX bioluminescent orthotopic models) of the resistant lines and their parental counterpart. A multidrug phenomenon by PgP induction was observed in the doxorubicin resistant cells. We show different mechanisms of acquired resistance to methotrexate according to the genetic background of the cell lines affecting either gene expression and copy number abnormalities. Different *in vivo* behavior of the resistant bioluminescent orthotopic CDX models compared to their parental counterparts were observed.

Finally, using human biopsy samples of osteosarcoma relapsing after usual anti-osteosarcoma chemotherapy were developed resistant patient-derived xenograft (PDX) models, either in subcutaneous as in orthotopic bone setting. The characterization of these models are still ongoing, in particular the comparison of their molecular characteristics, i.e. using whole exome and RNA sequencing, in comparison with the patient tumor at relapse and with the same patient tumor at diagnosis.

All these multiple models developed in different *in vitro* and *in vivo* contexts bring complementary information to other types of existing osteosarcoma models. They are needed to get more insight into the different processes involving osteosarcoma initiation, progression and in particular treatment sensitivity/resistance. They will further help drug testing to find solution to the current lack of efficient new drugs in osteosarcoma.

Most results presented in this thesis are part (integrated the main work) of the following papers of which Maria Eugénia Marques da Costa is the first author:

- ➔ **Marques da Costa ME**, Daudigeos-Dubus E, Gomez-Bouchet A, Bawa O, Rouffiac V, Serra M, Scotlandi K, Santos C, Geoerger B, Gaspar N. (-) Establishment and characterization of *in vivo* orthotopic bioluminescent xenograft models from human osteosarcoma cell lines in Swiss nude and NSG mice. *Published in Cancer Medicine: doi: 10.1002/cam4.1346*
- ➔ **Marques da Costa ME**, Daudigeos-Dubus E, Gomez-Bouchet A, Job B, Marchais A, Pata-Merci N, Leite B, Santos C, Geoerger B, Gaspar N. (-) *In vitro* and *in vivo* Establishment and Characterization of bioluminescent orthotopic chemo-resistant osteosarcoma models in NSG mice. *In preparation*
- ➔ **Marques da Costa ME**, Assoun N, Rondof W, Gomez-Bouchet A, Scoazec J-Y, Adam-de-Baumais T, Pasquet M, Santos C, Geoerger B, Daudigeos-Dubus E, Gaspar N. (-) Establishment and Characterization of *In vivo* orthotopic osteosarcoma patient-derived xenograft (PDX) models. *In preparation*

Chapter 1:.....	- 19 -
General Introduction.....	- 19 -
1.1. Bone.....	21
1.1.1. General Characteristics of the bone.....	21
1.1.2. Long Bones: structure, formation and growth.....	23
1.2. Osteosarcoma.....	28
1.2.1. Epidemiology and etiology.....	28
1.2.2. Clinical and radiological presentation	29
1.2.3. Histological diagnosis	30
1.2.4. Treatment and outcome	31
1.2.5. Osteosarcoma oncogenesis	34
1.2.5.1. Osteosarcoma genetic susceptibility	35
1.2.5.2. A complex somatic genomic/ epigenetic landscape.....	36
1.2.5.3. Cell of origin	38
1.2.5.4. Importance of the bone and immune microenvironment	40
1.2.6. Metastatic spread and resistance in osteosarcoma.....	44
1.3. Osteosarcoma pre-clinical Models	49
1.3.1. In vitro human osteosarcoma models	51
1.3.2. In vivo human osteosarcoma models.....	58
1.4. Aim of the study and conceptual framework.....	65
Chapter 2:.....	83
Establishment and characterization of <i>In vivo</i> orthotopic bioluminescent xenograft models from human osteosarcoma cell lines in Swiss nude and NSG mice.	83
Chapter 3:.....	115
<i>In vitro</i> and <i>in vivo</i> establishment and characterization of bioluminescent orthotopic chemo-resistant osteosarcoma models in NSG mice.....	115
Chapter 4:.....	153
Establishment and characterization of <i>in vivo</i> orthotopic osteosarcoma patient-derived xenograft (PDX) models	153
Chapter 5:.....	185
Discussion and Conclusions.....	185

List of abbreviations and symbols

v/v – Volume/volume

ABC – ATP binding cassette

AP – Doxorubicin-platinum

API-AI – Doxorubicin-platinum-ifosfamide

aCGH – array-based Comparative Genomic Hybridization

AYA – Adolescent and young adult osteosarcomas

BLI – Bioluminescence

BMSCs – Bone marrow-derived mesenchymal stem cells

CB – Chondroblastic subtype

CDX – Cell-line derived xenografts

CISP – Cisplatin/cisplatum

CR – Complete response

CSC – Cancer stem cells

CT – Computed tomography

CYP – Cytochrome P450

DHFR – Dihydrofolate reductase

DMEM – Dulbecco's modified Eagle medium

DMF – N,N-dimethylformamide

DOXO – Doxorubicin/adriamycin

ECM – Extracellular matrix

ETOP – Etoposide/VP16

EuroBoNeT – European Network of Excellence on bone tumors consortium

F – Female

FB – Fibroblastic subtype

FCT – Portuguese Foundation for Science and Technology

GEMOX – Gemcitabine-oxaliplatin

GHR – Good histological response (<10% residual viable tumor cells)

GST – Glutathione S-transferase

GSTP1 – Glutathione S-transferase P1

GWAS – Genome-wide association studies

HD-thiotepa – High-dose-thiotepa
HES – Hematoxilin-eosin-safranin
HG – High-Grade osteosarcoma
Histo – Histology
IC50 – 50 % inhibitory concentration
ITCC – European consortium Innovative Therapeutics for Children with Cancer
Luc – Luciferase
M – Male
MAP – Mafosfamide/ifosfamide
MAPPYACTS – Molecular Profiling for Pediatric and Young Adult Cancer Treatment Stratification
MDR – Multidrug resistance
MDR1 – Multidrug resistance protein 1
M-EI – Methotrexate-etoposide-ifosfamide
Met – Metastatic
MRP1 – Multidrug resistance-associated protein 1
MRI – Magnetic resonance imaging
MOI – Multiplicity of infection
MTX – Methotrexate
OB – Osteoblastic subtype
OS – Osteosarcoma
OS2006 – First-line treatment of osteosarcoma in France
OS2TTP – Second-line treatment of relapsed osteosarcoma in France
p/s – Photons/second
PCR – Polymerase chain reaction
PD – Progressive disease
PDX – Patient-derived xenografts
PgP – P-glycoprotein
PHR – Poor histological response ($\geq 10\%$ residual viable tumor cells)
PO – Para-osseous
PR – Partial response
PT – Primary tumor

Px – *In vivo* passage n°x

R – Relapse

R/DOXO – Doxorubicin Resistant

R/MTX – Methotrexate Resistant

RI – Resistance index

RFC – Reduced folate carrier

RNAseq – RNA sequencing

RT-qPCR – Real-time quantitative polymerase chain reaction

SC – Subcutaneous

SD – Stable disease

SNPs – Single nucleotide polymorphisms;

TAM – Tumor-associated macrophage

Td – Tumor doubling time

TOPO1 – Topoisomerase I

TOPO2 α/β – Topoisomerase II α and β

UGT1A – UDP glucuronosyltransferase family 1 member A

VCR – Vincristine

VER – Verapamil

VP16-Carbo – Etoposide-carboplatin

WB – Western-blot

WES – Whole exome sequencing

WHO – World Health Organization

Chapter 1:

General Introduction

1.1. Bone

1.1.1. *General Characteristics of the bone*

Bones are a mineralized specialized connective tissue that supports the body and are constantly undergoing modeling during life^{1,2}. Bones are characterized by their rigidity, hardness, and power of regeneration and repair^{3,4}. The bones of the skeleton support and protect muscles, vital organs and structures, allow movement and locomotion by providing levers for the muscles, provide maintenance of mineral homeostasis (eg. calcium) and acid-base balance, serve as a reservoir of growth factors and cytokines, and provide an environment for marrow (both blood formation and fat storage)^{1,3-5}. Bones support different processes throughout life to help on the adaptation to biomechanical force changes, as well as on the remodeling (remove microdamaged bone and replace it with new), becoming mechanically stronger bones to help on the bone strength preservation^{1,3,4}.

Bones are classified in four general categories (Fig.1.1): long bones, short bones, flat bones, and irregular bones. Long bones are found in the arms (humerus, ulna, radius) and legs (femur, tibia, fibula), as well as in the fingers (metacarpals, phalanges) and toes (metatarsals, phalanges) and the short bones include the carpal and tarsal bones. Flat bones include the skull, mandible, scapulae, sternum, and ribs and irregular bones for example the vertebrae¹.

Different types of cells are present in the bone (Fig.1.2): such as osteogenic cells (e.g stem cells), osteocytes, osteoblasts and osteoclasts, the two last cell types act continuously in the bones and they are responsible for the formation of new bone (osteoblasts) and old bone remodeling (osteoclasts)^{1,3,4,6}.

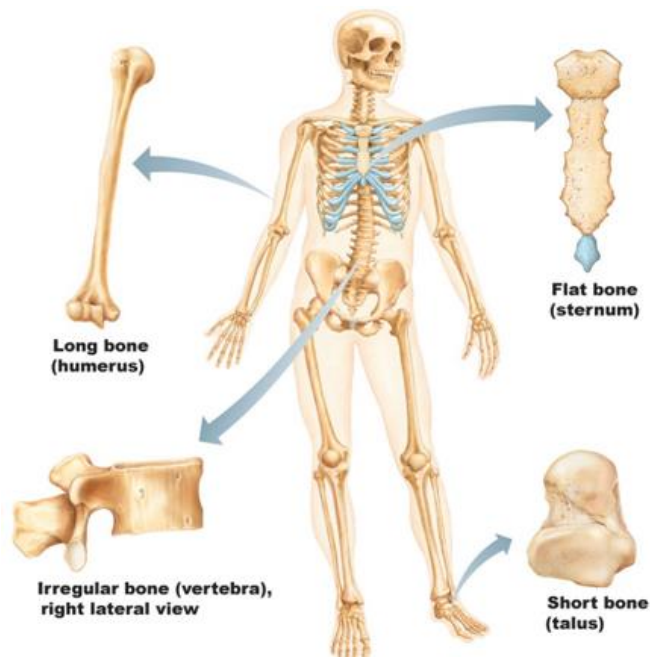


Figure 1.1: Classification of the bones in four groups: Long, short, flat and irregular bones⁷.

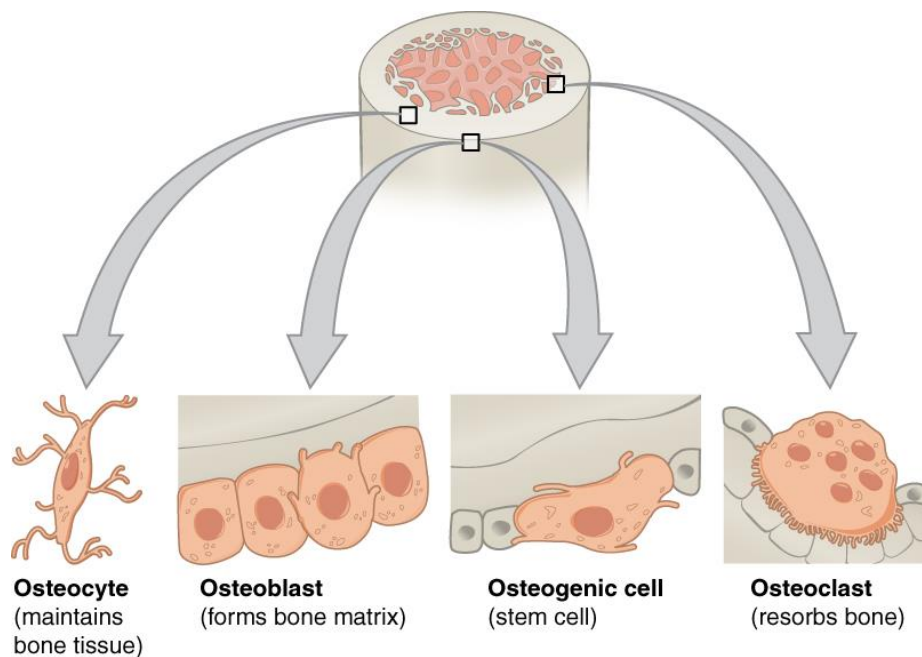


Figure 1.2: Cell types found within bone tissue. Osteogenic cells are undifferentiated cells and develop into osteoblasts. Osteoblasts are responsible to form new bone. Osteocytes maintain mineral concentration of matrix. Osteoclasts develop from monocytes and macrophages and are responsible for the bone resorption⁶.

1.1.2. Long Bones: structure, formation and growth

Long bones function as levers and have cylindrical shape (being longer than it is wide) (Fig.1.3). They are formed by thick outside layer of compact bone (cortical) and an inner medullary cavity containing bone marrow¹. They are divided in epiphysis, metaphysis and diaphysis. Epiphysis and metaphysis are composed of trabecular meshwork bone surrounded by a relatively thin shell of dense cortical bone whereas diaphysis is composed primarily of dense cortical bone. Embryos develop a cartilaginous skeleton and various membranes from sheets of mesenchymal connective tissue and during development these are replaced by bone during the endochondral (from cartilaginous cells) and membranar (from mesenchymal cells) ossification processes. In children and adolescent, the epiphyseal plate is the area of growth in long immature bones. It is composed of hyaline cartilage with its epiphyseal side which forms cartilage and its diaphysal side which forms new ossified bone to increase diaphysis length. In adult, this area is totally calcified and appears as the epiphyseal line without length growth potential^{1,3,6}. Two ossification types are described. The intramembranous ossification for flat bone formation is characterized by laying down of bone into the primitive connective tissue (mesenchyme). Endochondral ossification occurs in long bone through a cartilage forming bone model. Both ossification processes can be involved in fracture healing.

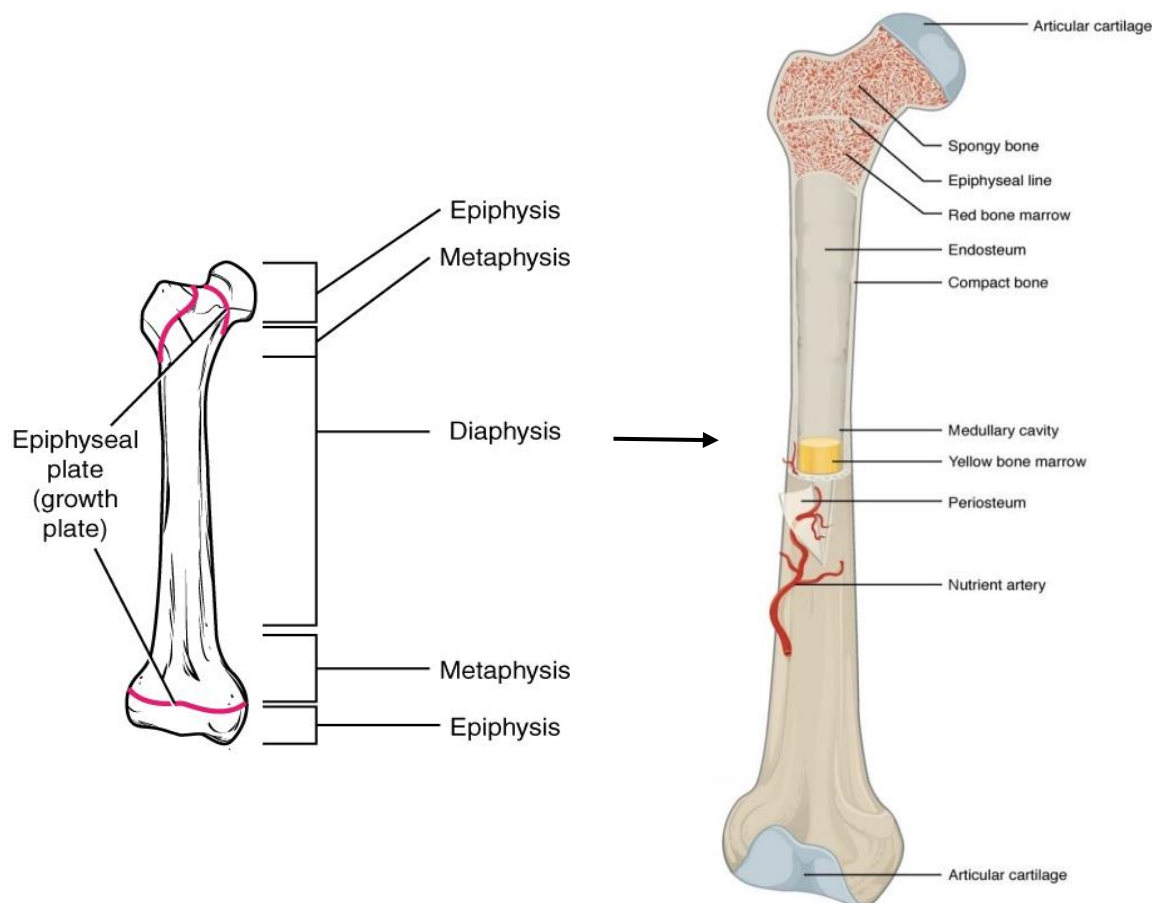


Figure 1.3: Long bone anatomical characteristics. A– Components of a growing bone. B– Interior components of a mature bone, epiphyseal plate progresses to an epiphyseal line. Adapted from⁶

Up to early adulthood, bone will undergo longitudinal growth (occurs at the growth plates, increasing in length), and throughout life, radial growth (increasing in diameter) and modeling (change of the general bone shape influenced by physiological or mechanical forces) and remodeling (bone renewal to maintain mineral homeostasis and bone strength)^{1–3,6} (Fig.1.4).

All these processes depend on the balanced actions between the opposite function of two cellular types (osteoblasts and osteoclasts), controlled by several hormones (e.g. growth, thyroid and the sex hormones) cytokines (e.g. RANK/RANKL) and growth factors⁴.

Osteoblasts originate from osteoprogenitor (osteoblast precursor) previously originated by mesenchymal stem cells of the bone marrow stroma are responsible for the three steps of new bone formation process also called ossification or osteogenesis, with synthesis of extracellular organic matrix (composed by 85 to 90% collagenous proteins, mainly type I collagen, and a 3D organization are the main component of the bone)¹, matrix mineralization leading to the formation of bone (by releasing small, membrane-bound matrix vesicles that concentrate calcium and phosphate and enzymatically destroy mineralization inhibitors such as pyrophosphate or proteoglycans) and remodeling of bone by resorption and reformation^{1,3}.

Osteocytes

Osteocytes originate from osteoblasts when these ones have been incorporated into the bone matrix. Surrounded by and buried within matrix, osteoblasts become osteocytes with an extensive canalicular network remaining in contact with bone surface lining cells, osteoblasts, and other osteocytes, via gap junction-coupled (required for osteocyte maturation, activity, and survival) cell processes passing through the matrix via small channels (canaliculi), that connect the cell body-containing lacunae with each other and with the outside world. Osteocytes express several matrix proteins that support intercellular adhesion and regulate exchange of mineral in the bone fluid within lacunae and the canalicular network. They are also active during osteolysis and may function as phagocytic cells (contain lysosomes)^{1,8}. Osteocytes represent terminally differentiated osteoblasts and function within syncytial networks to support bone structure and metabolism, more specifically osteocytes are possible actively involved in bone turnover; the osteocyte network is, through its large cell-matrix contact surface, involved in ion exchange; and osteocytes are the mechanosensory cells of bone, playing a pivotal role in functional adaptation of bone^{1,8}.

Bone-lining cells may regulate influx and efflux of mineral ions into and out of bone extracellular fluid, thereby serving as a blood-bone barrier, but retain the ability to redifferentiate into osteoblasts upon exposure to parathyroid hormone or mechanical forces. Bone-lining cells within the endosteum lift off the surface of bone

before bone resorption to form discrete bone remodelling compartments with a specialized microenvironment^{1,8}.

Osteoclasts derive from mononuclear precursor cells, hematopoietic stem cells that give rise to monocytes and macrophages⁴ and are responsible for bone resorption. The resorption area is limited by osteoclasts through a rearrangement of its cytoskeleton that forms a sealing zone wherein the degradation of bone tissue occurs^{5,9}. Bone resorption depends on osteoclast secretion of hydrogen (H^+) ions and cathepsin K enzyme. H^+ ions acidify the resorption compartment beneath osteoclasts to dissolve the mineral component of bone matrix, whereas cathepsin K digests the proteinaceous matrix (mostly composed of type I collagen)¹.

Osteoclasts activity can be inhibited for example by the osteoblasts, when they are stimulated to increase bone mass^{3,4}.

Bone modeling and remodeling is particularly highly dependent on the coupled action of osteoclasts and osteoblasts that sequentially break down and remove old bone and replace it with newly synthesized and mineralized bone matrix. The ongoing balance between osteoblasts and osteoclasts is responsible for the constant but subtle reshaping of bone, any imbalance in the osteoblast physiology may cause severe damages in the bone structure^{3,4}. Damages on these important processes can result in disease.

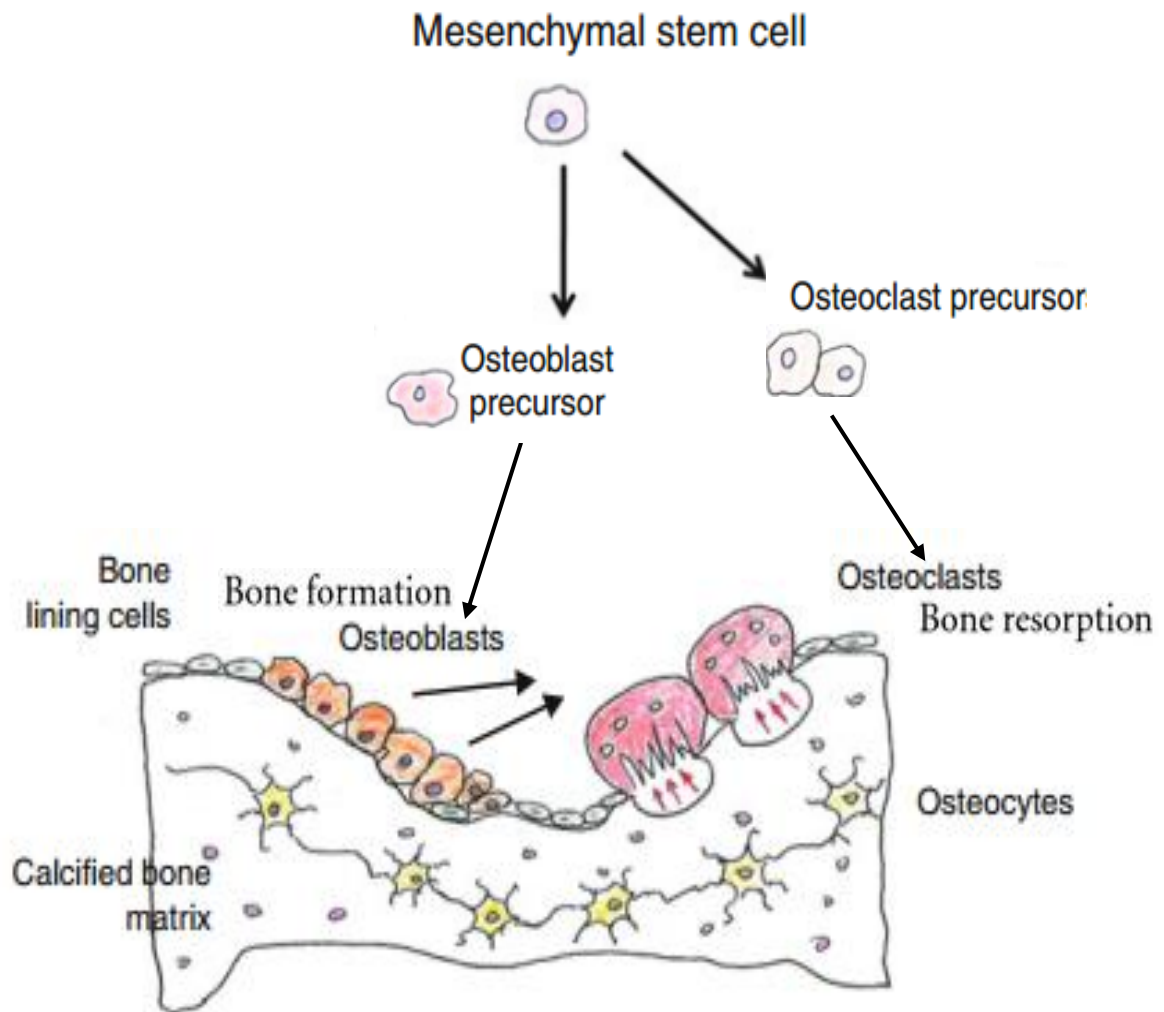


Figure 1.4: Osteoblasts and osteoclasts evolution and bone modeling (shows activated osteoclasts resorbing the underlying bone) and remodeling (shows formation phase where the osteoclasts are replaced by osteoblasts with underlying new osteoid matrix process). Adapted from³

1.2. Osteosarcoma

Sarcomas are a very heterogeneous group of malignant neoplasms of connective tissues, including bone and soft-tissues¹⁰.

Conventional osteosarcoma or osteogenic sarcoma is, according the World Health Organization (WHO) Classification of Tumors, a primary mesenchymal malignant bone tumor; high-grade and intra-osseous, in which the neoplastic cells produce bone^{11–14}.

1.2.1. *Epidemiology and etiology*

Osteosarcoma is a rare disease, with approximately 900 new cases/year reported in the United States or 300 in France, with a bimodal incidence. Extremely rare before 5th years of age^{11,12,15,16}, osteosarcoma has an initial peak of incidence during adolescence, around 14 years (during the pubertal growth spurt), and a second peak (smaller) after the 6th decade of life, usually on an abnormal bone^{12,16}. Indeed, adolescent and young adult (AYA) osteosarcomas are nearly always primary osteosarcomas, while 30-50% of the adult tumors are secondary tumors either post-irradiation or on pathological bone (e.g. Paget disease or, less commonly, other benign bone lesions). Exposure to radiation is the only well-established environmental risk factor already associated with osteosarcoma^{13,17}, and usually develops more than 10-20 years after radiation exposure^{13,18,19}.

We will focus our review and studies on the usual adolescent and young adult osteosarcoma (5-50 years). Boys are reported to be affected more frequently than girls (boys:girls ratio, 1.43:1). Girls have an osteosarcoma peak incidence a little earlier than boys, corresponding to the earlier age of growth spurt^{13,18,20}. A slight ethnic influence is observed in American population with a higher incidence in Asian/Pacific Islanders (5.3 per million of people), blacks (5.1 per million), Hispanics (4.9 per million) and whites (4.4 per million), compared to American Indian/Alaskan natives (3.0 per million)^{11–13}.

1.2.2. Clinical and radiological presentation

Osteosarcoma arises in children and adolescents with a typical metaphyseal location in long bones (80-90% of the cases) of the extremities (rapid bone growth areas), usually close to the knee (50%, distal femur and proximal tibia) and far from the elbow (proximal humerus)^{11–13,15,16,21,22}. In individuals over the 60 years old, low-grade tumors are typically found in axial sites²³. These differences may suggest different underlying mechanisms for the development of osteosarcoma in younger and older patients.

Pain is the most common and early symptom (2-4 months before diagnosis) of osteosarcoma and might appear after physical exercise or trauma, originated by the periosteum stretching or by bone deterioration due to stress fractures^{11,24}. Some patients also complain about swelling, related to soft tissue extension. Patients generally have symptoms for several months (average, 3–4 months, frequently more than 6 months) before a confirmed diagnosis^{11,24}.

Diagnosis is suspected on standard X-ray radiographs (or computed tomography) which detect aggressive bone lesions (cortical disruption), osteocondensation within the bone but also in the soft-tissue part of the tumor (new calcified material formation) as well as some osteolysis (bone destruction) (Fig.1.5).

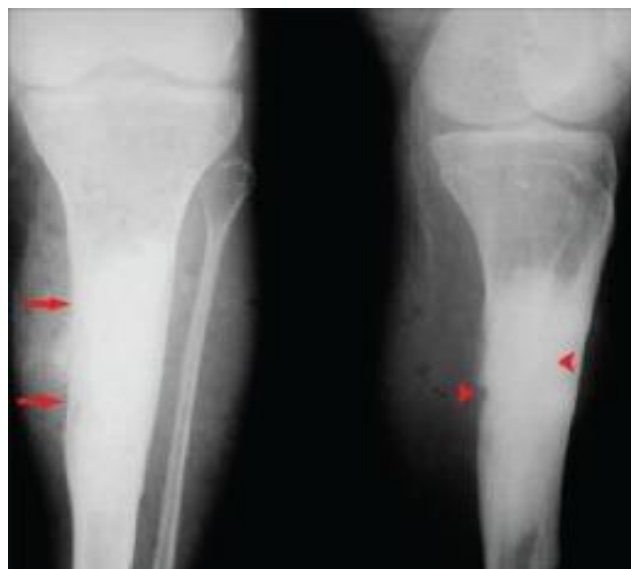


Figure 1.5: X-ray of proximal tibia and knee joint showing diaphyseal osteosarcoma of tibia with sclerosis (arrow), cortical destruction (arrow heads) and new bone formation in the soft tissues. Adapted from¹³

Magnetic resonance imaging (MRI) allows to better evaluate tumor extension through the growth plate, the articulation and soft-tissue extension to vessel and nerves, that will help to plan appropriate surgical resection^{11,13,25,26}.

Distant metastases are present in 20-30% of patient at diagnosis, mainly in the lung (90% of metastases)²³. A systematic thoracic CT-scan is performed at diagnosis. Metastatic bone localization is more rarely observed at diagnosis (<15%) and are usually detected by T99m bone scintigraphy. The occurrence of multiple bone metastases may actually reflect multifocal primary tumors, and constitute a distinct poorly known entity called osteosarcomatosis¹¹. "Skip metastases" small bone metastasis outside the reactive zone, but within the same bone can be detected only by RMI and not always seen in bone scintigraphy. Other metastatic localizations (e.g. lymph node, central nervous system) are extremely rare^{11,24}.

1.2.3. Histological diagnosis

Tumor biopsy prior to any treatment is mandatory for the diagnosis of osteosarcoma. No specific marker exists and the diagnosis is made on the detection of osteoid matrix formed by the malignant cells^{11,13,22,26}. Confrontation between histology and imaging is required.

Several sub-types are described according to the predominant type of stroma (osteoblastic, chondroblastic, fibroblastic, telangiectatic)¹⁴. Osteoblastic osteosarcoma is the most frequent sub-type (70% of the patients) and is characterized by the production of osteoid or bone as the main type of matrix and the presence of malignant plasmacytoid to epithelioid osteoblasts^{11,27}. Chondroblastic osteosarcomas (10% of the patients) present a predominant chondroid matrix with malignant cells within the lacunae. Fibroblastic osteosarcomas (10% of the patients) are composed of malignant spindle cells with scarce osteoid. In addition to these three conventional osteosarcoma subtypes, telangiectatic, giant cell-rich, anaplastic, and small cell osteosarcomas subtypes can be more rarely observed¹⁹.

1.2.4. Treatment and outcome

In the first half of the 20th century, when treated with limb amputation only, patients with osteosarcoma had lung metastases within the first two years and a survival rate of less than 20%²⁸. In the '70s-'80s, osteosarcoma chemosensitivity to various agent was demonstrated in phase-II trials (methotrexate/MTX, cisplatin, doxorubicin, ifosfamide, etoposide), with response rate of 19 to 40 % ²⁹ (Fig.1.6 and Table.1.I). These drugs are the principal chemotherapeutic agents used in the osteosarcoma treatment (Table.1.II). Neither complete surgical resection alone^{4,15}, neither chemotherapy alone are able to control osteosarcoma metastatic spread²¹. In addition to the gradually-improved surgical techniques, the introduction of these chemotherapeutic agents variously combined in multi-chemotherapy regimen, first in an adjuvant setting permitted to decreased metastasis occurrence, then in a neoadjuvant setting permitted to improved survival for patients with localized osteosarcoma to approximately 60%^{15,21,30–32}. The osteosarcoma radioresistance at standard doses, limited its use to unresectable tumors^{21,26}.

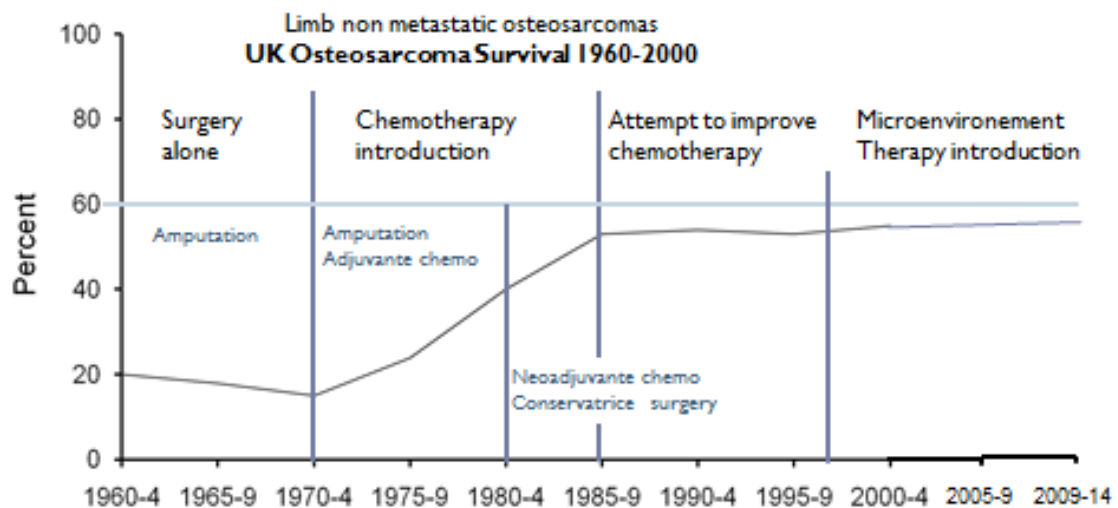


Figure 1.6: Osteosarcoma survival between 1960 and 2000. Kindly provided by Nathalie Gaspar

Table 1.I: Osteosarcoma phase-II trials (methotrexate, cisplatin, doxorubicin/adriamycin, ifosfamide, etoposide), with response rate of 19 to 40 % ²⁹.

Drug	Dose range (mg/m ² /course)	Number of patients	Number responding patients		Response rate (%)
			Complete remission (CR)	Partial remission (PR)	
Adriamycin	35–90	108	14	32	43
Ifosfamide	5.000–15.000	246	30	50	33
Methotrexate	80–15.000	164	26	26	32
Cisplatin	60–150	174	18	28	26
Etoposide	120–625	27	0	1	4

Table 1.II: The five principal chemotherapeutic agents used on the osteosarcoma treatment and the respective mechanism of action. Adapted from ^{24,33}.

Agent	Mechanism of action
Doxorubicin	Intercalates at point of local uncoiling of the DNA double helix and inhibits the synthesis of DNA and RNA (eg. DNA topoisomerase II-mediated DNA cleavage)
Cisplatin	Binds directly to tumor DNA and inhibits the synthesis of DNA through the formation of DNA cross-links
Ifosfamide	Causes crosslinking of DNA strands, inhibiting the synthesis of DNA and protein
Methotrexate	Inhibits the synthesis of purine and thymidylic acid by binding dihydrofolate reductase
Etoposide	Poisons the TopoII cleavage complexes (TopoIIcc) and inhibits the second step of the reaction (i.e. DNA religation), has also a high-affinity for chromatin and histones, in particular H1

Since the last 40 years, the first-line treatment of osteosarcoma includes neoadjuvant and adjuvant post-operative chemotherapy associated with surgical resection of the primary tumor and metastasis if present^{23,26,32,34}. MAP-based combinations (high-dose MTX, doxorubicin and cisplatin) are the most frequently used regimen³⁵, without adaptation to risk factors. In France, chemotherapy regimens depend on age. Patients <25 years receive MTX-etoposide/ifosfamide (M-EI) to avoid anthracycline cardiotoxicity and cisplatin ototoxicity; and patient from 18 years are offered API-AI (Doxorubicin/Platinum/Ifosfamide-Doxorubicin/Ifosfamide) by medical oncologist fear of methotrexate neurological and renal toxicities³², patients between 18-25 years are treated based on the clinical center of hospitalization. Chemotherapy is adapted to high risk factors of relapse after surgery to allow patients to receive all major anti-osteosarcoma drugs³². However, whatever the chemotherapy regimen used, and despite different attempt to modify chemotherapy, no improvement in survival has been observed and some patients have a persistent dismal outcome: patients at diagnosis with inoperable tumors^{36,37} or metastatic disease^{32,38}, tumors with poor response to neoadjuvant chemotherapy define as 10% of more persistent viable tumor cells in the surgical primary resection after neoadjuvant chemotherapy^{38,39}, and patients with refractory or recurrent disease⁴⁰. Several prospective phase-III trials have attempted to introduce additional agents targeting the immune or bone microenvironment, for either all patients or certain risk groups without further success; mifamurtide (a macrophage stimulating agent) in the controversial INT-0133 trial^{41,42}, interferon IFN α in localized osteosarcoma in EURAMOS-1 trial³⁵, zoledronic acid (bisphosphonate, osteoclast activity inhibitor) in OS2006 trial³² (Fig.1.7).

characterization of osteosarcoma. This fact together with the role of bone and immune microenvironment and the incomplete understanding of the metastatic spread program in these tumors might have participated to the lack in therapeutic advances in the last 40 years.

1.2.5.1. Osteosarcoma genetic susceptibility

Historically, several *de novo* and hereditary syndromes predisposing to cancers, are known to predispose to osteosarcoma, and involve genes implicated in DNA replication and repair, and cell cycle: Li-Fraumeni syndrome (autosomal dominant disorder characterized by a germline mutation of *TP53*), hereditary retinoblastoma (autosomal recessive disorders with germline mutation in the tumor suppressor gene *RB*), Rothmund-Thomson and RAPADILINO syndromes (autosomal recessive disorders with germline mutations of the DNA helicase *RECQL4*), Bloom syndromes (autosomal recessive disorders with germline mutations of the DNA helicase *BLM* or *RECQL3*), Werner syndrome (germline mutation of the *RECQL2* gene), among others^{13,19,22}.

More recently, human population-based studies, known as genome-wide association studies (GWAS), have reported 3 genetic variants (single nucleotide polymorphisms; SNPs) associated with risk for the development of osteosarcoma⁵¹ comparing genotypes of 941 human osteosarcoma cases with those of 3291 controls: rs1906953 ($P = 8.1 \times 10^{-9}$) located at 6p21.3 within intron 7 of the glutamate receptor metabotropic 4 (*GRM4*) gene. The metabotropic glutamate receptors are a family of G protein-coupled receptors linked to the inhibition of the cyclic AMP signaling cascade. In mice, a cAMP-dependent protein kinase (*Prkar1α*) is an osteosarcoma tumor suppressor gene involved in tumorigenesis⁵³, suggesting the cAMP pathway is important in osteosarcoma. rs7591996 ($P=1.0 \times 10^{-8}$) and rs10208273 ($P=2.9 \times 10^{-7}$) located at 2p25.2 in an intergenic region that neither contain active regulatory elements or transcription factor binding sites. This signal requires further investigation to determine which variants will be optimal for functional studies needed to explain the direct association.

1.2.5.2. A complex somatic genomic/ epigenetic landscape

Osteosarcomas are characterized by a highly complex genetic landscape that varies significantly between tumors (high genetic heterogeneity).

The development of osteosarcoma is best characterized by its disorganized genome. Osteosarcoma presents a high chromosomal instability with a high degree of losses and gains of full chromosomes or large chromosomal segments, associated with loss of function in cell cycle checkpoint and DNA damage response pathways (*RB* pathway > 80%, *TP53* pathway > 75%, *CDKN2A*, and others as *RECQL4* and *WWOX*) and/or gain of function of oncogenes (e.g. *E2F3* 60%, *CDK4* 10%, *MDM2*, *MET*, *RUNX2*, and *VEGFA*)⁵⁴.

The different mechanisms sustaining this complex genomic comprise: point mutations which are likely the result of errors in DNA replication and subsequent proof reading; aneuploidy which is the result of errors in chromosomal segregation during cell division and chromothripsis a phenomenon by which tens to hundreds of genomic rearrangements occur during cancer development in a one-off cellular crisis⁵⁴.

In addition, *BRCA1/2* (breast cancer gene 1/2 - important players in homologous recombination pathway) deficiency associated characteristics in single base substitutions, and large-scale genome instability signatures are evident in >80% of osteosarcomas⁵⁵. This suggests the possibility of an early defect in DNA repair/surveillance as a mechanism for osteosarcomagenesis and the resultant bizarre aneuploidy¹⁵.

A recent comprehensive assessment of somatic copy number alterations (SCNAs) performed in 160 osteosarcoma samples revealed recurrent genomic loss spatially clustered in certain locations, termed “broken regions”, containing tumor suppressor genes such as *LSAMP*, *CDKN2A*, *RB1* and *TP53* and most frequent gains at sites including the oncogene *MYC* and the gene *RUNX2* an important player in osteogenic differentiation⁵⁶. Chromosomal breakages in these regions occurred early and were influenced by local genomic context. Both aneuploidy and chromothripsis like pattern occurrence were found to be correlated with clinical outcome of patients with osteosarcoma. Chromosomal aberrations in *TP53*, *RB1*, *WWOX* and *DLG2* genes are strongly associated with chromothripsis-like pattern

in osteosarcoma and hyperploid had a greater chance to harbor chromothripsis events and less favorable outcomes⁵⁶.

Epigenetics is a more recent field, yet not fully explored in osteosarcoma. Which includes the regulatory mechanisms affecting the expression of DNA templates without altering the sequences themselves through DNA methylation, histone modification, nucleosome remodeling, and RNA mediated events (Non-coding RNAs)⁵⁴. Gene silencing through promoter hypermethylation is a phenomenon implicated in osteosarcoma and affecting suppressor gene function of the *Rb1* and *TP53* pathways and other proteins involved in DNA repair (e.g. *GADD45*). The expression and role of lysine-specific demethylase 1 (*LSD1*) been shown in osteosarcoma⁵⁴. *LSD1* demethylates histone H3 at lysine 4 inducing transcriptional repression and gene expression suppression⁵⁷, and demethylates, stabilizes⁵⁸ and inactivates non-histone proteins such as *TP53* and *DNMT1*⁵⁹ and destabilized other proteins (e.g. *MYPT1*, a negative regulator of *RB1* phosphorylation)⁶⁰. Alterations on *ATRX* gene, which is part of a multiprotein complex that regulates chromatin remodeling, nucleosome assembly, and telomere maintenance were also detected in osteosarcoma⁶¹. *ATRX* point mutations or focal deletions affecting the coding region of the gene were described in osteosarcoma⁶¹. Somatic *ATRX* gene mutations have been observed as recurrent alterations in osteosarcoma and the ATR-X syndrome was reported as a potential factor of osteosarcoma development⁶². MicroRNAs (miRNAs) act to fine-tune gene expression by binding to messenger RNA transcripts and inhibit translation or induce degradation. The miRNAs expressed in osteosarcoma include members of signaling pathways that are key to osteosarcoma pathogenesis, including Ras, Wnt, mitogen-activated protein kinase (MAPK), and Notch. Long noncoding RNAs (lncRNAs) are defined as any non-protein-coding transcripts over 200 base pairs in length and are key regulators of a number of critical biological processes. lncRNAs LOC285194 and BC040587 were associated with copy number alteration (usually deletion) in 80% of osteosarcomas, resulting in reduced expression of the associated lncRNAs across osteosarcoma samples⁵⁴.

1.2.5.3. Cell of origin

Each cell of osteoblastic lineage can be a target for malignant transformation, leading to a large panel of more or less differentiated phenotypes for osteosarcomas. Adolescents and Young Adults rather develop osteosarcoma in bone growth areas of long bones ^{11,12,15,16,22}.

More recent data suggest that the osteosarcoma-transforming event occurs in multipotent mesenchymal stem cells⁵⁴. Bone marrow-derived mesenchymal stem cells (BMSCs) are proposed as the cells of origin of several subtypes of osteosarcoma (Fig.1.8) and an attractive hypothesis is that oncogenes and/or tumor suppressors regulate the lineage choices of BMSCs and, thus, the subtypes of osteosarcoma^{19,27}.

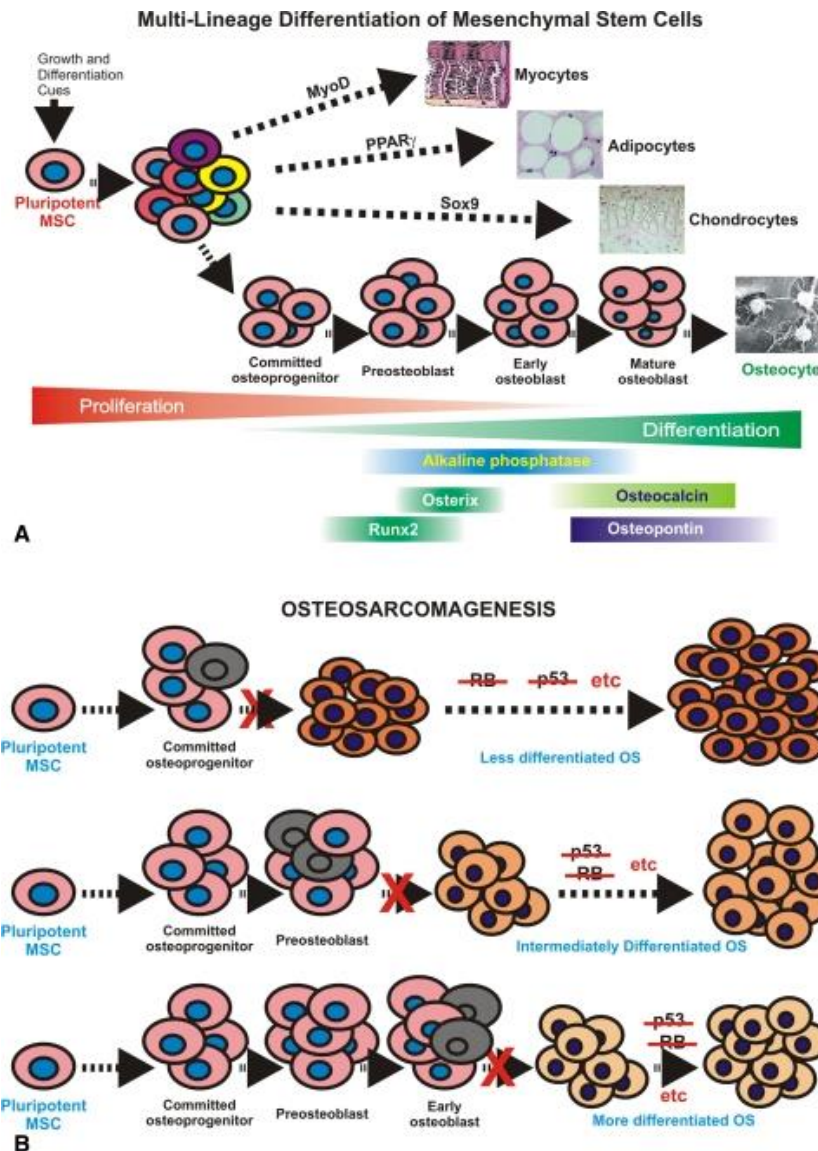


Figure 1.8: **(A)** Osteogenic differentiation. Mesenchymal stem cells (MSCs) can give rise to several cell types such as myocytes, adipocytes, chondrocytes, and osteocytes, with appropriate stimuli, presumably by activating proper lineage-specific regulators, eg, MyoD, PPAR γ , Sox9, or Runx2/Osterix. Osteogenic differentiation can be monitored by using alkaline phosphatase as an early marker and osteocalcin and osteopontin as late markers. **(B)** Disruption of osteogenic differentiation, due to genetic defects (eg, activation of oncogenes or inactivation of *TP53* and *RB* tumor suppressor genes) and epigenetic alterations at different stages may lead to OS development. Defects at the early stages may lead to the development of more aggressive and undifferentiated OS. The cells filled with black color indicate cancer-initiating cells¹⁹.

1.2.5.4. Importance of the bone and immune microenvironment

In addition to the complexity of osteosarcoma cells, the microenvironment plays an important role in the osteosarcoma pathogenesis, once is dynamic and variable, with a complex bone extracellular matrix (ECM) and diverse cell populations implicated^{15,63}. Osteosarcoma microenvironment contributes in several processes, participating to osteosarcoma aggressiveness: the dysregulation of bone remodeling (bone niche), the induction of a tolerant environment (immune niche), and the facilitation of the transport of gas and nutrients to cancer cells and extravasation to their metastatic location (vascular niche) (Fig.1.9)^{63,64}.

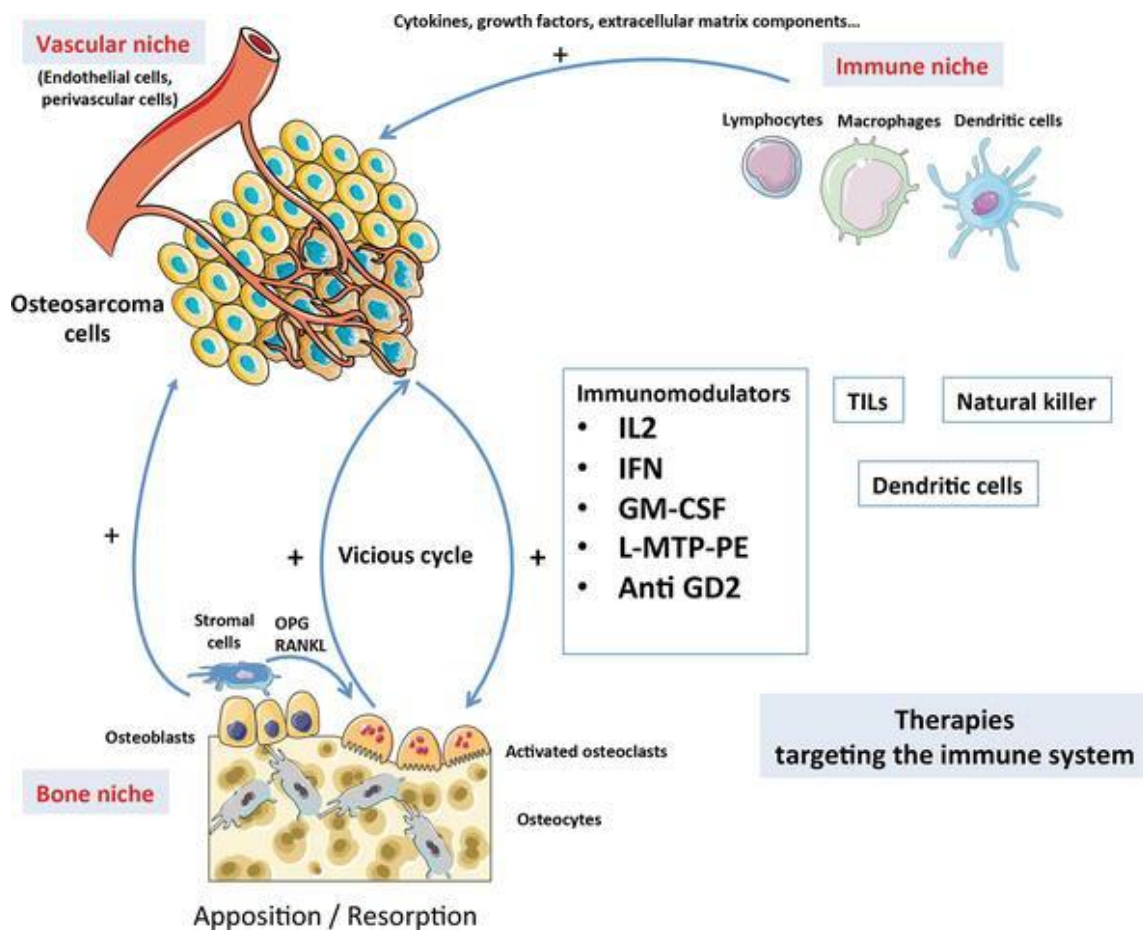


Figure 1.9: Osteosarcoma and its niches (bone, immune and vascular niche). Adapted from⁶³.

Bone-tumor vicious cycle

Osteosarcoma microenvironment is characterized by abundant transforming growth factor- β 1 (TGF- β 1) and hypoxia, resulting on the acquisition of cancer stem cell characteristics by the non-stem-like osteosarcoma cells (eg. self-renew capacity, proliferation), promoting tumorigenesis and chemoresistance^{15,65}. The bone is relatively hypoxic in comparison with other tissues ($\leq 2\%$ O₂). What in conjunction with a rather high proliferation capacity of cancer cells, resulting in increased hypoxia levels that can often lead to poor prognosis in osteosarcoma. Low oxygen tension may be important for the development of osteosarcoma but also for other solid tumors, particularly in those that grow rapidly. In tumor areas of low oxygenation, reduced cell division can be observed which might result in resistance to both radiotherapy and chemotherapy. Cellular responses to hypoxia are commonly regulated by the hypoxia inducible factor (HIF) family of transcription factors^{15,65,66}.

Once an osteosarcoma develops in the bone, tumor cells are capable of secreting factors that initiate osteoclast-mediated bone destruction, and matrix-derived growth factors, especially TGF- β 1 (released from bone matrix). At this time, osteosarcoma cells also release TGF- β 1 directly. TGF- β 1 is a pleiotropic cytokine that acts as a mediator upon the tumor to promote further tumor expansion, metastasis, and cytokine production. Recent findings suggest that genetic and epigenetic events mediate the acquisition of oncogenic activity by TGF- β 1, as do the aberrant alterations within the tumor microenvironments^{15,65,66}.

The molecular OPG/RANKL/RANK triad (osteoprotegerin/ Receptor activator of nuclear factor kappa-B ligand/ Receptor activator of nuclear factor kappa-B) plays an important role in physiological management of the bone niche (Fig.1.9)^{63,64}. Its dysregulation in osteosarcoma causes exacerbated local bone remodeling. In a normal bone, the RANK receptor is expressed at the surface of osteoclasts and precursors, while OPG and RANKL are secreted by osteoblasts and/or stromal cells. In a bone tumor environment, RANKL can also be produced by other normal cell types (e.g. fibroblasts, epithelial cells, or T-lymphocytes) or by tumor cells in response to chemokines, cytokines, hormones, and growth factors. In addition, a reduced OPG production might aggravate the vicious cycle between osteosarcoma

cells and bone niche^{63,64}. Such high levels of RANKL and RANK and low levels of OPG are associated with worse outcomes in osteosarcoma^{63,64}.

Immune microenvironment

Although the immune microenvironment of osteosarcoma is not fully understood yet, some evidences suggest its huge importance in acquisition of metastatic phenotype and outcome. It has been reported that localized tumors at diagnosis might present higher levels of tumor-infiltrating macrophage (TAM, CD68+ or CD14+) with M1-polarisation⁶⁷ associated to low levels of tumor infiltrating lymphocytes (TIL) with a balance in favor of CD8 effectors⁶⁸. These data associated with low metastases risk and improved outcome. Conversely, metastatic disease might present primary tumor with M2-polarised TAM (CD163+ IL10+) harboring immunosuppressive, tissue remodeling and pro-angiogenic properties⁶⁹. Their immunosuppressive effect is mediated by exhaustion/energy of CD8+ TIL⁷⁰ and a balance favoring FOXP3+ T regulator lymphocytes (Treg)⁶⁸. This pro-tumor immune contexture appears increased in lung metastasis samples^{67,71}.

High expression levels of immunosuppressive molecules such as PD-L1⁷¹, B7-H3⁷², and indoleamine 2,3-dioxygenase (IDO)⁷³, high peripheral levels of CSF1⁷⁴, and high expression of intra-tumor IL34 (another CSF1R ligand)⁷⁵ in tumors at diagnosis have been associated with poor metastases-free and overall survival.

Rather than a clear situation of dichotomy, a continuum between both states might better mimic the reality of osteosarcoma microenvironment explaining some apparent recent conflicting results⁷⁶.

Vascular niche

The vascular niche regulates osteogenesis and hematopoiesis and support the self-renewal of Hematopoietic Stem Cells (HSCs). Vascular niche was also associated with tumor cell extravasation/migration to their metastatic location (e.g. lung, bone and liver), facilitating the transport of gas and nutrients to cancer cells^{63,77,78}. Similarly to other tumor types that have their own vascular system, osteosarcoma has abundant blood vessels. Increased vasculature has been reported as a poor prognostic factor in human OS¹⁵. Bone vasculature might regulate multiple cellular

and developmental processes, including, stem cell and progenitor cell proliferation and cancer cell metastasis, and is involved in several steps of the metastatic cascade^{68,70}. Complex microenvironment involving multiple cell populations (eg. endothelial cells), vessels (extensive vascularization of the skeletal tissue) as well as matrix and growth factors (eg. transforming growth factor beta-TGF β) abundant in vascular bone microenvironments, not only provide a fertile soil for the metastatic growth but also support the dormancy of Disseminated Tumor Cells (DTCs) and their reactivation. During the later stages of the disease, blood vessels enhance the metastatic outgrowth by mediating higher delivery of oxygen, nutrients and growth factors^{77,80}. Angiogenesis, a dynamic and programmed process in which new blood vessel are formed from preexisting vessels induced by different triggers (e.g., hypoxia), has been described as a major process in the development of tumor vascularization system, which supplies cancer cells with blood^{15,81}. A study based on a cohort of 131 osteosarcoma samples suggested that patients with low OS vascularization have a prolonged survival and good response to neoadjuvant chemotherapy¹⁵.

The vascular endothelial growth factor (VEGF) and its receptor (VEGFR) are key inducers of physiological or pathological angiogenesis by promoting endothelial cell growth, migration, and survival from pre-existing vasculature. Besides that, VEGF mediates vessel permeability, and more recently, was associated to mobilization of endothelial progenitor cells from the bone marrow to distant sites of neovascularization^{15,81}. Elevated expression of VEGF in primary OS promotes angiogenesis, leading to higher rate of pulmonary metastasis¹⁴, and is also associated to drug sensitivity^{15,81}. Platelet-derived growth factor (PDGF) and its receptor PDGFR have been also associated with poor prognosis. PDGF-AA expression in osteosarcoma patient samples associate with decreased disease-survival⁸². Others suggest that osteosarcoma-platelet interactions induce the release of PDGF from platelets, which promotes the proliferation of osteosarcomas by activating the PDGFR and then Akt⁸³.

1.2.6. Metastatic spread and resistance in osteosarcoma

The different steps and some of the key elements required for metastatic spread are starting to be known in osteosarcoma. But the understanding of the timing of events leading to metastatic progression and the events themselves are far from complete. Osteosarcoma metastatic potential and the ways of targeting it, are active research fields.

The metastatic cascade (Fig.1.10) represents a series of processes that start as a cell leaves the primary tumor and invades the surrounding tumor microenvironment, leading to intravasation. In osteosarcoma, intravasation is mediated by integrin $\alpha_5\beta_1$, ANGPTL2 through integrin $\alpha_5\beta_1$, p38 MAPK and MMPs, such as MMP9 expression⁸⁵, and promoted by increased TGF- β s expression⁸⁶) into existing or new vascular structures, survival in the circulation, and eventual arrest and extravasation at distant secondary sites, followed by the development or recruitment of a blood supply and growth at the secondary site⁵⁴. Cells must then rapidly adapt to this new and maybe hostile environment to survive, usually the lung in osteosarcoma.

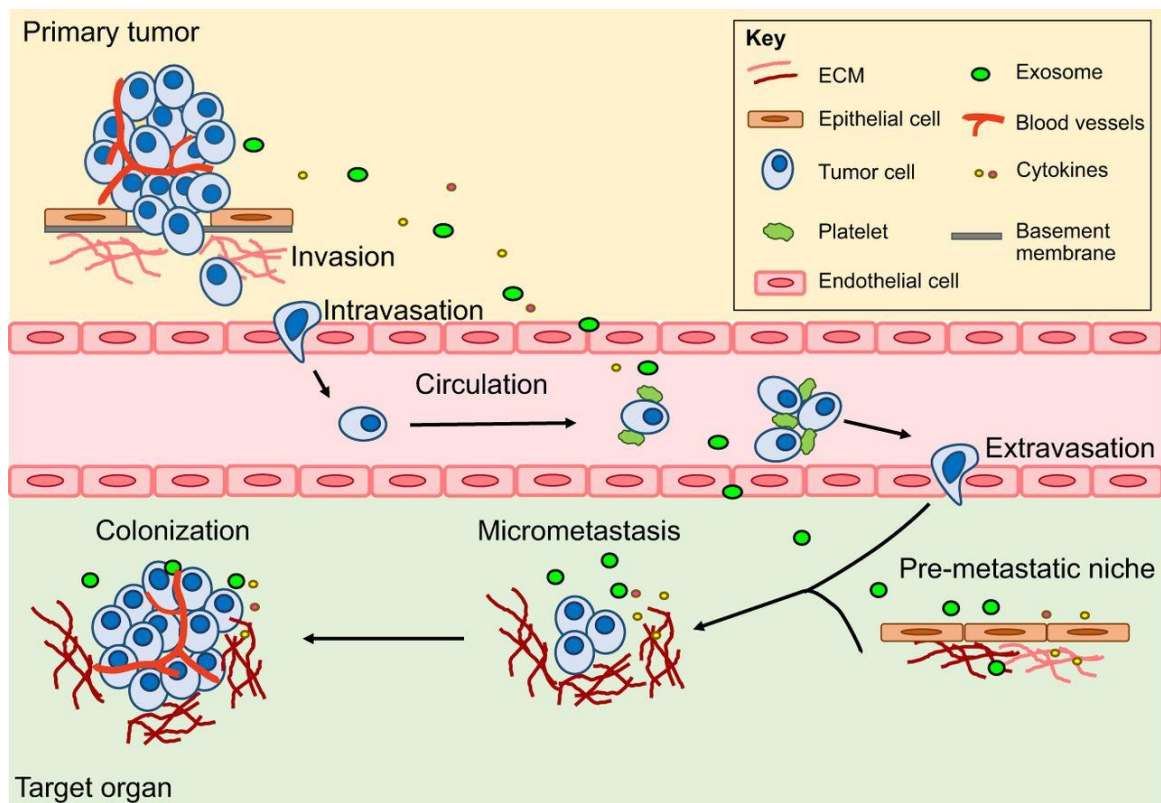


Figure 1.10: Metastatic cascade. Initially, tumor cells migrate into adjacent tissues (invasion), involving the breakdown of the basement membrane and invasion into the surrounding ECM. Intravasation then allows cells to enter the circulation. In blood vessels, circulating tumor cells exist as single cells or clusters, coated with platelets. They need to survive shear stress and evade clearance by the immune system to successfully reach distant organs. Tumor cells then attach to endothelial cells, which facilitates their extravasation. After settling in the metastatic target organ, tumor cells must survive in this foreign environment and establish micrometastases. These disseminated tumor cells can remain dormant for many years before proliferating into large macrometastases in a process termed colonization. The primary site also regulates the development of metastasis via secretion of factors (such as cytokines) that can prime a pre-metastatic niche and support survival of disseminated tumor cells⁸⁷.

Although osteosarcoma resistance to chemotherapy phenomenon is not fully known⁶⁵, several mechanisms have been described, depending on the cell state, the microenvironment of the osteosarcoma cells and the drug pressure.

Resistance mechanisms might intervene at different levels:

1- **Reduced drug accumulation in tumor cells** can be due to either a reduced drug uptake, an increase of drug efflux, or an increase of drug detoxification. As an example, methotrexate resistance by low expression of the reduced folate carrier (RFC) without gene deletion. Such decreased RFC expression is found in 65% of tumor biopsies at diagnosis^{65,88,89}. Multidrug resistance to increased vinca alkaloids, epipodophyllotoxins, anthracyclines, taxanes, and kinase inhibitors have been observed following increased expression of multidrug resistance proteins such as PgP=MDR1=ABCB1, MRP1=ABCC1 and others^{65,88,90–93} (Fig.1.11). Finally, resistance to cisplatin by GSH (Glutathione S-transferase) xenobiotic detoxification pathway^{65,94} with increased GSTP1 (Glutathione S-transferase P1) levels⁹⁴, resistance to methotrexate⁹⁵ by increased levels of UGT1A (UDP glucuronosyltransferase family 1 member A) an enzyme inactivating different xenobiotics through covalent addition of glucuronic acid⁹⁶; ifosfamide resistance by increased CYP (Cytochrome P450) system⁹⁰.

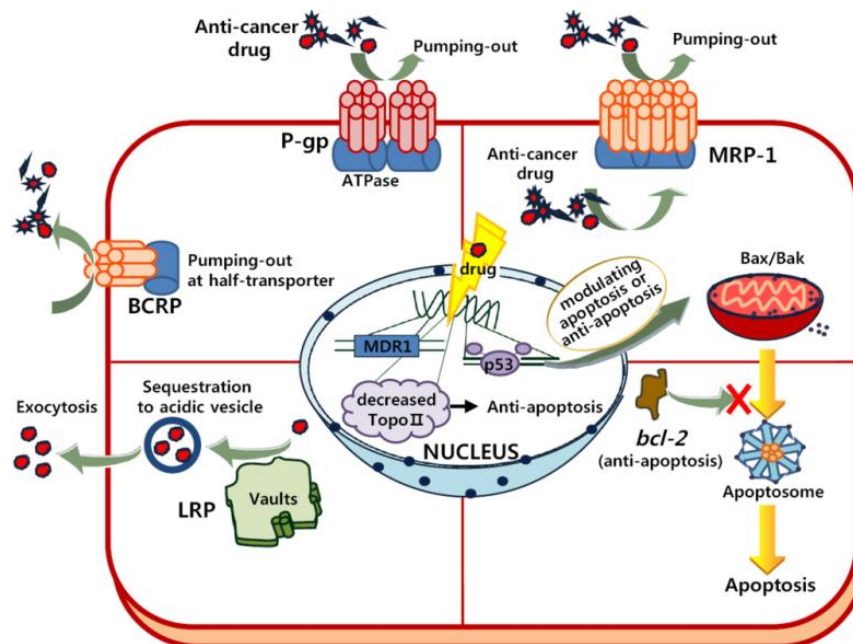


Figure 1.11: Drug-resistance mechanisms (such as PgP, MRP, *BCRP*, *LRP*, *TP53*, *bcl-2*, and Topo 2) in tumor cells⁸⁸.

2- Drug target molecular abnormalities can induce resistance to a specific drug or a class of drug. For example, methotrexate resistance may be due to an increased expression of DHFR (dihydrofolate reductase), a key enzyme for intracellular folate metabolism. An increased DHFR expression was found in 10% of tumor biopsies at diagnosis^{84,85,92}. Resistance to topoisomerase inhibitors, doxorubicin and etoposide, may be due to low expression levels of topoisomerase II (TOPO2) through gene mutation/alteration⁹⁸.

3- Drug action impairment by specific cellular characteristics might result from alterations of the inter-related cell cycle and DNA repair processes, from resistance to apoptosis or to autophagy, or from activation of survival stimulatory genes. For example, TP53 mutations⁹⁹ or *STAT3*⁶⁵ and G2/M arrest allow DNA repair, whereas alterations in expression levels of *AARS*, *AURKA*, *AURKB*, *CENPA*, *CCNB1*, *CCNE2* and *CDK*¹⁰⁰ are linked to MTX resistance. Alteration in the *Wnt* signaling pathway by repression of syndecan-2 expression influences both caspases-dependent and independent apoptosis in response to doxorubicin¹⁰¹. Finally, overexpression of BAX, BCL2 or Survivin confers resistance to cell death^{65,102}.

Inter-relations between all these mechanisms of resistance are complex and not yet completely elucidated. The activity of key factors may be regulated at a gene level through several molecular alterations in their coding sequences such as deletion/amplification (e.g. DHFR amplification in many osteosarcoma cell lines¹⁰³ but rarely found in patient samples⁸⁹), mutation (e.g. mutation in RFC observed in 9,2% osteosarcoma samples results in serine-to-asparagine substitution at amino acid 46)¹⁰⁴, epigenetic modulation and miRNA regulation (e.g. decreased expression level of miR-15b is linked to doxorubicin resistance on osteosarcoma cells¹⁰⁵).

4- Osteosarcoma cancer stem cells (CSC). There is growing evidence that osteosarcoma may arise from cancer stem cells (CSCs). Using CD117 and Stro-1 as potential candidates for CSC markers^{106,66}, some positive cells have been detected in osteosarcoma cell lines and in biopsies of human tumors⁶⁵. These osteosarcoma CSCs have the potential for self-renewal, the ability to proliferate and differentiate⁶⁵. They also present resistance to chemotherapy, and several mechanisms have been identified : increased PgP/*MDR1* or GST expression, low

levels of topoisomerase II expression, increased DNA repair capacity and anti-apoptotic protein overexpression^{65,98,106,107}, capacity to maintain in a quiescent state for prolonged periods of time (resting in G0)^{106,66}. Hypoxia is also reported to instigate inflammation-like conditions in the tumor microenvironment which are generally favorable to survival of (stem-like) cancer cells⁶⁵.

5- Metastatic cells, even at diagnosis and before any drug exposure, present higher chemoresistance compared to primary tumor cells^{89,108}. For example, they present increased PgP expression comparatively to primary tumors, increased DHFR expression (10% at diagnosis in primary tumors and 62% in metastatic lesions); decreased RFC expression (65% at diagnosis and 45% at definitive surgery and relapse)^{89,108}. The capacity of tumor cells to metastasize reflect their aggressiveness and their ability to adapt to a different niche (bone niche for the primary tumor and lung niche for metastases). How this selection might influence the differential drug sensitivity between metastatic and from primary tumor, is not known. At diagnosis, non-detectable and non-proliferating (dormant) single cancer cells or micrometastases might already be present in tumors defined as “localized”, and may be responsible for a number of relapses. Non-proliferating cells present natural resistance to agents requiring an active cell cycle to be fully active (e.g. DNA damaging agents).

6- Induced chemotherapy drug resistance. In addition to intrinsic resistance detectable even in the absence of treatment, resistance to therapy can as well be acquired during/after treatment with chemotherapeutic agents^{65,107}. Exposure to the drug may cause clonal selection or induced resistance mechanisms, detectable in surgical samples of patients with poor histological response to neoadjuvant chemotherapy after induction chemotherapy or at relapse (e.g. DHFR levels 10% in primary tumor sample at diagnosis and 62% in relapse samples⁸⁹).

The inter-relation between metastatic process beginning and cells acquire resistance to chemotherapy are not clear but their possible occurrence at different time point might explain different osteosarcoma behavior. Micrometastases at diagnosis might explain metastatic relapse in patients with a good histological response or after amputation alone. The metastatic process during pre-operative chemotherapy might lead to drug selection process by the metastatic process itself

and/or by drug pressure. At the end, metastatic relapse might present a mix of all these different mechanisms of resistance and improving outcome in osteosarcoma would require to target several of the key steps of the metastatic process and resistance phenomena at the same time. Preclinical models for drug testing would need to reflect all this diversity to approach at best the real effect to be expected in patients.

1.3. Osteosarcoma pre-clinical Models

Preclinical *in vitro* and *in vivo* models are important tools in cancer research, to identify etiologic factors, to provide insight into the molecular mechanisms of tumor growth and metastases, as well as for drug screening, development of new therapies and understanding the mechanisms of resistance¹⁰⁹.

Fully representing the genetic complexity and tumor heterogeneity, the unique clinical (rapid bone tumor growth, local aggressiveness, lung and bone metastases) and biological behavior (expression of osteoblastic biomarkers such as alkaline phosphatase (ALP), osteocalcin (OCN), or osteopontin (OP), and osteoid production) of human osteosarcoma in pre-clinical models has proven to be particularly difficult under practical lab conditions and requires multiples models from different origins^{110,111}.

Several osteosarcoma models, issued from animal or human sources have been developed and characterized in the last decades (Fig. 1.12)¹¹⁰. Those models have been generated or implanted in different animal species (immunocompetent or variously immunocompromised), and in different *in vivo* setting (e.g. heterotopic and orthotopic).

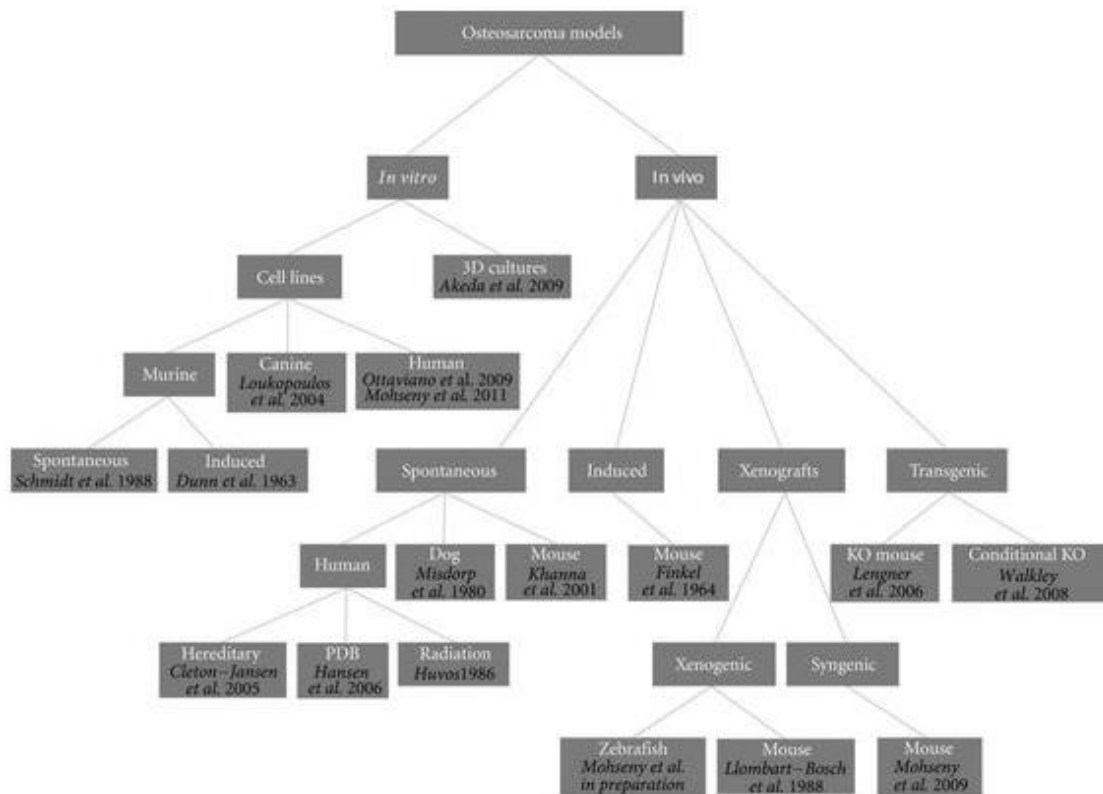


Figure 1.12: Existing osteosarcoma models. References are provided for each model¹¹⁰.

Animal osteosarcoma models were used for different purposes, from understanding osteosarcoma oncogenesis to study the role of the immune system in this tumor. However, neither isolated cells or tumors derived from these animal models, might accurately reflect the human disease^{112,113}. **Transgenic** models, genetically engineered/knock-out mouse to mimic the human disease at the molecular level, have been successfully used to study the importance of a particular gene in cancer development and progression (e.g. *TP53* or *RB1* genes in osteosarcoma)^{113,114}. However, tumors that develop in transgenic models tend to be less heterogeneous, which may influence their progression and metastatic behavior¹¹³. **Syngeneic** models, issued from murine cancer cells induced by chemical or surgical intervention are subsequently implanted/injected into immunocompetent mice (same mouse strain)^{112,113}, showed appropriate interaction

of introduced malignant cell lines with host stroma elements and retains full immunoreactivity allowing immune microenvironment studies^{112,115}. *In vivo* **spontaneous** osteosarcoma animal models exist in mice and in dogs, allowing studying osteosarcoma in the full *in vivo* context with the bone, immune and vascular niches. Again, they might not reflect the whole human disease. Indeed, spontaneous osteosarcoma in dogs affects mainly geriatric dogs, while the peak of incidence in human disease occurs during adolescence, and dogs are not easy to use for laboratory research¹¹⁴.

To overcome these pitfalls, several *in vitro* and *in vivo* human osteosarcoma models have been developed, issued from human tumor samples and their description are detail below.

1.3.1. *In vitro* human osteosarcoma models

The development of cell isolation and culturing techniques conducted to the emergence of multiple cancer cell culture models issued from patient samples. They are easy to grow, form the basis for study numerous cellular processes, general tumor cell biology, and help to identify promising therapeutic agents and novel targets for new treatments^{109,110,116}. They allow the control of most experimental variables and permit quantitative analysis. They could be used as excellent *in vitro* models as long as they are representative of the original tumor (molecular profiles of a large number of human cancer cell lines available in the Cancer Cell Line Encyclopedia, to be compared to the profiles of human tumors, compiled as part of the Cancer Genome Atlas Research Network)¹⁰⁹. However, cancer-cell *in vitro* models have reduced physiological relevance, capturing only limited aspects of the tumor microenvironment.

Osteosarcoma cell lines derived from patient samples usually retain many markers of the osteoblast phenotype and present most of their parental tumors characteristics^{117,118}. They are used as *in vitro* osteosarcoma models for their altered molecular background and high proliferative rate, despite the questioning about the additional genetic alterations acquired *in vitro* and the extent of their representativeness of the original tumors they are issued of¹¹⁷. *In vitro* culture has

an inherent risk of selection of certain cellular sub-clones (e.g. through changes in cellular adhesion properties or proliferation rates), as a consequence of ongoing genomic instability¹¹⁹.

The Eurobonet consortium has characterized 19 human osteosarcoma cell lines, mainly issued from primary tumor biopsy at diagnosis (n=12) of female patients (sex ratio M/F = 9/10, with the most frequently used osteosarcoma cell lines being issued from females, while male patients are more frequent), of a teenage age (around 13 years-old, range 7 to 41 years; one patient below 10 and 3 patients above 25 years old). These cell lines usually present an osteoblastic subtype and different essential genetic alterations implicated in osteosarcoma oncogenesis (eg. *TP53*, *RB* pathways) (table 1.III)^{117,120,121}. Very few cell lines were issued from metastasis samples (n=4) or resistant tumors after drug exposure (post-operative or relapse samples), which usually present less sensitivity to chemotherapy (e.g. IOR/OS18)^{29,38–40,122}. Some of these cell lines have been continuously exposed to increasing drug concentration of different agent to select resistant clone to these agents (eg. Saos-2 resistant to doxorubicin, U2OS resistant to methotrexate; U2OS resistant to cisplatin)¹²³.

These cell lines have been widely used and proven to be useful to understand osteosarcoma oncogenesis, to dissect different cellular mechanisms linked to osteosarcoma aggressiveness (proliferation, migration/invasion, apoptosis/autophagy) and to test sensitivity/resistance to different drugs and to analyze the underlying mechanisms^{120,124,125}. However, studying osteosarcoma metastatic behavior and the interactions with the microenvironment further requires *in vivo* models.

In the current thesis, several of these established human osteosarcoma cell lines were used: MG-63, Saos-2, U2OS, HOS, HOS-143B and IOR/OS18. We checked that their described *in vitro* characteristics were present in our culture conditions: performing copy number analysis by array-based Comparative Genomic Hybridization (aCGH) (Fig.1.13): our cell batches presented similar aCGH profiles to those described in the literature¹²², the hierarchical clustering classified our cell lines with the respective cell lines of the literature. Two different culture flasks of

Saos-2 showed slight differences in aCGH profile and we carried on the experiment with both, calling the second one Saos-2-B. The main loss of *CDKN2A*, *TP53* and *RB1* status were retained in our cells (Table 1.IV).

- observing their proliferative, migratory and invasive potential (Incucyte) under basal *in vitro* culture conditions (DMEM supplemented with 10% FBS and incubated at 37°C in a humidified atmosphere -5% CO₂ and 95% air) (Table 1.V)
- their *in vitro* drug sensitivity to classical anti-osteosarcoma chemotherapeutic agents (doxorubicin, methotrexate, cisplatin, mafosfamide, etoposide) (Table 1.VI).

Table 1.III: Characteristics of Osteosarcoma cell lines. Patients and samples characteristics from where the cell lines were derived, the principal genetic alterations and the *in vivo* development^{111,117,119,121,122,126–130}. F-female, M-male, OB-osteoblastic, FB-fibroblastic, NA-not available, PT-primary tumor, Met- metastases, a- in SCID mice¹²⁶, b-in Nude mice, IM-Intramuscular, SC-Subcutaneous, PO-Para-osseous

Cell line	Patients and samples characteristics				Principal Genetic alterations				<i>In vivo</i> mice models			
	Gender	Age	Subtype	Tumor sample	TP53	RB1	CDKN2A	ATRX	Orthotopic In SCID ^a or nude ^b		SC in nude	
									PT	Met	PT	Met
U2OS	F	15	OB/FB	Primary biopsy from tibia	Normal	Normal	Hemizygous deletion	Deleted	Yes (IM) ^b	No (IM) ^b	Yes (SC)	No (SC)
MG-63	M	14	FB	Primary biopsy	First intron Rearrangements	NA	Homozygous deletion	Homozygous deletion	Yes (PO) ^a	No (PO) ^a	No (SC)	No (SC)
IOR/OS18	M	33	OB	Metastatic biopsy	Del>EX3/EX4	Normal	Homozygous deletion	NA	No (IM) ^b	No (IM) ^b	No (SC)	No (SC)
Saos-2	F	11	NA	Primary biopsy	Del>EX4/EX8	Mutated	Normal	Normal	Yes (PO) ^a	Yes (PO) ^a	No (SC)	No (SC)
HOS	F	13	NA	Primary biopsy from distal femur	Mutated (p.Arg156Pro)	Normal	Homozygous deletion	NA	Yes (PO) ^a	No (PO) ^a	No (SC)	No (SC)
HOS-143B	F	13	NA	Ki-ras oncogene transformation of the HOS	Mutated (p.Arg156Pro)	Normal	Homozygous deletion	NA	Yes (PO) ^a	Yes (PO) ^a	Yes (SC)	Yes (SC)
HOS-MNNG	F	13	NA	HOS transformation with 0.01 mcg/ml MNNG (a carcinogenic nitrosamine)	Mutated (p.Arg156Pro)	Normal	Homozygous deletion	NA	Yes (PO) ^a	Yes (PO) ^a	Yes (SC)	No (SC)
IOR/MOS	F	13	OB	Primary biopsy	Mutated (c.249_572del)	Mutated	Normal	NA	No (IM) ^b	No (IM) ^b	No (SC)	No (SC)
IOR/OS9	M	15	OB	Metastatic biopsy	Normal	NA	Homozygous deletion	NA	Yes (IM) ^b	No (IM) ^b	Yes (SC)	No (SC)
IOR/OS10	F	10	FB	Primary biopsy	Mutated (splicing ex9/10)	Heterozygous deletion	Homozygous deletion	NA	No (IM) ^b	No (IM) ^b	No (SC)	No (SC)
IOR/OS14	M	13	OB	Primary biopsy	Normal	NA	Normal	NA	Yes (IM) ^b	No (IM) ^b	Yes (SC)	No (SC)
IOR/OS15	F	12	OB	Primary biopsy	Normal	NA	Homozygous deletion	NA	No (IM) ^b	No (IM) ^b	No (SC)	No (SC)
OSA	M	19	FB	Primary biopsy from femur	Normal	NA	Hemizygous deletion	NA	Yes (IM) ^b	No (IM) ^b	Yes (SC)	No (SC)
SARG	M	25	NA	Primary biopsy	Mutated (p.Tyr205X)	copy number increase (breakpoint)	Hemizygous deletion	NA	No (IM) ^b	No (IM) ^b	No (SC)	No (SC)
KPD	F	7	OB	Primary biopsy	Normal	NA	Normal	NA	No (IM) ^b	No (IM) ^b	No (SC)	No (SC)
OHS	M	14	OB	Primary biopsy	Mutated (p.Glu286Lys)	NA	Normal	NA	Yes (IM) ^b	No (IM) ^b	Yes (SC)	No (SC)
HAL	M	16	NA	Bone marrow	Normal	NA	Normal	NA	No (IM) ^b	No (IM) ^b	No (SC)	No (SC)
ZK-58	M	21	OB	NA	Normal	NA	Normal	NA	No (IM) ^b	No (IM) ^b	No (SC)	No (SC)
MHM	F	41	FB	Metastatic biopsy	Normal	NA	Hemizygous deletion	NA	Yes (IM) ^b	No (IM) ^b	Yes (SC)	No (SC)

Figure 1.13: aCGH hierarchical clustering of the osteosarcoma cell lines used compared to the literature data. Unpublished data from the lab.

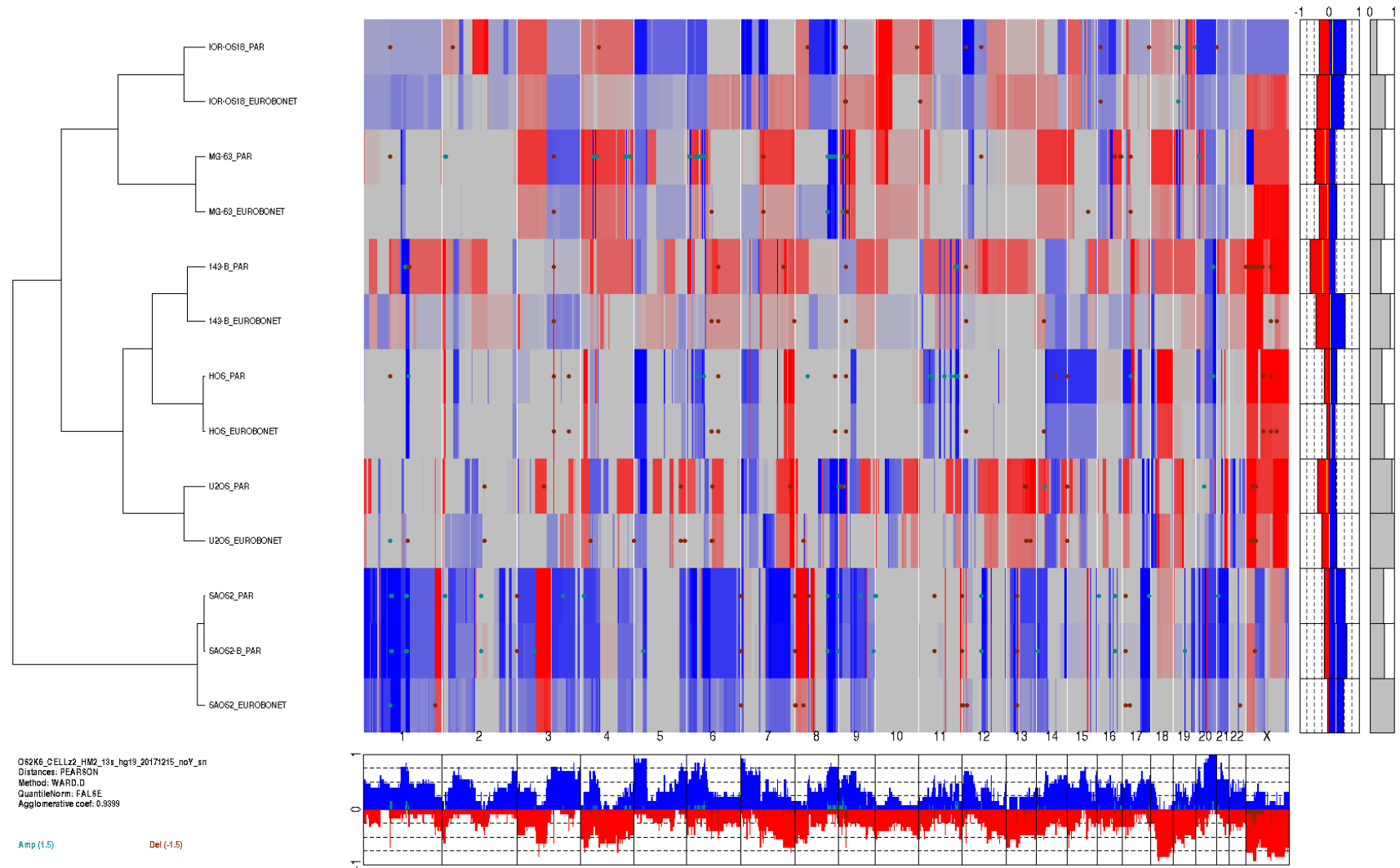


Table 1.IV: Basal characteristics of the most used osteosarcoma cell lines obtained by aCGH analysis. Where zero, positive and negatives values represent respectively normal, a gain or a loss status of the gene. Unpublished data from the lab.

Cell lines aCGH	HOS	143B	Saos-2	Saos-2-B	MG-63	IOR/OS18
ABCB1 (MDR1) Chr7: 87,503,633- 87,713,323	0	0	0.56757	0.56201	-0.47213	0.38875
DHFR Chr5:79,922,044- 79,950,800	0	0.37769	0	0	-0.39298	0.32455
SLC19A1 (RFC gene) Chr21:46,934,628- 46,962,385	0	0.33396	0.69829	0.62839	0.29289	0.22172
MTHFR Chr1:11,845,786- 11,866,160	0	0.35286	0.94115	0.97643	-0.05033	0.12133
TP53 Chr17: 7,661,779- 7,687,550	0.60445	0.47133	0	0	0	-0.49461
RB1 Chr13: 48,303,751- 48,481,986	0	0	0.46966	0.39403	-0.059991	-0.06233
CDKN2A Chr9: 21,967,753- 21,995,301	-3.10149	-3.13089	0.33569	0.30065	-3.72571	-3.45441
ATRX ChrX: 77,504,878- 77,786,269	-0.84526	-0.07896	0	-	-0.46597	0.27468

Table 1.V: *In vitro* characteristics of osteosarcoma cell lines, namely proliferative, invasive and migratory capacities obtained through Incucyte, cell cycle phase arrest and apoptosis rate by flow cytometry under the most used chemotherapeutical agents for 72h using the IC50 for treatment (observed in table 1.VI): DOXO- doxorubicin, MTX- methotrexate, ETOP- etoposide, MAF- mafosfamide, CISP- cisplatin. Unpublished data from the lab.

Cell line	<i>In vitro</i> characteristics												
	Proliferation rate	Invasion capacity	Migration capacity	Cell cycle(IC50, 72h) arrest					Apoptosis (%death cells IC50, 72h)				
				DOXO	MTX	ETOP	MAF	CISP	DOXO	MTX	ETOP	MAF	CISP
U2OS	++++	-	+++	G2	G1	G2	G2	G2	10%	15%	22%	38%	30%
MG-63	++++	++	++++	G2	G1	G2	G2	G2	10%	20%	19%	15%	15%
IOR/OS18	+++	++	++++	G2	G1	G2	G2	G2	15%	20%	24%	34%	26%
HOS	++++	-	+++	G1	G1	G2	G1	G2	40%	18%	23%	8%	29%
143B	+++++	++	+++++	G1	G1	G1	G1	G2	15%	10%	17%	10%	11%
Saos-2	++	-	++	G2	G1	G2	G2	G2	40%	13%	36%	42%	25%

Table.1.VI: IC50 of the different cell lines to the most used chemotherapeutic agents obtained at 72h by MTS assay. Unpublished data from the lab. MTX- methotrexate, DOXO- doxorubicin, ETOP- etoposide, CISP- cisplatin, MAF- mafosfamide.

		IC50 (μM)				
		MTX	DOXO	ETOP	CISP	MAF
HOS	Parental	0.04	0.05	0.70	4.80	12.70
HOS-143B	Parental	0.04	0.04	0.68	1.68	14.30
Saos-2	Parental	0.05	0.05	2.97	4.28	17.60
Saos-2-B	Parental	0.05	0.06	2.80	5.20	20.30
MG-63	Parental	0.05	0.10	2.00	2.48	13.30
U2OS	Parental	0.05	0.10	4.40	10.00	33.00
IOR/OS18	Parental	1.30	0.18	5.86	4.62	27.13


1.3.2. *In vivo* human osteosarcoma models

In vivo models might allow to better capture the complexity of the metastatic process in a living system as well as the influence of the microenvironment on tumor behavior¹⁰⁹. Indeed, cancer cells migrate through vastly different microenvironments: stroma, blood vessel endothelium, vascular system, and tissue at a secondary site. Their ability to successfully form metastases depends on the interactions between the cancer cell and the local microenvironment^{18,109}. Another advantage of *in vivo* models is to allow to access to *in vivo* response to various therapeutic agents, not only at the primary site, but also in terms of the metastatic development¹¹¹. They also provide valuable tools to investigate the underlying mechanisms of sensitivity and resistance to drugs^{18,109}.

Different *in vivo* models exist, depending on the integrity of the source of osteosarcoma cells (spontaneous osteosarcoma models, osteosarcoma cell derived from either human or non-human osteosarcoma), on the recipient animal species (e.g. mice, rats, dogs), or immune system status (immune-competent or immune-compromised), and the implantation localization in animal (heterotopic or orthotopic).

Several ***in vivo* xenogeneic human osteosarcoma models** were developed in the last decades, issued from human cancer cells implanted in immune-deficient mice. Although several animals have more similarity to humans with regard to genetics and morphology, rodents are frequently chosen as they are easy to manipulate in laboratory facilities. They reproduce easily, in a short time period, with low cost and can be manipulated genetically^{111,113,131} (Table.1.VII). Swiss *nude* mouse strains result from a homozygous recessive mutation of FOXP1^{nu} gene¹¹¹, born without thymus and hair. They present a T cell depletion, with some innate immunity preserved (with age an increase in NK cells and $\alpha\beta$ TCR lymphocytes maturation is observed)¹³². Several more immune compromised SCID (severe combined immunodeficient) models exist with lack of mature T and B lymphocytes, and defective dendritic and macrophage cells however present functional NK cells¹³². The NSG mouse strains (NOD.Cg-Prkdc^{scid} Il2rg^{tm1Wjl}/SzJ) are more immune-compromised, presenting deficient B, T and NK cells and defective for macrophages and dendritic cells, minimizing the risk of xenograft rejection^{131,132,133}.

Table 1.VII: Characteristics of some mouse strains used for *in vivo* models establishment. NA- not available. Adapted from¹³².

Common name	NSG	SCID	Outbred Nude
Major Phenotypes	NOD. <i>Cg-Prkdc^{scid} Il2rg^{tm1Wjl}/SzJ</i>	BALB/c SCID: CbySmn.CB17- <i>Prkdc^{scid}/J</i>	Swiss Nude: CrI:NU(Ico)- <i>Foxn1^{nu}</i>
Mature B cells	Absent	Absent	Present
Mature T cells	Absent	Absent	Absent
Natural killer cells	Absent	Present	Present
Dendritic cells	Defective	Present	Present
Macrophages	Defective	Present	Present
Hemolytic complement	Absent	Present	Present
Leakiness	Very low	Low	NA
Radiation tolerance	Low	Low	High
Spontaneous tumor incidence (type)	Low	High (thymic lymphoma)	Low
Medial survival	>89 weeks	Not determined	Not determined
Features and research applications	-No functional B, T, NK cells -Best engraftment of primary cells, tissues and tumors -Permits long-term experiments	-No functional B, T cells -Engrafts hematopoietic cancer cells lines, some primary cells -Suitable for therapeutic antibody testing due to functional complement	-Athymic and T cells deficient -Engraftment of solid cancer cell lines -Hairless -Outbred to maximize genetic diversity and hybrid vigor
Limitations	Poor radiation tolerance	-NK activity limits engraftment -Poor radiation tolerance	-Innate immunity intact -Little engraftment of hematopoietic cancer cells -Not suitable for primary cells
Degree of immunodeficiency			

The main source of osteosarcoma cells used to create human xenograft models were cell lines established from patients tumor and cultured *in vitro* before injection into immune-compromised mice leading to **osteosarcoma cell-line-derived xenograft (CDX) models**^{110,134}. Several osteosarcoma cell lines have been used to develop CDX models (Table.1.III), in *nude* mice and with a subcutaneous heterotopic implantation (implantation in a different site of tumor origin), rendering tumors easier to detect. But their tumorigenic rate (6/17 osteosarcoma cells lines) and metastatic potential (1/6 tumorigenic osteosarcoma cells lines) are low¹¹⁷, poorly reflecting human osteosarcoma behavior. In this context, some human osteosarcoma cell lines have been engineered, like HOS virally transformed (Ki-RAS oncogene) to 143B and chemically transformed to MNNG cell lines, becoming successfully tumorigenic and metastatic *in vivo*¹¹⁷. Others highly metastatic osteosarcoma cell lines were derived from their low metastatic parental cells through single clone selection in cell culture (Hu09-H3 derived from Hu09 parental cell line)¹²⁶ or *in vivo* selection in the mouse (LM7 derived from Saos-2 by repeated cycling through the lungs of nude mice¹³⁵; MG-63.2 derived from MG-63 through serial passages in nude mice via intratibial injections¹³⁶; MG-63.3 derived from MG-63.2 by a process of experimental metastasis¹²⁶; Hu09-M112 and Hu09-M132 derived from Hu09 cells injected subcutaneously in nude mice¹³⁷). To increase tumorigenicity of the osteosarcoma cell lines, other methods have been used such as implantation in a different, more physiological area, either heterotopic (eg. subcutaneous) or orthotopic (implantation in the site of tumor origin, the bone for osteosarcoma, either para-osseous (eg. paratibial) or intra-osseous (eg. intratibial) implantation; Fig.1.14), as well as implantation in more immune compromised animals (e.g. NSG mice).

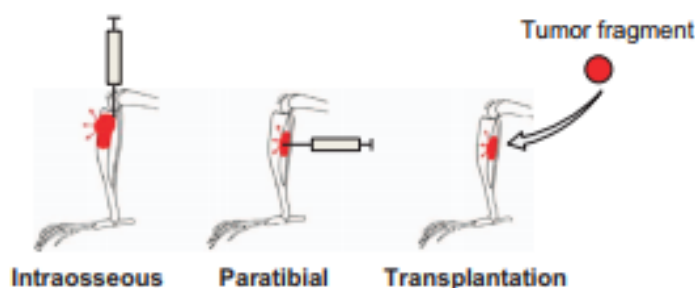


Figure 1.14: Illustration of the different orthotopic injection (intraosseous and paratibial) and implantation (transplantation, normally used for the PDXs) models. Adapted from²⁸.

Intramuscular injection in *nude* mice did not massively increase the tumorigenicity and metastatic potential of osteosarcoma cell lines¹¹⁷. The more recent **orthotopic osteosarcoma CDX-models** (paratibial and intraosseous), especially in NSG mice, in addition to develop more easily, present several advantages. They develop in the bone, better mimicking the initial tumor site including the osseous microenvironment, and reveal different tumor behavior in terms of primary tumor growth, metastatic potential and response to treatment as observed in patients^{117,138–140}. The disadvantage of these orthotopic osteosarcoma models is that primary tumor detection is more difficult *in vivo*. Several **imaging techniques** have been developed and used for real time *in vivo* (live mice) or *ex vivo* (dead animals or isolated parts like bones/organs) CDX detection, such as the IVIS spectrumCT system. This system combines longitudinal computed tomography (CT), bioluminescence (luciferase/luciferin) real-time detection, and a 3D image reconstruction¹⁴¹ (Fig.1.15). It detects and quantifies the signal produced (photons) by an enzymatic reaction in which the substrate luciferin is oxidized by luciferase expressing tumor cells, in the presence of oxygen and ATP^{138,142}. The IVIS spectrumCT system allows the detection in real time of *in vivo* CDX primary tumor growth and metastatic spread, as well as the analysis of tumor-induced bone alterations¹⁴¹ in a non-invasive manner, leading to the reduction of the number of animals used.

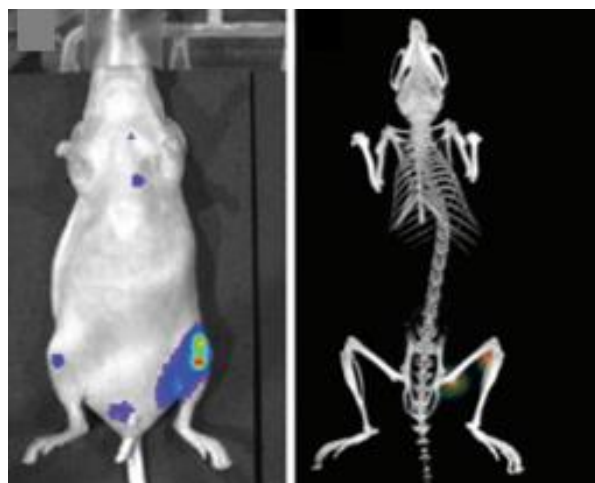


Figure 1.15: Bioluminescence detection and 3D reconstruction using the IVIS spectrumCT system. Adapted from¹⁴¹.

CDX models proved to be excellent models, allowing the study of the tumor cells and microenvironment interaction, of the metastatic potential and others mechanisms, and more importantly for drugs screening^{110,117}, once cell lines adequately represents the tumors where they are originating from, especially at the genetic level¹¹⁷. However, these models are derived from *in vitro* cultured cells that sometimes can suffer several alterations (eg. cells selection, genetic alterations, cross-contamination)¹¹⁷. Furthermore, their representativeness compared with the original tumors is being questioned, once these cells have been cultured in the absence of stroma, hence lacking the proper microenvironment and the original tissue architecture¹¹⁷. They also not fully reflected tumor heterogeneity observed in osteosarcoma patients.

More recently, to better approach the human disease, **patient-derived xenograft, (PDX) models** were developed by direct transplantation of a tumor fragment issued from human patient disease(or circulating tumor cells, CTCs) into immune-compromised mice¹³⁴ (Fig.1.16). There are still few PDXs models, mainly by lack of available cancer material. However, international effort through several programs are now trying to increase the availability of these PDX models, either for adult cancers (EuroPDX consortium, the Public Repository of Xenografts, and the National Cancer Institute Patient Derived Models Repository)¹⁴³ or more recently for pediatric cancer (MAST protocol, NCT01050296¹⁴³; MAPPYACTS protocol, NCT02613962¹⁴⁴; and IPI-4).

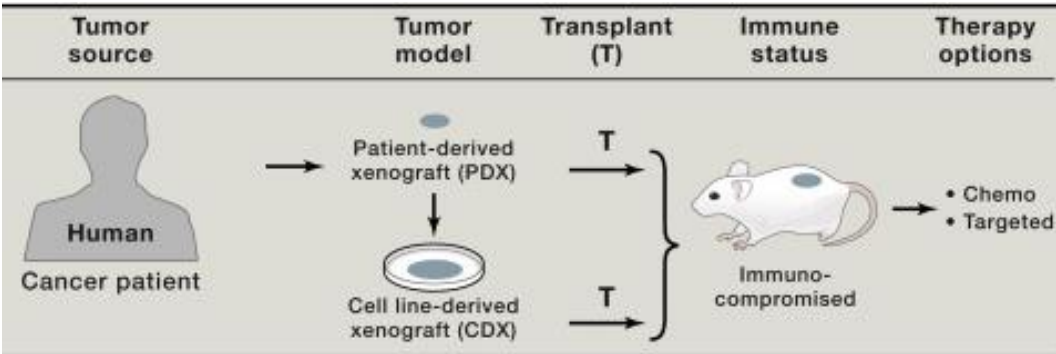


Figure 1.16: Preclinical Cancer Models (CDX and PDX) derived from human patients, using immunocompromised mice. Adapted from¹³⁴

PDXs allow the tumor cells to grow in their own stroma, which is essential for the tumor behavior¹¹⁰ and the preservation of tumor heterogeneity, and in some cases, the tumor histomorphology and global gene expression profile^{18,109}. These PDX models might further help to identify and validate predictive biomarkers of sensitivity to different molecularly targeted therapeutics¹⁴³. Beside these advantages, engraftment into a mouse or matrix material exerts a selection pressure that may change the clonal composition, and infiltration by mouse cells may also influence human tumor cell properties^{110,109}.

Few osteosarcoma PDX models have been published yet. Between 2010 and 2015, the Molecular Analysis of Solid Tumors (MAST) protocol (NCT01050296), collected 192 fresh tumors samples of 15 different types of tumors from 168 patients to establish PDX models¹⁴³. Comparing the PDXs tumors with the originating tumor from the patient, PDXs models retained the molecular and cellular features, the epigenetic landscape of their developmental origins and clonal preservation¹⁴³. This cohort included 31 osteosarcoma patient samples (from diagnosis n=17 and relapse n=14) that were inserted into the intercondylar femur of NSG female mice, after both mechanic and enzymatic dissociation. The engraftment rate was 48% (n=15/31), from either diagnostic primary tumor samples (n=8) or recurrence (n=7, including 2 local relapses). The metastatic potential of these models were not described and no drug testing was performed.

All these *in vivo* CDX or PDX orthotopic models, allow better understanding the bone microenvironment influence, metastatic potential, and tumor heterogeneity (in PDX models). However, in these immune-deficient animals the immune contexture is not preserved. New models are being developed such as **humanized PDX models** to mimic the human immune system¹⁴⁵. Up to now no osteosarcoma humanized PDX models have been published.

1.4. Aim of the study and conceptual framework

The natural evolution of osteosarcoma without chemotherapy is to metastasize, even when the primary tumor has been removed. Metastatic progression/relapse is the main cause of failure to current anti-osteosarcoma strategy with chemotherapy plus surgery, whatever the chemotherapy used ^{26,146}. The main factors which prognoses this metastasis risk are the absence of primary tumor removal (inoperable tumor), a disease that has already spread at primary bone tumor distance (metastasis at diagnosis) and an observed resistance to chemotherapy (poor histological response at the end of neoadjuvant chemotherapy)^{34,106}. “Chemoresistant” osteosarcoma cells, by not being killed by chemotherapy, will then have free space to express their metastatic program. Understanding osteosarcoma metastatic potential and timing, osteosarcoma chemoresistance (intrinsic or acquired) and the interconnection of these two phenomena is then crucial to improve osteosarcoma outcome.

Getting more appropriate and numerous pre-clinical models *in vitro* and *in vivo* will help to access the complexity and heterogeneity of the disease, with the objective to find new drugs that can target the metastatic phenotype and chemoresistant osteosarcoma cells. Thus, the general objective of my thesis was to develop and characterize *in vitro* and *in vivo* models that mimic the patients disease (eg. metastases), including resistant models, in order to:

- Understand osteosarcoma resistant and metastatic phenotype
- Test new therapies to overcome these problems and improve survival

Specific objectives:

- **Chapter 1-** Evaluation of different parameters in order to improve our *in vivo* models development
- **Chapter 2 –** Development of bioluminescent resistant models *in vitro* and *in vivo* and understand the resistant mechanism involved
- **Chapter 3 –** Development of models derived from patients samples at relapse in different sites, including orthotopic site and molecular characterization

After **chapter 1** which introduced the problematic and in order to perform this work, different approaches were carried out.

Firstly, we developed and characterized *in vivo* orthotopic bioluminescent CDX models derived from the Saos-2-B parental cell line by two different methods (paratibial and intratibial injections), into different mice strains (NSG and Swiss *nude* mice) in order to evaluate which are the best techniques to develop orthotopic osteosarcoma models. We used a second parental cell line (HOS) with different genetic background, and we analyzed the different behavior of both lines (**Chapter 2**).

We then established and characterized *in vitro* chemoresistant models and their *in vitro* and *in vivo* behavior. Several cell lines were selected to be rendered resistant *in vitro* to MTX and doxorubicin, and from these, two were selected to develop orthotopic bioluminescent CDX models (derived from the parental and resistant lines - Saos-2-B and HOS) and further analysis of their *in vivo* primary tumor and metastatic behavior (**Chapter 3**).

We finally established *in vivo* models directly derived from patients biopsy/surgery at the relapse time and characterized three patient derived xenografts (PDX) models in both subcutaneous and paratibial setting. A molecular (WES and RNAseq) comparison between the established PDX sample and the patient sample at relapse but also at diagnosis is also planned (**Chapter 4**).

Finally, the conclusion and final remarks/perspectives are presented in **chapter 5**.

References

1. Clarke B. Normal bone anatomy and physiology. *Clin J Am Soc Nephrol*. 2008;3 Suppl 3(Supplement 3):S131-9.
2. Florencio-Silva R, Sasso GR da S, Sasso-Cerri E, et al. Biology of Bone Tissue: Structure, Function, and Factors That Influence Bone Cells. *Biomed Res Int*. 2015;2015:421746.
3. Fogelman I, Van Der Wall H, Gnanasegaran G. *Radionuclide and Hybrid Bone Imaging*. (Fogelman I, Gnanasegaran G, Van Der Wall H, eds.). Springer, 2012.
4. Kansara M, Teng MW, Smyth MJ, Thomas DM. Translational biology of osteosarcoma. *Nat Rev Cancer*. 2014;14.
5. Taichman RS, Liu ZY, Groopman JE. Blood and bone: two tissues whose fates are intertwined to create the hematopoietic stem-cell niche. *Blood*. 2005;105(7):2631-2639.
6. OpenStax College A and POC <http://cnx.org/contents/14fb4ad.-39a1-4eee-ab6e-3ef2482e3e22@8>. 108. *Bone Formation and Development · Anatomy and Physiology*.
7. <http://antranik.org/wp-content/uploads/2011/09/classification-of-bones-long-flat-irregular-short.png>.
8. Aarden EM, Nijweide PJ, Burger EH. Function of osteocytes in bone. *J Cell Biochem*. 1994;55(3):287-299.
9. Väänänen H.K, Zhao H MM and HJ. The cell biology of osteoclast function. *J Cell Sci*. 2000;(113):377-381.
10. Demetri GD. *209-Sarcomas of Soft Tissue and Bone, and Other Neoplasms of Connective Tissues - Goldman's Cecil Medicine*. 24th ed. (Goldman, Lee and Schafer AI, ed.). Philadelphia: Saunders - Elsevier, 2012.

11. Marina N, Gebhardt M, Teot L, Gorlick R. Biology and therapeutic advances for pediatric osteosarcoma. *Oncologist*. 2004;9(4):422-441.
12. Geller DS, Gorlick R. Osteosarcoma: a review of diagnosis, management, and treatment strategies. *Clin Adv Hematol Oncol*. 2010;8(10):705-718.
13. Kundu ZS. Classification, imaging, biopsy and staging of osteosarcoma. *Indian J Orthop*. 2014;48(3):238-246.
14. Fletcher CDM, Bridge JA, Hogendoorn PCW MF, ed. World Health Organization, Classification of Tumours: Pathology and Genetics, Classification of Tumours: Pathology and Genetics of Tumors of Soft Tissue and Bone. Lyon: *IARC Press*; 2013.
15. Zhang Y, Mai Q, Zhang X, Xie C, Zhang Y. Microenvironment Signals and Mechanisms in the Regulation of Osteosarcoma. In: *Osteosarcoma - Biology, Behavior and Mechanisms*. InTechOpen, London, UK. 2017.
16. Durfee Maryam Mohammed Hue H Luu RA. Review of Osteosarcoma and Current Management. *Rheumatol Ther*. 2016;3.
17. Weatherby RP, Dahlin DC, Ivins JC. Postradiation sarcoma of bone: review of 78 Mayo Clinic cases. *Mayo Clin Proc*. 1981;56(5):294-306.
18. Guijarro M V, Ghivizzani SC, Parker Gibbs C, Blanco Aparicio C. Animal models in osteosarcoma. 2014.
19. Tang N, Song W-X, Luo J, Haydon RC, He T-C. Osteosarcoma development and stem cell differentiation. *Clin Orthop Relat Res*. 2008;466(9):2114-2130.
20. Rytting M, Pearson P, Raymond AK et al. Osteosarcoma in Preadolescent Patients. : Clinical Orthopaedics and Related Research. *Clinical Orthopaedics & Related Research*. 2000; 373:39-50.
21. Ando K, Oise Heymann M-F, Stresing V, et al. Current Therapeutic Strategies and Novel Approaches in Osteosarcoma. *Cancers (Basel)*. 1960;5:591-616.

22. Abarrategi A, Tornin J, Martinez-Cruzado L, et al. Osteosarcoma: Cells-of-Origin, Cancer Stem Cells, and Targeted Therapies. *Stem Cells Int.* 2016;2016:1-13.
23. Gorlick R, Khanna C. Osteosarcoma. *J Bone Miner Res.* 2010;25(4):683-691.
24. Ta HT, Dass CR, Choong PFM, Dunstan DE. Osteosarcoma treatment: state of the art. *Cancer Metastasis Rev.* 2009;28(1-2):247-263.
25. Panicek DM, Gatsonis C, Rosenthal DI et al. CT and MR imaging in the local staging of primary malignant musculoskeletal neoplasms. *Radiology.* 1997. 202:237-246.
26. Picci P. Osteosarcoma (Osteogenic sarcoma) Disease name and synonyms. *Orphanet J Rare Dis.* 2007; 2: 6.
27. He Y, Zhu W, Shin MH, et al. cFOS-SOX9 Axis Reprograms Bone Marrow-Derived Mesenchymal Stem Cells into Chondroblastic Osteosarcoma. *Stem Cell Reports.* 2017;8(6):1630-1644.
28. Uluçkan Z, Segaliny A, Botter S, Santiago JM, Mutsaers AJ. Preclinical mouse models of osteosarcoma. *Bonekey Rep.* 2015;4.
29. Anninga JK, Gelderblom H, Fiocco M, et al. Chemotherapeutic adjuvant treatment for osteosarcoma: where do we stand? *Eur J Cancer.* 2011;47(16):2431-2445.
30. Trama A, Botta L, Foschi R, et al. Survival of European adolescents and young adults diagnosed with cancer in 2000–07: population-based data from EURO CARE-5. *Lancet Oncol.* 2016;17(7):896-906.
31. Bielack SS, Smeland S, Whelan JS, et al. Methotrexate, Doxorubicin, and Cisplatin (MAP) Plus Maintenance Pegylated Interferon Alfa-2b Versus MAP Alone in Patients With Resectable High-Grade Osteosarcoma and Good Histologic Response to Preoperative MAP: First Results of the EURAMOS-1 Good Response Randomized Controlled Trial. *J Clin Oncol.*

2015;33(20):2279-2287.

32. Piperno-Neumann S, Le Deley M-C, Rédini F, et al. Zoledronate in combination with chemotherapy and surgery to treat osteosarcoma (OS2006): a randomised, multicentre, open-label, phase 3 trial. *Lancet Oncol.* 2016;17(8):1070-1080.
33. Montecucco A, Zanetta F, Biamonti G. Molecular mechanisms of etoposide. *Excli J.* 2015;14:95-108.
34. PosthumaDeBoer J, van Royen B., Helder M. Mechanisms of therapy resistance in osteosarcoma: a review. *Oncol Discov.* 2013;1(1):8. d
35. Bielack SS, Hecker-Nolting S, Blattmann C, Kager L. Advances in the management of osteosarcoma. *F1000Research.* 2016;5:2767.
36. Bielack SS, Kempf-Bielack B, Delling G, et al. Prognostic factors in high-grade osteosarcoma of the extremities or trunk: an analysis of 1,702 patients treated on neoadjuvant cooperative osteosarcoma study group protocols. *J Clin Oncol.* 2002;20(3):776-790.
37. Ozaki T, Flege S, Kevric M, et al. Osteosarcoma of the pelvis: Experience of the Cooperative Osteosarcoma Study Group. *J Clin Oncol.* 2003;21(2):334-341.
38. Marina NM, Smeland S, Bielack SS, et al. Comparison of MAPIE versus MAP in patients with a poor response to preoperative chemotherapy for newly diagnosed high-grade osteosarcoma (EURAMOS-1): an open-label, international, randomised controlled trial. *Lancet Oncol.* 2016;17:1396-1408.
39. Le Deley M-C, Guinebretière J-M, Gentet J-C, et al. SFOP OS94: A randomised trial comparing preoperative high-dose methotrexate plus doxorubicin to high-dose methotrexate plus etoposide and ifosfamide in osteosarcoma patients. *Eur J Cancer.* 2007;43(4):752-761.
40. Bielack SS, Kempf-Bielack B, Branscheid D, et al. Second and subsequent

- recurrences of osteosarcoma: presentation, treatment, and outcomes of 249 consecutive cooperative osteosarcoma study group patients. *J Clin Oncol*. 2009;27(4):557-565.
41. Meyers PA, Schwartz CL, Krailo M, et al. Osteosarcoma: a randomized, prospective trial of the addition of ifosfamide and/or muramyl tripeptide to cisplatin, doxorubicin, and high-dose methotrexate. *J Clin Oncol*. 2005;23(9):2004-2011.
 42. Meyers PA, Schwartz CL, Krailo MD, et al. Osteosarcoma: the addition of muramyl tripeptide to chemotherapy improves overall survival--a report from the Children's Oncology Group. *J Clin Oncol*. 2008;26(4):633-638.
 43. Kempf-Bielack B, Bielack SS, Jürgens H, et al. Osteosarcoma relapse after combined modality therapy: An analysis of unselected patients in the Cooperative Osteosarcoma Study Group (COSS). *J Clin Oncol*. 2005;23(3):559-568.
 44. Gelderblom H, Jinks RC, Sydes M, et al. Survival after recurrent osteosarcoma: data from 3 European Osteosarcoma Intergroup (EOI) randomized controlled trials. *Eur J Cancer*. 2011;47(6):895-902.
 45. Leary SES, Wozniak AW, Billups CA, et al. Survival of pediatric patients after relapsed osteosarcoma: The St. Jude Children's Research Hospital experience. *Cancer*. 2013;119(14):2645-2653.
 46. Bacci G, Briccoli A, Longhi A, et al. Treatment and outcome of recurrent osteosarcoma: Experience at Rizzoli in 235 patients initially treated with neoadjuvant chemotherapy. *Acta Oncol (Madr)*. 2005;44(7):748-755.
 47. Briccoli A, Rocca M, Salone M, Guzzardella GA, Balladelli A, Bacci G. High grade osteosarcoma of the extremities metastatic to the lung: Long-term results in 323 patients treated combining surgery and chemotherapy, 1985e2005. *Surg Oncol*. 2010;19:193-199.
 48. Marec-Berard P, Segura-Ferlay C, Tabone MD, et al. High dose thiotepa in

- patients with relapsed or refractory osteosarcomas: Experience of the SFCE group. *Sarcoma*. 2014.
49. Errani C, Longhi A, Rossi G, et al. Palliative therapy for osteosarcoma. *Expert Rev Anticancer Ther*. 2011;11(2):217-227.
 50. Omer N, Le Deley M-C, Piperno-Neumann S, et al. Phase-II trials in osteosarcoma recurrences: A systematic review of past experience. *Eur J Cancer*. 2017;75:98-108.
 51. Savage SA, Mirabello L, Wang Z, et al. Genome-wide Association Study Identifies Two Susceptibility Loci for Osteosarcoma. *Nat Genet*. 2013;45(7):799–803.
 52. Karlsson. Genome-wide analyses implicate 33 loci in heritable dog osteosarcoma, including regulatory variants near CDKN2A/B. *Genome Biol*. 2013;14.
 53. Molyneux SD, Di Grappa MA, Beristain AG, et al. Prkar1a is an osteosarcoma tumor suppressor that defines a molecular subclass in mice. *J Clin Invest*. 2010;120(9):3310-3325.
 54. Morrow JJ, Khanna C. Osteosarcoma Genetics and Epigenetics: Emerging Biology and Candidate Therapies. *Crit Rev Oncog*. 2015;20(3-4):173-97.
 55. Kovac M, Blattmann C, Ribi S, et al. Exome sequencing of osteosarcoma reveals mutation signatures reminiscent of BRCA deficiency. *Nat Commun*. 2015;6:8940.
 56. Smida J, Xu H, Zhang Y, et al. Genome-wide analysis of somatic copy number alterations and chromosomal breakages in osteosarcoma. *Int J Cancer*. 2017;141(4):816-828.
 57. Scoumanne A, Chen X. Protein methylation: a new mechanism of p53 tumor suppressor regulation. *Histol Histopathol*. 2008;23(9):1143-1149.

58. Jin L, Hanigan CL, Wu Y, et al. Loss of LSD1 (lysine-specific demethylase 1) suppresses growth and alters gene expression of human colon cancer cells in a p53- and DNMT1(DNA methyltransferase 1)-independent manner. *Biochem J.* 2013;449(2):459-468.
59. Huang J, Sengupta R, Espejo AB, et al. p53 is regulated by the lysine demethylase LSD1. *Nature.* 2007;449(7158):105-108.
60. Cho H-S, Suzuki T, Dohmae N, et al. Demethylation of RB regulator MYPT1 by histone demethylase LSD1 promotes cell cycle progression in cancer cells. *Cancer Res.* 2011;71(3):655-660.
61. Chen X, Bahrami A, Pappo A, et al. Recurrent Somatic Structural Variations Contribute to Tumorigenesis in Pediatric Osteosarcoma. *Cell Rep.* 2014;7(1):104-112.
62. Ji J, Quindipan C, Parham D, et al. Inherited germline *ATRX* mutation in two brothers with ATR-X syndrome and osteosarcoma. *Am J Med Genet Part A.* 2017;173(5):1390-1395.
63. Heymann M-F, Heymann D. Immune Environment and Osteosarcoma. In: *Osteosarcoma - Biology, Behavior and Mechanisms.* InTechOpen, London, UK. 2017.
64. Redini F, Heymann D. Bone Tumor Environment as a Potential Therapeutic Target in Ewing Sarcoma. *Front Oncol.* 2015;5:279.
65. Posthumadeboer. Mechanisms of Resistance Molecular involvement Drug Target Drug References. *Oncol Discov.* 2013.
66. Zhang H, Wu H, Zheng J, et al. Transforming Growth Factor β 1 Signal is Crucial for Dedifferentiation of Cancer Cells to Cancer Stem Cells in Osteosarcoma. *Stem Cells.* 2013;31(3):433-446.
67. Buddingh EP, Kuijjer ML, Duim RA, et al. Tumor-infiltrating macrophages are associated with metastasis suppression in high-grade osteosarcoma: a

- rationale for treatment with macrophage-activating agents. *Clin Cancer Res*. 2011; 15;17(8):2110-9.
68. Fritzsching B, Fellenberg J, Moskovszky L, et al. CD8(+)/FOXP3(+)-ratio in osteosarcoma microenvironment separates survivors from non-survivors: a multicenter validated retrospective study. *Oncoimmunology*. 2015;4(3):e990800.
 69. Dumars C, Ngyuen J-M, Gaultier A, et al. Dysregulation of macrophage polarization is associated with the metastatic process in osteosarcoma. *Oncotarget*. 2016;7(48):78343-78354.
 70. Han Q, Shi H, Liu F. CD163+ M2-type tumor-associated macrophage support the suppression of tumor-infiltrating T cells in osteosarcoma. *Int Immunopharmacol*. 2016;34:101-106.
 71. Sundara YT, Kostine M, Cleven AHG, Bovée JVMG, Schilham MW, Cleton-Jansen AM. Increased PD-L1 and T-cell infiltration in the presence of HLA class I expression in metastatic high-grade osteosarcoma: a rationale for T-cell-based immunotherapy. *Cancer Immunol Immunother*. 2017;66(1):119-128.
 72. Wang L, Zhang Q, Chen W, et al. B7-H3 is Overexpressed in Patients Suffering Osteosarcoma and Associated with Tumor Aggressiveness and Metastasis. *PLoS One*. 2013;8(8):4-11.
 73. Urakawa H, Nishida Y, Nakashima H, Shimoyama Y, Nakamura S, Ishiguro N. Prognostic value of indoleamine 2,3-dioxygenase expression in high grade osteosarcoma. *Clin Exp Metastasis*. 2009;26(8):1005-1012.
 74. Rutkowski P, Kamińska J, Kowalska M, Ruka W, Steffen J. Cytokine and Cytokine Receptor Serum Levels in Adult Bone Sarcoma Patients: Correlations With Local Tumor Extent and Prognosis. *J Surg Oncol*. 2003;84(3):151-159.
 75. Ségaliny AI, Mohamadi A, Dizier B, et al. Interleukin-34 promotes tumor

- progression and metastatic process in osteosarcoma through induction of angiogenesis and macrophage recruitment. *Int J Cancer*. 2015;137(1):73-85.
76. Gomez-Bouchet A, Illac C, Gilhodes J, et al. CD163-positive tumor-associated macrophages and CD8-positive cytotoxic lymphocytes are powerful diagnostic markers for the therapeutic stratification of osteosarcoma patients: An immunohistochemical analysis of the biopsies from the French OS2006 phase 3 trial. *Oncoimmunology*. 2017;6(9):e1331193.
 77. Kusumbe AP. Vascular niches for disseminated tumour cells in bone. *J bone Oncol*. 2016;5(3):112-116.
 78. Tamma R, Ribatti D. Bone niches, hematopoietic stem cells, and vessel formation. *Int J Mol Sci*. 2017;18(1).
 79. Nikolova G, Strilic B, Lammert E. The vascular niche and its basement membrane. *Trends Cell Biol*. 2007;17(1):19-25.
 80. Siclari VA, Qin L. Targeting the osteosarcoma cancer stem cell. *J Orthop Surg Res*. 2010;5:78.
 81. Bajpai J, Sharma M, Sreenivas V, et al. VEGF expression as a prognostic marker in osteosarcoma. *Pediatr Blood Cancer*. 2009;53(6):1035-1039.
 82. DuBois S, Demetri G. Markers of angiogenesis and clinical features in patients with sarcoma. *Cancer*. 2007;109(5):813-819.
 83. Takagi S, Takemoto A, Takami M, Oh-Hara T, Fujita N. Platelets promote osteosarcoma cell growth through activation of the platelet-derived growth factor receptor-Akt signaling axis. *Cancer Sci*. 2014;105(8):983-988.
 84. Yang M, Liu B, Jin L, Tao H, Yang Z. Estrogen receptor β exhibited anti-tumor effects on osteosarcoma cells by regulating integrin, IAP, NF- κ B/BCL-2 and PI3K/Akt signal pathway. *J Bone Oncol*. 2017;9:15-20.
 85. Odagiri H, Kadomatsu T, Endo M, et al. The secreted protein ANGPTL2

promotes metastasis of osteosarcoma cells through integrin $\alpha 5 \beta 1$, p38 MAPK, and matrix metalloproteinases. *Sci Signal*. 2014;7(309):ra7.

86. Lamora A, Talbot J, Mullard M, Brounais-Le Royer B, Redini F, Verrecchia F. TGF- β Signaling in Bone Remodeling and Osteosarcoma Progression. *J Clin Med*. 2016;5(11).
87. Gómez-Cuadrado L, Tracey N, Ma R, Qian B, Brunton VG. Mouse models of metastasis: progress and prospects. *Dis Model Mech*. 2017;10(9):1061-1074.
88. Oh KT, Baik HJ, Lee AH, Oh YT, Youn YS, Lee ES. The Reversal of Drug-Resistance in Tumors Using a Drug-Carrying Nanoparticulate System. *Int J Mol Sci*. 2009;10(9):3776-3792.
89. Guo W, Healey JH, Meyers PA, et al. Mechanisms of Methotrexate Resistance in Osteosarcoma Mechanisms of Methotrexate Resistance in Osteosarcoma 1. 1999:621-627.
90. Housman G, Byler S, Heerboth S, et al. Drug resistance in cancer: an overview. *Cancers (Basel)*. 2014;6(3):1769-1792.
91. Okada T, Tanaka K, Nakatani F, et al. Involvement of P-glycoprotein and MRP1 in resistance to cyclic tetrapeptide subfamily of histone deacetylase inhibitors in the drug-resistant osteosarcoma and Ewing's sarcoma cells. *Int J Cancer*. 2006;118(1):90-97.
92. Yang X, Yang P, Shen J, et al. Prevention of multidrug resistance (MDR) in osteosarcoma by NSC23925. *Br J Cancer*. 2014;110(12):2896-2904.
93. Györfy B, Surowiak P, Kiesslich O, et al. Gene expression profiling of 30 cancer cell lines predicts resistance towards 11 anticancer drugs at clinically achieved concentrations. *Int J Cancer*. 2006;118(7):1699-1712.
94. Pasello M, Michelacci F, Scionti I, et al. Overcoming glutathione S-transferase P1-related cisplatin resistance in osteosarcoma. *Cancer Res*. 2008;68(16):6661-6668.

95. Selga E, Oleaga C, Ramírez S, de Almagro MC, Noé V, Ciudad CJ. Networking of differentially expressed genes in human cancer cells resistant to methotrexate. *Genome Med.* 2009;1(9):83.
96. Borden KLB. When will resistance be futile? *Cancer Res.* 2014;74(24):7175-7180.
97. Sowers R, Wenzel BD, Richardson C, et al. Impairment of methotrexate transport is common in osteosarcoma tumor samples. *Sarcoma.* 2011;2011:834170.
98. Ganapathi RN, Ganapathi MK. Mechanisms regulating resistance to inhibitors of topoisomerase II. *Front Pharmacol.* 2013;4:89.
99. Harisi R, Dudas J, Nagy-Olah J, Timar F, Szendroi M, Jeney A. Cancer Biology & Therapy Extracellular matrix induces doxorubicin- resistance in human osteosarcoma cells by suppression of p53 function. *Mikl Szendroi Andras Jeney Cancer Biol Ther Biol Ther.* 2007;68(8):1251-1257.
100. Yang X-R, Xiong Y, Duan H, Gong R-R. Identification of genes associated with methotrexate resistance in methotrexate-resistant osteosarcoma cell lines. *J Orthop Surg Res.* 2015;10:136.
101. Dieudonné F-X, Marion A, Marie PJ, Modrowski D. Targeted inhibition of T-cell factor activity promotes syndecan-2 expression and sensitization to doxorubicin in osteosarcoma cells and bone tumors in mice. *J Bone Miner Res.* 2012;27(10):2118-2129.
102. Gaspar N, Di Giannatale A, Geoerger B, et al. Bone sarcomas: from biology to targeted therapies. *Sarcoma.* 2012;2012:301975.
103. Hattinger CM, Stoico G, Michelacci F, et al. Mechanisms of gene amplification and evidence of coamplification in drug-resistant human osteosarcoma cell lines. *Genes, Chromosom Cancer.* 2009;48(4):289-309.
104. Kaufman Y, Drori S, Cole PD, et al. Reduced folate carrier mutations are not

- the mechanism underlying methotrexate resistance in childhood acute lymphoblastic leukemia. *Cancer*. 2004;100(4):773-782.
105. Duan Z, Gao Y, Shen J, et al. miR-15b modulates multidrug resistance in human osteosarcoma in vitro and in vivo. *Mol Oncol*. 2017;11(2):151-166.
 106. Yang J, Guo W, Wang L, et al. Cisplatin-resistant osteosarcoma cells possess cancer stem cell properties in a mouse model. *Oncol Lett*. 2016;12(4):2599-2605.
 107. Gorlick R, Anderson P, Andrulis I, et al. Biology of childhood osteogenic sarcoma and potential targets for therapeutic development: meeting summary. *Clin Cancer Res*. 2003;9(15):5442-5453.
 108. Baldini N, Scotlandi K, Barbanti-Bròdano G, et al. Expression of P-Glycoprotein in High-Grade Osteosarcomas in Relation to Clinical Outcome. *N Engl J Med*. 1995;333(21):1380-1385.
 109. Katt ME, Placone AL, Wong AD, Xu ZS, Searson PC. In Vitro Tumor Models: Advantages, Disadvantages, Variables, and Selecting the Right Platform. *Front Bioeng Biotechnol*. 2016;4:12.
 110. Mohseny AB, Hogendoorn PCW, Cleton-Jansen A-M. Osteosarcoma Models: From Cell Lines to Zebrafish. *Sarcoma*. 2012;2012:1-11.
 111. Ek ETH, Dass CR, Choong PFM. Commonly used mouse models of osteosarcoma. *Crit Rev Oncol*. 2006;60:1-8.
 112. de Jong M, Maina T. Of mice and humans: are they the same?--Implications in cancer translational research. *J Nucl Med*. 2010;51(4):501-504.
 113. Zhang N, Li D, Shao J, Wang X. Animal models for bladder cancer: The model establishment and evaluation (Review). *Oncol Lett*. 2015;9(4):1515-1519.
 114. Guijarro M V, Ghivizzani SC, Parker Gibbs C, Blanco Aparicio C. Animal models in osteosarcoma. *Front Oncol*. 2014; 4: 189.

115. Biteau K, Guiho R, Chatelais M, et al. L-MTP-PE and zoledronic acid combination in osteosarcoma: preclinical evidence of positive therapeutic combination for clinical transfer. *Am J Cancer Res*. 2016;6(3):677-689.
116. Sharma S V., Haber DA, Settleman J. Cell line-based platforms to evaluate the therapeutic efficacy of candidate anticancer agents. *Nat Rev Cancer*. 2010;10(4):241-253.
117. Mohseny AB, Machado I, Cai Y, et al. Functional characterization of osteosarcoma cell lines provides representative models to study the human disease. *Lab Invest*. 2011;91(8):1195-1205.
118. Pautke C, Schieker M, Tischer T, et al. Characterization of osteosarcoma cell lines MG-63, Saos-2 and U-2 OS in comparison to human osteoblasts. *Anticancer Res*. 24(6):3743-3748.
119. Muff R, Rath P, Mohan R, et al. Genomic Instability of Osteosarcoma Cell Lines in Culture: Impact on the Prediction of Metastasis Relevant Genes. *PLoS One*. 2015;19;10(5):e0125611
120. Lauvrak SU, Munthe E, Kresse SH, et al. Functional characterisation of osteosarcoma cell lines and identification of mRNAs and miRNAs associated with aggressive cancer phenotypes. *Br J Cancer*. 2013;109(8):2228-2236.
121. Ottaviano L, Schaefer K-L, Gajewski M, et al. Molecular characterization of commonly used cell lines for bone tumor research: A trans-European EuroBoNet effort. *Genes, Chromosom Cancer*. 2010;49(1):40-51.
122. Kresse SH, Rydbeck H, Skårn M, et al. Integrative Analysis Reveals Relationships of Genetic and Epigenetic Alterations in Osteosarcoma. *PLoS One*. 2012;7(11).
123. Vella S, Tavanti E, Hattinger CM, et al. Targeting CDKs with Roscovitine Increases Sensitivity to DNA Damaging Drugs of Human Osteosarcoma Cells. Heymann D, ed. *PLoS One*. 2016;11(11):e0166233.

124. Huang J, Ni J, Liu K, et al. HMGB1 Promotes Drug Resistance in Osteosarcoma. *Cancer Res.* 2012. 1;72(1):230-8
125. Graat HCA, Witlox MA, Schagen FHE, et al. Different susceptibility of osteosarcoma cell lines and primary cells to treatment with oncolytic adenovirus and doxorubicin or cisplatin. *Br J Cancer.* 2006;94(12):1837-1844.
126. Ren L, Mendoza A, Zhu J, et al. Characterization of the metastatic phenotype of a panel of established osteosarcoma cells. *Oncotarget.* 2015;6(30):29469-29481.
127. Lovejoy CA, Li W, Reisenweber S, et al. Loss of ATRX, Genome Instability, and an Altered DNA Damage Response Are Hallmarks of the Alternative Lengthening of Telomeres Pathway. Scott HS, ed. *PLoS Genet.* 2012;8(7):e1002772.
128. <http://cancer.sanger.ac.uk/cosmic>.
129. Serra M, Reverter-Branchat G, Maurici D, et al. Analysis of dihydrofolate reductase and reduced folate carrier gene status in relation to methotrexate resistance in osteosarcoma cells. *Ann Oncol.* 2004;15(1):151-160.
130. Lorenz S, Barøy T, Sun J, et al. Unscrambling the genomic chaos of osteosarcoma reveals extensive transcript fusion, recurrent rearrangements and frequent novel TP53 aberrations. *Oncotarget.* 2016;7(5):5273-5288.
131. Belizário JE. Immunodeficient Mouse Models: An Overview. *Open Immunol J.* 2009;2:79-85.
132. <https://www.jax.org/jax-mice-and-services/find-and-order-jax-mice/most-popular-jax-mice-strains/immunodeficient-mouse-and-xenograft-host-comparisons>.
133. Puchalapalli M, Zeng X, Mu L, et al. NSG Mice Provide a Better Spontaneous Model of Breast Cancer Metastasis than Athymic (Nude) Mice. Cukierman E, ed. *PLoS One.* 2016;11(9):e0163521.

134. Day C-P, Merlino G, Van Dyke T. Preclinical mouse cancer models: a maze of opportunities and challenges. *Cell*. 2015;163(1):39-53.
135. Worth LL, Jia SF, Zhou Z, et al. Intranasal therapy with an adenoviral vector containing the murine interleukin-12 gene eradicates osteosarcoma lung metastases. *Clin Cancer Res*. 2000;6(9):3713-3718.
136. Su Y, Luo X, He B-C, et al. Establishment and characterization of a new highly metastatic human osteosarcoma cell line. *Clin Exp Metastasis*. 2009;26(7):599-610.
137. Kimura K, Nakano T, Park Y-B, et al. Establishment of human osteosarcoma cell lines with high metastatic potential to lungs and their utilities for therapeutic studies on metastatic osteosarcoma. *Clin Exp Metastasis*. 2002;19(6):477-485.
138. Garimella R, Eskew J, Bhamidi P, et al. Biological characterization of preclinical Bioluminescent Osteosarcoma Orthotopic Mouse (BOOM) model: A multi-modality approach. *J Bone Oncol*. 2013;2(1):11-21.
139. Vormoor B, Knizia HK, Batey MA, et al. Development of a Preclinical Orthotopic Xenograft Model of Ewing Sarcoma and Other Human Malignant Bone Disease Using Advanced In Vivo Imaging. Nurminskaya M, ed. *PLoS One*. 2014;9(1):e85128.
140. Creen V, Biteau K, Amiaud J, et al. Bone microenvironment has an influence on the histological response of osteosarcoma to chemotherapy: retrospective analysis and preclinical modeling. *Am J Cancer Res*. 2017;1;7(11):2333-2349
141. [Http://www.ivis.ku.dk/about/](http://www.ivis.ku.dk/about/).
142. Uluçkan Ö, Bakiri L, Wagner EF. Characterization of Mouse Model-Derived Osteosarcoma (OS) Cells In Vitro and In Vivo. In: *Humana Press*, New York, NY; 2015:297-305.
143. Stewart E, Federico SM, Chen X, et al. Orthotopic patient-derived xenografts

- of paediatric solid tumours. *Nat Publ Gr*. 2017;549.
144. <https://clinicaltrials.gov/ct2/show/NCT02613962>.
145. Walsh NC, Kenney LL, Jangalwe S, et al. Humanized Mouse Models of Clinical Disease. *Annu Rev Pathol*. 2017;12:187-215.
146. Ritter J, Bielack SS. Osteosarcoma. *Ann Oncol*. 2010;21(Supplement 7):vii320-vii325.

Chapter 2:

Establishment and characterization of *in vivo* orthotopic bioluminescent xenograft models from human osteosarcoma cell lines in Swiss nude and NSG mice.

Establishment and characterization of *in vivo* orthotopic bioluminescent xenograft models from human osteosarcoma cell lines in Swiss nude and NSG mice

Maria Eugenia Marques da Costa^{1,2}, Estelle Daudigeos-Dubus, PhD¹, Anne Gomez-Brouchet MD, PhD³, Olivia Bawa⁴, Valerie Rouffiac, PhD⁵, Massimo Serra PhD⁶, Katia Scotlandi, PhD⁶, Conceição Santos PR⁷, Birgit Geoerger, MD, PhD^{1,8}, Nathalie Gaspar, MD, PhD^{1,8}

¹ Vectorology and Anticancer Therapies, CNRS UMR 8203, Paris-Sud University, Gustave Roussy, Paris-Saclay University, 94 805 Villejuif, France

² CESAM & Department of Biology, University of Aveiro, 3810 Aveiro, Portugal

³ Department of Pathology, IUCT-Oncopole, CHU of Toulouse and University of Toulouse; Pharmacology and structural biology institut, CNRS UMR5089, 31059 Toulouse, France

⁴ Plateforme HistoCytoPathologie, UMS AMMICA, Gustave Roussy, 94805 Villejuif, France

⁵ Imaging and Cytometry Platform, UMS 3655 & US23, Gustave Roussy, Paris-Saclay University, 94805, Villejuif, France

⁶ Laboratory of Experimental Oncology, Orthopaedic Rizzoli Institute, 40136 Bologna, Italy

⁷ Department of Biology, Faculty of Sciences, University of Porto, Rua do Campo Alegre, 4000 Porto, Portugal

⁸ Department of Oncology for Children and Adolescents, Gustave Roussy, 94805 Villejuif, France

Abstract

Osteosarcoma is one of the most common primary bone tumors in childhood and adolescence. Metastases occurrence at diagnosis or during disease evolution is the main therapeutic challenge. New drug evaluation to improve patient survival requires the development of various preclinical models mimicking at best the complexity of the disease and its metastatic potential. We describe here the development and characteristics of two orthotopic bioluminescent (Luc/mKate2) cell-derived xenograft (CDX) models, Saos-2-B-Luc/mKate2-CDX and HOS-Luc/mKate2-CDX, in different immune (nude and NSG mouse strains) and bone (intratibial and paratibial with periosteum activation) contexts. IVIS SpectrumCT system allowed both longitudinal computed tomography (CT) and bioluminescence real-time follow-up of primary tumor growth and metastatic spread, which was confirmed by histology. The murine immune context influenced tumor engraftment, primary tumor growth, and metastatic spread to lungs, bone, and spleen (an unusual localization in humans). Engraftment in NSG mice was found superior to that found in nude mice and intratibial bone environment more favourable to engraftment compared to paratibial injection. The genetic background of the two CDX models also led to distinct primary tumor behaviour observed on CT scan. Saos-2-B-Luc/mKate2-CDX showed osteocondensed, HOS-Luc/mKate2-CDX osteolytic morphology. Bioluminescence defined a faster growth of the primary tumor and metastases in Saos-2-B-Luc/mKate2-CDX than in HOS-Luc/mKate2-CDX. The early detection of primary tumor growth and metastatic spread by bioluminescence allows an improved exploration of osteosarcoma disease at tumor progression, and metastatic spread, as well as the evaluations of anticancer treatments. Our orthotopic models with metastatic spread bring complementary information to other types of existing osteosarcoma models.

Key words: human osteosarcoma, *In vivo* orthotopic, cell-derived xenograft, bioluminescenc

Introduction

Osteosarcoma is a rare although the most frequent primary malignant bone tumor with a peak incidence in adolescence and young adulthood¹. The survival of patients with osteosarcoma has not improved in the last 30 years since the introduction of chemotherapy in the 70s-80s¹⁻³. The development of metastasis, mainly lung metastases, remains the main cause of treatment failure⁴. The main prognostic factors of relapse are the metastatic status at diagnosis and the histological response to neoadjuvant chemotherapy (surrogate marker of osteosarcoma chemosensitivity)^{5,6}. Several aspects might have participated in this disappointing situation, the insufficient understanding of osteosarcoma oncogenesis, the non-optimal phase-II clinical trial designs⁷ and the unsatisfactory low number of preclinical osteosarcoma models.

Due to the complex osteosarcoma genetic background and the importance of bone and immune microenvironment in this tumor type⁸⁻¹⁰, multiple osteosarcoma models representative of the human disease in different *in vitro* and *in vivo* contexts are needed to get more insight into different processes involving osteosarcoma initiation, progression especially metastatic and treatment sensitivity. The EuroBoNeT (European Network of Excellence on bone tumors) consortium has characterized 19 osteosarcoma cell lines^{9,11,12} and described their tumorigenic capacities under simplified conditions (subcutaneous and intra-muscular/paratibial xenograft conditions) to identify technically practical models⁹. Although covering a large panel of osteosarcoma genetic abnormalities, these mice models might not be fully clinically relevant because osteosarcoma cells are not spontaneously arisen and do not grow in the proper site. It can be hypothesized that *in vivo* models in an orthotopic setting might reveal different tumor behavior: primary tumor growth, metastatic potential and response to treatment¹³⁻¹⁵, by better mimicking the initial bone site of the disease in patients. The major difficulty in using these preclinical orthotopic bone models is the measurement of the disease burden in a non-accessible site, which requires the use of non-invasive techniques such as radiography¹⁶, computed tomography (CT), magnetic resonance imaging (MRI) or bioluminescence^{13,14}.

In this work we used cell lines transduced with luciferase (bioluminescence) and CT imaging to facilitate *in vivo* follow-up of primary tumor growth, changes in bone microarchitecture and metastatic development. Therefore, we developed and characterized distinct orthotopic Cell-Derived Xenograft (CDX) human osteosarcoma models in mice with different immune backgrounds with metastatic potential.

Methods

Cell culture

A panel of 7 human osteosarcoma cell lines (HOS, 143B, U2OS, MG-63, Saos-2, Saos-2-B and IOR/OS18) mycoplasma free were used. The 143B cell line was purchased from the American Type Culture Collection. All other osteosarcoma cell lines were kindly provided within the scope of the European Consortium Innovative Therapies for Children with Cancer (ITCC). Testing Saos-2 issued from two different culture flasks, we observed two slightly different CGH profile. We continued the experiments with both, and named the second one Saos-2-B.

The cell lines were cultured, using early passages in Dulbecco's modified Eagle medium (DMEM, GIBCO/Invitrogen, Saint Aubin, France) supplemented with 10% (v/v) fetal bovine serum (FBS, GIBCO/Invitrogen, Saint Aubin, France) at 37°C in a humidified atmosphere (5% CO₂ and 95% air). Mycoplasma test was performed each month by PCR.

Transfection and cell transduction with Luc/mKate2 (transgene) *in vitro*

Procedures were performed in sterile and safe conditions. The procedures using genetically modified organisms (GMO) were approved by the Ministry of Higher Education and Research and performed under the conditions established according to Decree n°2011-1177. Lentiviral particles were produced by transfecting HEK 293T cells 24 hours after plating, with transfection solution containing jetPRIME Transfection Reagent kit (Polyplus-transfection, Illkirch, France), envelope plasmids - 29.4 µg of VSVG (pMD2G) and 54.6 µg of GAGPOL (psPax2) and 48 µg of plasmid Plvx-CAG-luc-2A-mKate2 that contains the gene of interest. Plasmids were provided by David Castel from UMR8203 Research Unit, at Gustave Roussy¹⁷.

The supernatant containing the virus was collected 48h later and centrifuged for 5 min at 5000 rpm and 4°C, the pellet was discarded and the supernatant was centrifuged at 22,000 rpm and 4°C for 70 minutes. The pellet was resuspended in PBS, incubated under agitation for 1h at 4°C, centrifuged 1 min at 5000 rpm and 4°C and aliquoted at -80°C.

For virus titration, serial dilutions of supernatants had been tested on HCT116 cells, which were then analyzed for mKate2 detection by cytometry (BD Biosciences, Le-Pont-De-Claix, France), 4/5 days post-infection.

All 7 cell lines were plated at 1×10^5 cells per well in a 6-well plate and infected with viral supernatant with a high multiplicity of infection (MOI). After cells reached confluency a selection of the cells marked with Luc/mKate2 was performed by flow cytometry using FACSDiva version 6.1.3. software (BD Biosciences, Le-Pont-De-Claix, France). The cells expressing the transgene were amplified for further use. Expression and activity were measured by bioluminescence using IVIS SpectrumCT system (Perkin Elmer, Courtaboeuf, France).

***In vivo* bioluminescent CDX orthotopic models**

Animal experiments were approved by the CEEA26, CEEA PdL N°6 Ethics Committee and the Ministry of Agriculture (approval number: APAFIS#1648-2015090713516480) and performed under the conditions established by the European Community (Directive 2010/63/UE).

We have established osteosarcoma orthotopic models derived from two human cell lines, using two different 7 week-old immunodeficient mouse strains and two different types of bone injection conditions.

Osteosarcoma cell lines used for CDX. Two cell lines were used for *in vivo* CDX establishment based on its different genetic background, tumorigenic and metastatic capacity depending on mouse strains and injection type, Saos-2-B-Luc/mKate2 and HOS-Luc/mKate2. The non-bioluminescent human Saos-2-B osteosarcoma cell line was established from a primary osteosarcoma of an 11-year old Caucasian female patient. In Saos-2-B cell line, *TP53* (del²>EX4-EX8) gene is deleted, *Rb1* mutated and *CDKN2A* normal^{9,11,18}. Non-bioluminescent human HOS osteosarcoma cell line was established from a primary tumor of a 13- year-old

female patient. HOS (*TP53* mutation p.Arg156Pro and *CDKN2A* homozygous deletion)¹¹.

Immunodeficient mouse strains. Swiss Nude and NSG mouse strains were purchased at Gustave Roussy (Villejuif, France) They were born and bred at the animal facilities at Gustave Roussy and maintained under controlled conditions. NSG mouse strains are deficient in B and T lymphocytes and with low NK cell activity¹⁹, minimizing the chance of xenograft rejection, while nude mouse strains have T cell depletion, but with age an increase in NK cells and $\alpha\beta$ TCR lymphocytes maturation is observed. Innate immunity of the nude mice is less compromised than in the NSG strain¹⁹.

Paratibial and Intratibial injection. 1.5×10^6 Saos-2-B-Luc/mKate2 or HOS-Luc/mKate2 cells were injected in a total volume of 10 μ l Matrigel (Corning, Wiesbaden, Germany) solution at 4 mg/ml, whatever the injection method used. Procedures were performed under a sterile atmosphere and with the mice being anesthetized using 3% isoflurane. Paratibial injection with periosteum denudation and intratibial injection were performed according Uluçkan et al, with some modifications²⁰.

Paratibial injection was performed applying a 30G needle perpendicular to the tibia after a 0.5 cm skin incision. Before cell injection, periosteum was gently activated with the needle (periosteum denudation).

For intratibial injection, a 0.5 cm skin incision was performed just below the knee joint and cells were injected into the intramedullary cavity of the tibia with a 30G syringe, then skin was sutured. To avoid bone pain, an analgesic (buprenorphine at 0.3 mg/kg) was applied in addition to general anesthesia.

Mice were clinically monitored every week, for general symptoms, weight, and tumor size. They were euthanized at the onset of general symptoms (e.g. weight loss, difficulty to walk).

In vivo bioluminescence and CT imaging

Images were acquired using IVIS SpectrumCT (Perkin Elmer, Courtaboeuf, France). This multimodality imaging system allows the detection of tumors and metastases in X-ray tomography co-registered with optical images of tagged tumor cells without

image adjustment for anatomical correspondence. As light is only emitted by tumor cells without any background signal, bioluminescence is a highly specific and sensitive methodology for tumor detection and follow up over time¹³. For optical detection, mice were injected intraperitoneally with 150 mg/kg of D-luciferin (Beetle luciferin, Promega, Charbonnières, France) and then anesthetized with 3% isoflurane. For primary tumor detection, the lower section of the body (area of the lower legs) was imaged. For metastatic spread, especially lung metastases, primary tumor was covered to exclude its signal and chest was imaged. For primary tumors as for metastases, acquisition parameters were automatically computed by the SpectrumCT software in order to optimize bioluminescence signals (photons per second (p/s)) detection.

***Ex vivo* organs imaging**

After sacrifice, anatomical parts (legs, lungs, and spleen) were collected and immersed in 150 µg/mL of D-luciferin, then imaged individually for luciferase detection using IVIS SpectrumCT system.

Histology

Organs were fixed in 4% paraformaldehyde, and embedded in paraffin. Tissues were stained with hematoxylin-eosin-safranin (HES) for morphology. Paraffin sections were processed following heat-induced antigen retrieval using a mouse anti-firefly luciferase monoclonal antibody (1:200, ThermoFisher Scientific, Waltham, MA, USA). The cytoplasmic signal was revealed with klear mouse kit (GBI labs). Slides were examined using light microscopy (Zeiss, Marly-Le-Roy, France). IGR-N91-Luc neuroblastoma cells²¹ were used as positive control. Single representative whole tumor tissue section from each animal was digitized using a slide scanner NanoZoomer 2.0-HT (C9600-13, Hamamatsu Photonics). Histology was reviewed by an expert pathologist of human bone.

Statistical analysis

In vitro and *in vivo* bioluminescence intensity is shown as the mean \pm standard error of mean (SEM) using Graphpad Prism® Software version 5.00 (Graphpad Software Inc, La Jolla, CA, USA).

Results

Osteosarcoma cell transduction

All 7 osteosarcoma cell lines were successfully transduced with a rate above 90% of Luc/mKate2 positive cells (Fig.2.1; supplementary Fig.2.S1), including HOS and MG-63 cell lines after selection by flow cytometry. Data are shown for Saos-2-B-Luc/mKate2 and HOS-Luc/mKate2 which were also used for the *in vivo* model establishment (Fig.2.1). Cell transduction with Plvx-CAG-luc-2A-mKate2 plasmid using the viral vector resulted in 98% and 68% of luciferase/mKate2 positive cells for Saos-2-B and HOS, respectively. HOS cells were subjected to an additional selection using mKate2 positivity by flow cytometry which resulted in a 99% rate of HOS positive cells (Fig.2.1A). Using IVIS system, we were able to detect bioluminescence $>10^5$ photons/sec in both Luc/mKate2 transduced cells at a concentration of 1000 cells. Bioluminescence intensity increased with the number of cells in both bioluminescent cell lines in the presence of luciferin substrate (Fig.2.1B). No genetic alterations were observed by aCGH between the cell lines without and with the luciferase gene (data not shown).

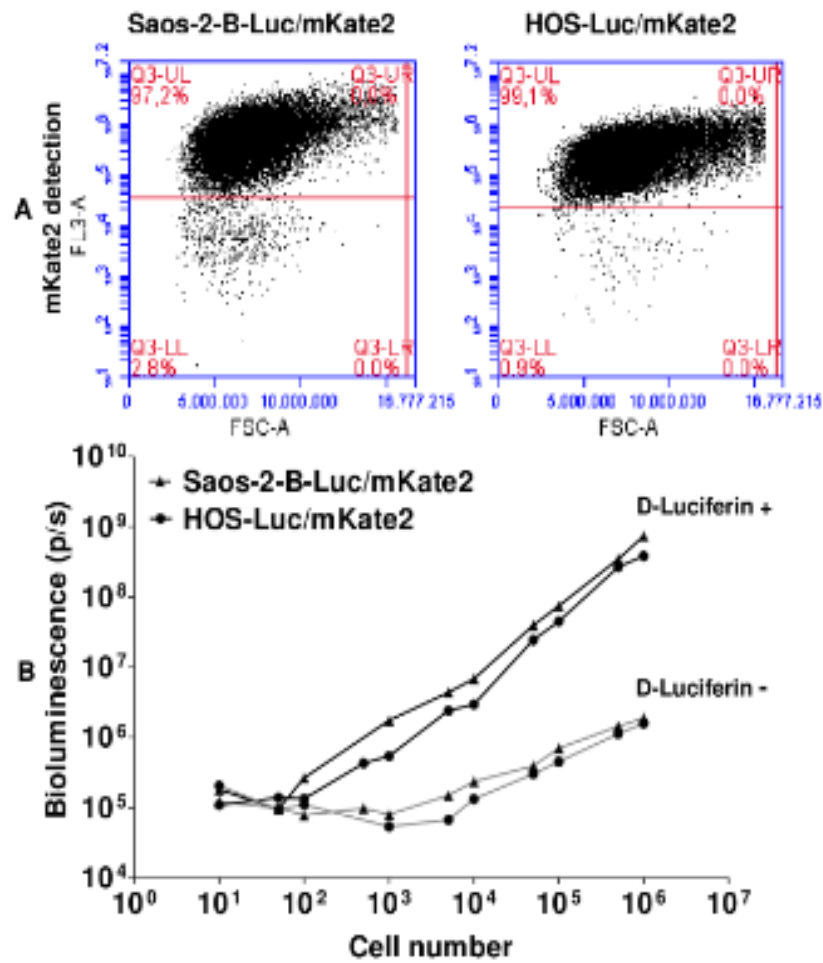


Figure 2.1: Characterization of luciferase-transduced osteosarcoma cells. A- mKate2 (FL3-A) selection by flow cytometry of transduced Saos-2-B-Luc/mKate2 and HOS-Luc/mKate2 cells showed a rate of more than 90% positive cells. B- Bioluminescence detection using IVIS SpectrumCT system showed increased bioluminescence signal paralleling the increase numbers of Plvx-CAG-luc-2A-mKate2 transfected osteosarcoma cells Saos-2-B and HOS (black ▲ and ●, respectively) in the presence of luciferin, but not without luciferin (grey ▲ and ●, for Saos-2-B and HOS, respectively).

Tumorigenicity and metastatic potential of osteosarcoma cell lines in an orthotopic setting to the bone using bioluminescence *in vivo*

We first developed the Saos-2-B-Luc/mKate2 cell line model. Saos-2-B engraftment rate appeared higher (Fig.2.2A) and primary tumor (Fig.2.2B) and metastases growth (Fig.2.2C) were faster in NSG than in nude mice. Bioluminescence was detectable much earlier than clinical deformation of the leg.

Primary tumor bioluminescence was detectable *in vivo* as early as 5 days after Saos-2-B-Luc/mKate2 cell injection (the first evaluation time point) for both mouse strains and both injection conditions used (Fig.2.2B). Bioluminescence $>10^{10}$ was reached at 40-50 days and 90-163 days in NSG and nude mice, respectively. Between paratibial and intratibial injection, no difference in primary tumor growth was observed in NSG mice. In nude mice, primary Saos-2-B-Luc/mKate2 tumors showed an initial decrease in bioluminescent signals with a subsequent recovery of tumor growth. This phenomenon was more prominent for intratibial injection (Fig.2.2B), resulting in delayed tumor growth. Bioluminescence allowed to detect metastases that occurred earlier in NSG than in nude mice (26-42 and 78-104 days after intratibial and paratibial injection in NSG and Nude, respectively) (Fig.2.2C). In nude mice, metastases occurred earlier after paratibial injection than intratibial injection, as observed for the primary tumors (Fig.2.2C). In NSG mice, intratibial injection seemed slightly favorable for metastatic growth as compared to paratibial Saos-2-B-Luc/mKate2-CDX with first detection at 26 and 42 days, respectively (Fig.2.2C).

Consistent with the bioluminescent observations, clinical deformation of the leg appeared later in nude as compared to NSG mice (100 and 40 days, respectively) and later after intratibial injection as compared to paratibial one in NSG mice (60 and 40 days, respectively). Difficulties in moving led to NSG mice sacrifice between 67 and 77 days after paratibial and intratibial injections, respectively, and for nude mice between 114 and 191 days after paratibial and intratibial injections respectively.

For the HOS-Luc/mKate2 cell line, we used the best conditions observed with Saos-2-B-Luc/mKate2-CDX, i.e. intratibial injection in NSG mice. Primary tumors developed in all 5 mice injected (Fig.2.2A) but barely grew locally (Fig.2.2B).

Bioluminescence values were 10^7 - 10^8 at day 0 and 3.5×10^9 at day 160 when mice were sacrificed. However, lung metastases were detected 26 days after injection in 4 out of 5 animals (Fig.2.2C). In total, the growth rate of primary tumors and metastases of the intratibial HOS model were slower than those seen with intratibial Saos-2-B-Luc/mKate2-CDX in NSG. Metastasis bioluminescence values reached $>10^8$ at 110 and 70 days, respectively.

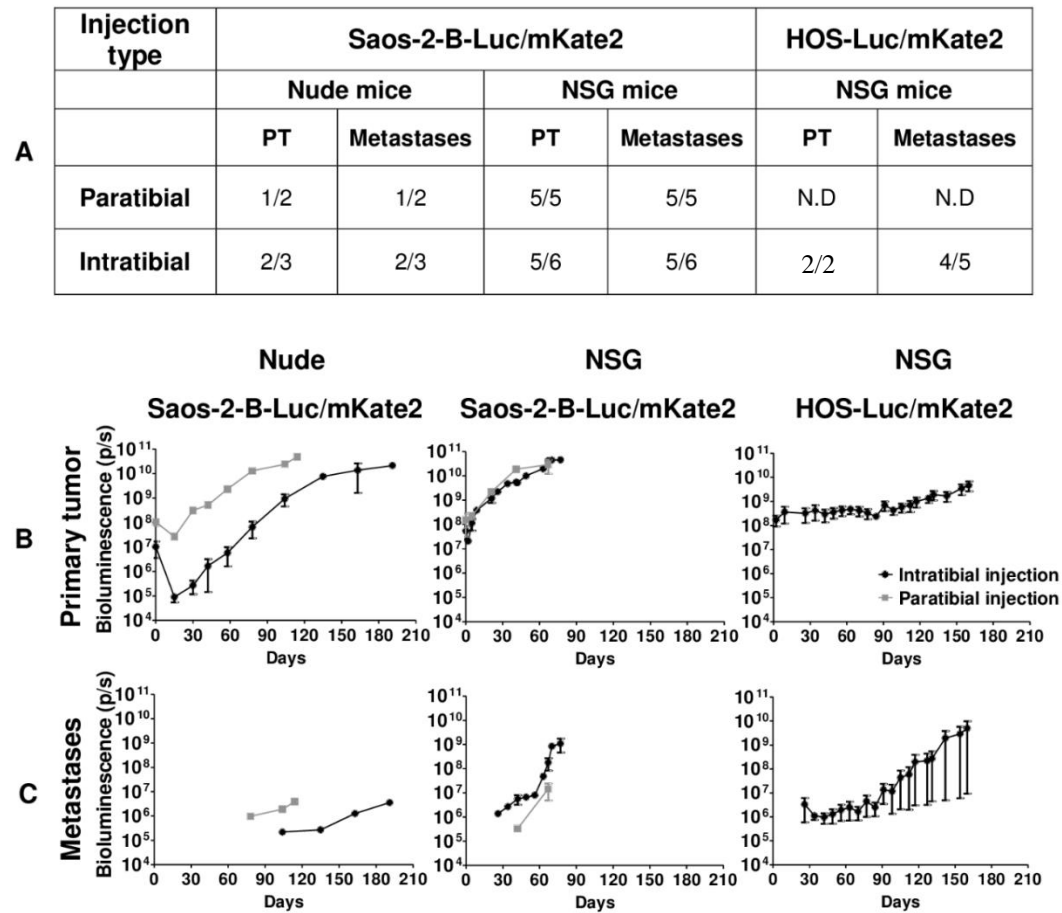


Figure 2.2: *In vivo* tumor growth and metastatic potential of Saos-2-B-Luc/mKate2-CDX and HOS-Luc/mKate2-CDX orthotopic bioluminescent models. A-Primary tumor growth engraftment and metastatic rate according to osteosarcoma cell line, mouse strain, and type of injection. B- Primary tumor *in vivo* bioluminescence detection overtime. C- Metastases *in vivo* bioluminescence detection overtime. Orthotopic osteosarcoma bioluminescent models: Saos-2-B-Luc/mKate2-CDX in Nude (left panel) and NSG mice (central panel); HOS-Luc/mKate2-CDX in NSG mice (right panel). 1.5×10^6 Luc/mKate2 transduced cells were injected in NSG mice by intratibial injection (black) for both cell lines (Saos-2-B and HOS). Saos-2-B-Luc/mKate2 was also injected by paratibial injection (grey) on the left tibia for NSG as well as in nude with intratibial and paratibial injection. NSG and Nude mice were imaged for bioluminescence with IVIS SpectrumCT system until 67 or 77 days (paratibial or intratibial) and 114 or 191 days (paratibial or intratibial), respectively in Saos-2-B-Luc/mKate2-CDX and 160 days for NSG in HOS-Luc/mKate2-CDX. ND=Not done.

Radiological and morphological characteristics of the orthotopic Saos-2-B and HOS osteosarcoma Luc/mKate2-CDX models

CT-imaging allowed real-time detection of tumor growth and modifications of the bone structures in the CDX models (Fig.2.3A), but did not detect lung or any other metastases. Saos-2-B-Luc/mKate2-CDX scans revealed tumor-bearing tibia bone structure abnormalities similar to those observed in the human disease. Aggressive bone lesions (cortical rupture, periosteal reaction), detection of aberrant new bone formation extending within the extra-osseous mass (osteocondensation, new calcified material), and some osteolysis (bone destruction) were found as shown in Fig.2.3A when mice were sacrificed at day 67 and 77 for paratibial and intratibial, respectively. Osteocondensation was also observed inside the bone of intratibial models, but less in paratibial models (Fig.2.3A). These changes were first noted 41 days after Saos-2-B-Luc/mKate2 injection in NSG mice and 78 days in nude mice, independently of injection localization (data not shown). In HOS-Luc/mKate2-CDX intratibial model, bone structure alterations had more osteolytic characteristics (Fig.2.3A, lower panel) and were detected later (> day 100) with slight osteocondensation only inside the bone detected even later. Overlying the *in vivo* bioluminescence analysis and the CTscan images allowed to confirm that CT abnormalities correspond to the injected human osteosarcoma cells transduced with luciferase in both models (Fig.2.3B).

For both Saos-2-B-Luc/mKate2-CDX and HOS-Luc/mKate2-CDX, HES staining confirmed the osteosarcoma nature of primary tumors (osteoid formation), mostly osteoblastic with some fibroblastic components in some animals (Fig.2.3C, Table I). *Ex vivo* bioluminescence analysis (data not shown) and luciferase positive staining (Fig.2.3C) in bone paraffin embedded sections confirmed that histological features correspond to the injected human osteosarcoma cells transduced with luciferase in both models.

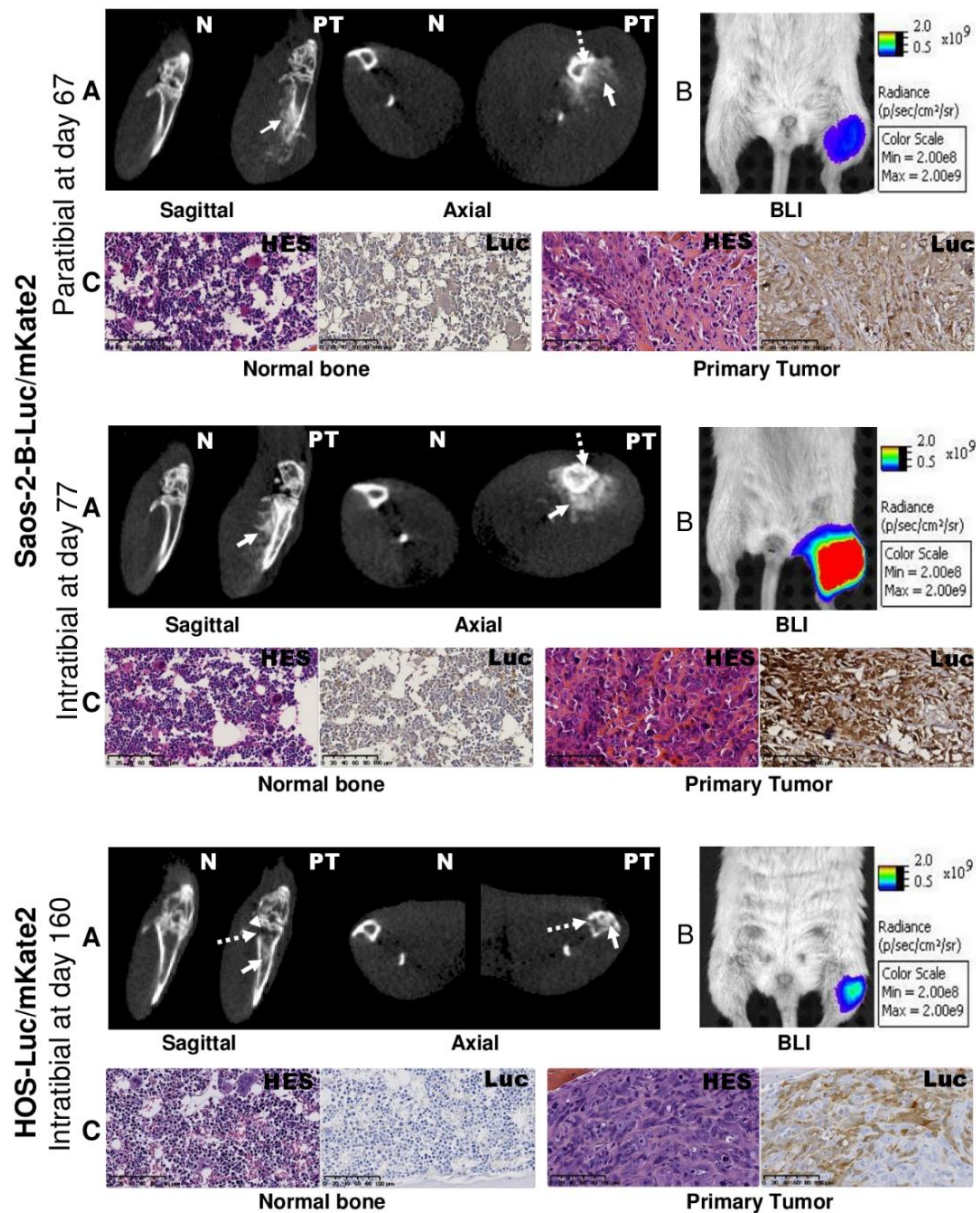


Figure 2.3: Primary bone tumor - morphological and histological characteristics of Saos-2-B-Luc/mKate2-CDX and HOS-Luc/mKate2-CDX orthotopic models in NSG mice. Orthotopic osteosarcoma bioluminescent models in NSG mice at sacrifice time: paratibial Saos-2-B-Luc/mKate2-CDX (top panel), intratibial Saos-2-B-Luc/mKate2-CDX (middle panel) and intratibial HOS-Luc/mKate2-CDX (bottom panel). A- *In vivo* CTscan imaging by IVIS SepectrumCT system of the normal leg (N) and Primary tumor (PT), by sagittal and axial view showing osteocondensation (plain arrow) and osteolysis (dotted arrow). B- *In vivo* bioluminescence imaging by IVIS SepectrumCT system of the primary tumor (left leg) compared to the control leg (right leg). C- Histology using Hematoxylin Eosin Saffron (HES) and luciferase stainings of the primary tumor and normal bone at 16x magnification.

Table 2.I: Morphological and histological characteristics of all osteosarcoma bioluminescent orthotopic CDX. BLI-Bioluminescence; CT-Computed Tomography; FB-fibroblastic subtype; HG-High-Grade osteosarcoma; N.A-Not Available; OB-Osteoblastic subtype; + -Positive detection; - -Negative detection; Met-Metastases

Cell line Luc/mKate2	Mouse Strain	Injection Type	Mouse Number	Primary tumor			Metastases					
				Histology		CT	Lung		Bone		Spleen	
				Sub-type	Necrosis	Calcification	Histology	BLI	Histology	BLI	Histology	BLI
Saos-2-B	Nude	paratibial	32773	HG OB	-	++	-	++ (78days)	-	-	-	-
Saos-2-B	Nude	intratibial	33535	HG OB	10%	++	-	++ (100days)	-	-	-	-
			33536	HG OB	-	+++	-	++ (100days)	-	+	-	-
Saos-2-B	NSG	paratibial	32752	HG OB	-	+++	-	++	-	N.A	+	+
			32753	HG OB	<1%	+++	-	++	+	N.A	+	+
			32754	HG FB+OB	-	+++	-	++	-	N.A	-	+
			32755	HG FB+OB	-	+++	-	++	-	N.A	+	+
			32756	HG OB	-	+++	-	++	-	N.A	+	+
Saos-2-B	NSG	intratibial	32769	HG OB	-	++++	-	++	-	N.A	+	+
			32770	HG FB+OB	40%	++++	+	++++ (32 met)	-	N.A	-	+
			32771	HG OB	-	++++	+	++++ (6 met)	-	N.A	+	+
			32772	HG OB	30%	++++	+	++++ (22 met)	+	N.A	-	+
			34104	HG OB	-	++++	+	+++ (6 met)	+	+	-	+
HOS	NSG	intratibial	34662	HG FB+OB	-	+	+	++ (19 met)	-	-	+	+
			34663	HG FB+OB	-	+	+	++ (29 met)	-	+	-	-

Ex vivo bioluminescence and histology (HES and luciferase staining) also confirmed the presence of lung metastases in both models (Fig.2.4). Saos-2-B-Luc/mKate2-CDX pulmonary metastases were more frequent and more numerous (range 6-32) when injected intratibially than paratibially in NSG mice as detected by bioluminescence *in vivo* (Fig.2.4A) and *ex vivo* (Fig.2.4B-C). However, lung metastases in the paratibial model could not be confirmed by histology, despite *in vivo* and *ex vivo* bioluminescent positivity (Fig.2.4D-E-F top panel; Table I). In intratibial Saos-2-B-Luc/mKate2-CDX, lung metastases were visible even macroscopically (Fig.2.4G). For intratibial HOS-Luc/mKate2-CDX, lung metastases were also frequent and numerous (<29) but of smaller size than those in intratibial Saos-2-B-Luc/mKate2-CDX in NSG mice (Fig.2.4D-E-F; Table I). Spleen metastases were detected in all model types, except in Saos-2-B-Luc/mKate2-CDX nude mouse model (Fig.2.4H-I). Histology also revealed a unique bone metastasis on the opposite leg (not injected) in two Saos-2-B-Luc/mKate2-CDX NSG mice (one after intratibial and one after paratibial injections), and one in the homolateral femur of one HOS-Luc/mKate2-CDX model detected by *in vivo* and *ex vivo* bioluminescence which could not be detected histologically (Fig.2.4J-K).

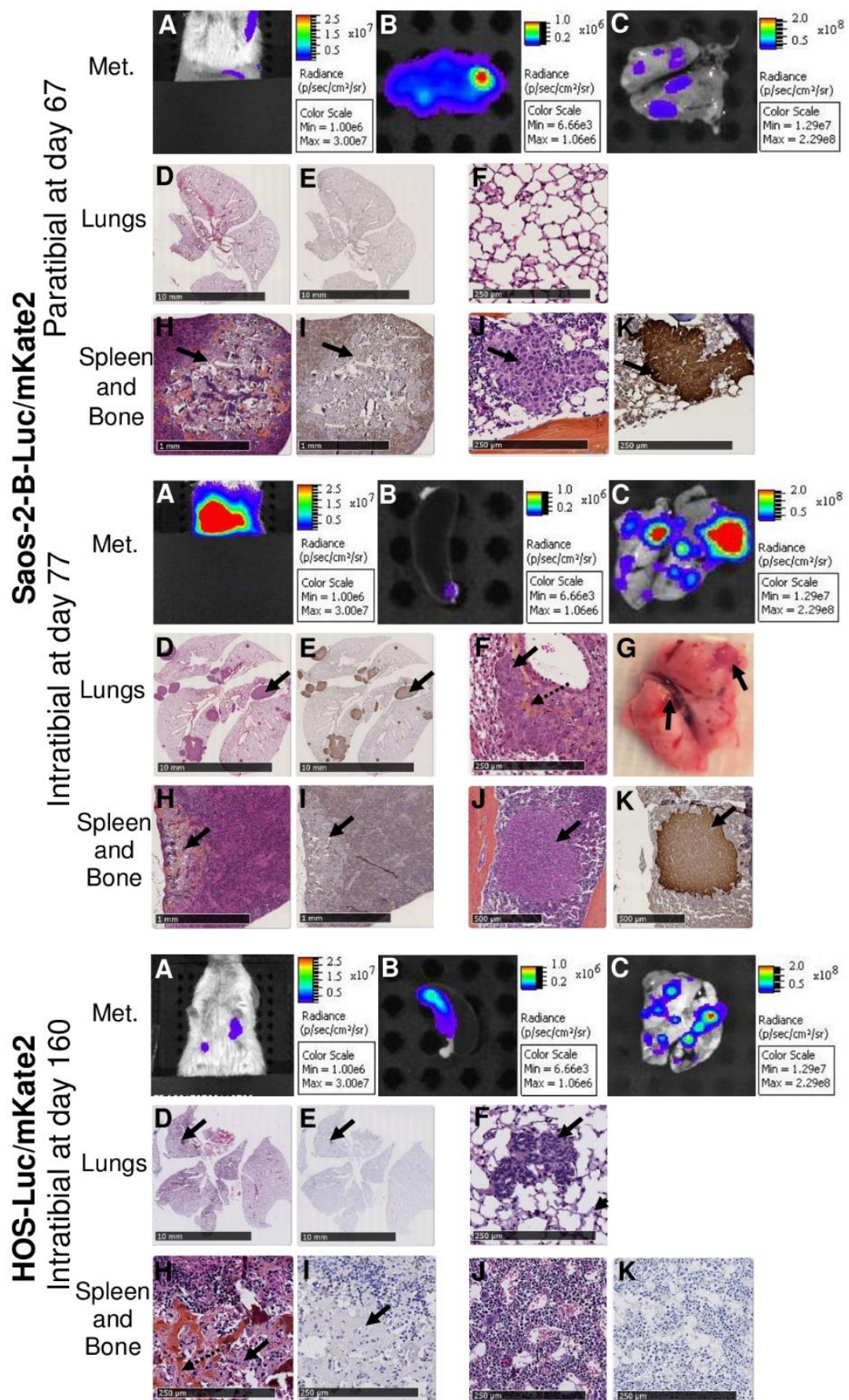


Figure 2.4 (previous page): Metastases - morphological and histological characteristics of Saos-2-B-Luc/mKate2-CDX and HOS-Luc/mKate2-CDX orthotopic models in NSG mice. Orthotopic osteosarcoma bioluminescent models in NSG mice at sacrifice time: paratibial Saos-2-B-Luc/mKate2-CDX (top panel), intratibial Saos-2-B-Luc/mKate2-CDX (middle panel) and intratibial HOS-Luc/mKate2-CDX (bottom panel). *In vivo* bioluminescence of metastases (A). *Ex vivo* bioluminescence of spleen (B) and lungs (C). Lung Hematoxylin Eosin Saffron (HES) (D) and luciferase staining (E) at 0.24x and 0.26x magnification for paratibial and intratibial Saos-2-B-Luc/mKate2-CDX respectively and 0.22x magnification for intratibial HOS-Luc/mKate2-CDX. Lung HES staining at 10x magnification (F). Lung macroscopic view (G). Spleen HES (H) and luciferase stainings (I) at 2x magnification (paratibial and intratibial Saos-2-B-Luc/mKate2) and 10x HOS-Luc/mKate2 intratibial. Bone of not injected leg HES (J) and luciferase stainings (K) at 10x and 4x magnification for paratibial and intratibial respectively. Plain arrows showed metastases. Dotted arrows showed the intraosseous osteoid matrix. Met=metastases

Discussion

We developed two novel bioluminescent osteosarcoma orthotopic xenograft models with spontaneous metastatic spread, derived from two osteosarcoma cell lines (Saos-2-B and HOS).

We used IVIS SpectrumCT, a multimodality imaging system combining X-ray tomography (CT scan) with optical detection (bioluminescence), and showed advantages of this technique in our orthotopic bone CDX osteosarcoma models.

The bioluminescence was valuable and presents advantages to detect and follow in real-time without animal sacrifice, both showed bone primary growth and spread to metastatic sites, especially in the lung. The signal appears before clinical and radiological detection capacity, as previously described²¹. We had more difficulties in detecting other metastatic localizations (e.g. bone, spleen) when the *in vivo* bioluminescent signal was close to the background noise, then either *ex vivo* bioluminescent detection or histological confirmation at mice sacrifice were required for metastases detection²¹.

CT scans were also valuable and efficient for the analysis of important tumor-associated bone modifications induced by primary tumor growth, either bone destruction (osteolysis) or aberrant new bone formation (ostecondensation)¹⁴.

However in our models, lung metastases were not detectable by CT scan. IVIS X-rays capacities are not as good as those reached with a specific X-ray tomography, giving lower limit detection and resolution. Because of resolution and signal to noise ratio, tumor volumes under 1 mm remain difficult to detect which could explain the absence of lung metastases detection in CT scans observed in our study.

The combination of different techniques, *in vivo* and *ex vivo* bioluminescence detection, CT scan and histology using HES and luciferase staining allowed us to verify that bone alterations and metastases were due to the presence of the human osteosarcoma cells injected. Thus, these cell lines have the potential to develop primary tumors that mimic different osteosarcoma primary tumors within the *in vivo* bone environment and usual metastases in lung and bone which are the typical metastatic homing observed in patients.

Using the osteosarcoma cell line Saos-2-B-Luc/mKate2, we compared CDX engraftment and metastatic potential within different immune (nude and NSG mice) and bone (intratibial and periosteum-denuded paratibial injections) contexts. We observed a differential impact of these conditions on the *in vivo* primary bone tumor and metastatic behavior, as reported in other models²².

The NSG mouse strain used proved to be excellent recipients for osteosarcoma orthotopic xenografts allowing bone tumor engraftment in almost 100% of Saos-2-B-Luc/mKate2-CDX injected animals in a shorter period of time and more rapid metastatic spread compared to nude mice. The NSG strain also allowed intratibial HOS-Luc/mKate2-CDX engraftment in all tested animals and metastatic spread, while the literature reports lack of engraftment in nude mice (subcutaneous and intra-muscular injections)⁹ and no metastatic potential in SCID mice (paratibial injection)²³. The more profound immune-deficiency of NSG mice compared to nude mice (B-cell preserved and some innate immunity as macrophages, dendritic cells and NK cells) not just maximize the chance of xenograft engraftment¹⁹ but favored osteosarcoma primary tumor growth and metastatic spread^{14,21,24}. Lung metastases in Saos-2-B-Luc/mKate2-CDX models were indeed more frequent in NSG than in nude mice as well as the unusual spleen metastases, not observed in a human context. Spleen metastases were also observed in HOS-Luc/mKate2-CDX NSG mice. Others unusual metastatic localizations such as kidney metastases were

previously described in 143B-intratibial CDX Nu/Nu mice models¹³, or lymph nodes, liver, adrenal gland, kidney or ovary in Saos-2 paratibial CDX in SCID mice²³. These findings suggest the importance of macrophages and innate immunity in osteosarcoma oncogenesis and metastatic potential. Indeed, macrophages intra-tumor environment is an important aspect of osteosarcoma aggressiveness. High tumor-associated macrophage (TAM) infiltrates were found associated with better survival and lower risk of metastases²⁵. Thus, NSG strains might represent an advantage in having osteosarcoma models rapidly developing and spreading to test new drugs. However, therapeutics targeting the immune environment cannot be tested appropriately in these immune-deficient mice strains.

Bone is a site composed of many distinct cell types (e.g. osteoblasts, osteoclasts, immune cells) leading to a complex bone microenvironment. This complexity influences the development and progression of osteosarcoma tumors^{26,27}. The bone microenvironment allows engraftment and metastatic spread with Saos-2-B-Luc/mKate2-CDX model in nude mice, while Saos-2 was described as non-tumorigenic after subcutaneous and intramuscular injection in this mouse strain⁹. The different bone microenvironment of the primary tumor in Saos-2-B-Luc/mKate2-CDX model influences primary tumor engraftment and growth behavior as well as metastatic spread. Intratibial models better mimic primary bone tumor, reflecting the range of radiological (CT scan) changes seen in patients with osteosarcoma and developed early, frequent, numerous and visible lung metastases. In the paratibial setting, lung metastases were not confirmed by histology, although detected by both *in vivo* and *ex vivo* bioluminescence analysis. The metastases might have been missed by the slide sampling, due to their small size. In HOS-Luc/mKate2-CDX NSG mouse models, we observed barely any primary bone growth but rapid metastatic spread from day 30, while when injected subcutaneously in NSG mice a fast primary growth within 20 days was described²⁴, and when injected para-osseous in SCID don't show metastatic potential²³, highlighting different behaviors in distinct microenvironment context. Recently, tumor microenvironment has been shown to influence drug sensitivity in osteosarcoma MOS-J syngeneic model using C57BL/6J mice, where a higher response to doxorubicin was observed in intratibial model compared to intra-muscular model for tumor growth and necrosis¹⁵.

The genetic background of osteosarcoma may also have influenced the *in vivo* behavior in terms of local and metastatic potential. Saos-2-B-Luc/mKate2-CDX does not express the *TP53* gene, exhibits *RB1* mutation and normal *CDKN2A* whereas HOS-Luc/mKate2-CDX is *TP53* mutated and has *CDKN2A* homozygous deletion^{11,18}, hallmarks of aggressive osteosarcoma. When comparing the same *in vivo* conditions (intratibial in NSG mice), Saos-2-B has a high local growth potential leading to big osteocondensated aggressive bone tumors while HOS grew very slowly and is more osteolytic. Lung metastases developed at the same time in both models but grew faster with Saos-2-B-Luc/mKate2-CDX than in HOS-Luc/mKate2-CDX. Genetic transformation of these cell lines (Ki-RAS transformed HOS cell line, 143B^{11,13} and *in vivo* metastatic selection of Saos-2 leading to LM7 cell line²³) led to CDX models with higher metastatic potential than the parental cell line: 143B-subcutaneous-CDX models in nude mice presented tumorigenic and metastatic potential while parental HOS was not tumorigenic^{11,13}, LM7 paratibial-CDX was more metastatic than the parental Saos-2 in SCID mice²³.

Conclusion

Our two CDX orthotopic osteosarcoma bioluminescent models with different primary bone behavior and metastatic potential completed those previously published, the “aggressive” HOS-143B intratibial model in nude mice¹³, and the Saos-2 intrafemoral model in NSG mice¹⁴. These orthotopic models might further help to better follow osteosarcoma human disease in terms of tumor, progression, and metastatic spread, especially under different treatment conditions. They might bring complementary information to other types of existing osteosarcoma models (sub-cutaneous CDX, syngeneic models in mice or spontaneous osteosarcoma in dogs)²⁸, with the advantage of real-time *in vivo* follow-up in orthotopic and metastatic conditions. Several programs (e.g MAPPYACTS, IMI2-P4) are also developing patient-derived xenograft (PDX) models²⁹, which are missing in this disease, as well as humanized models. In osteosarcoma, all these multiple models developed in different *in vitro* and *in vivo* contexts are needed to get more insight into the different processes involving osteosarcoma initiation, progression and treatment sensitivity/resistance.

Acknowledgments

We thank Claudia Silva Evangelista for help on virus transduction, the Platform of Preclinical Evaluation for providing immunocompromised mice and animal care, Irene Villa for performing the histology slides scans and Carole Lecinse for critical reading of the manuscript, Brenda Mallon for editing the manuscript and to the Portuguese Foundation for Science and Technology (FCT) for the financial support through the PhD fellowship to Maria Eugénia Marques da Costa (SFRH/BD/89137/2012).

References

1. Trama A, Botta L, Foschi R, et al. Survival of European adolescents and young adults diagnosed with cancer in 2000–07: population-based data from EUROCARE-5. *Lancet Oncol.* 2016;17(7):896-906.
2. Bielack SS, Smeland S, Whelan JS, et al. Methotrexate, Doxorubicin, and Cisplatin (MAP) Plus Maintenance Pegylated Interferon Alfa-2b Versus MAP Alone in Patients With Resectable High-Grade Osteosarcoma and Good Histologic Response to Preoperative MAP: First Results of the EURAMOS-1 Good Response Randomized Controlled Trial. *J Clin Oncol.* 2015;33(20):2279-2287.
3. Piperno-Neumann S, Le Deley M-C, Rédini F, et al. Zoledronate in combination with chemotherapy and surgery to treat osteosarcoma (OS2006): a randomised, multicentre, open-label, phase 3 trial. *Lancet Oncol.* 2016;17(8):1070-1080.
4. Ritter J, Bielack SS. Osteosarcoma. *Ann Oncol.* 2010;21:vii320-vii325.
5. Collins M, Wilhelm M, Conyers R, et al. Benefits and adverse events in younger versus older patients receiving neoadjuvant chemotherapy for osteosarcoma: findings from a meta-analysis. *J Clin Oncol.* 2013;31(18):2303-2312.
6. Isakoff MS, Bielack SS, Meltzer P, Gorlick R. Osteosarcoma: Current Treatment and a Collaborative Pathway to Success. *J Clin Oncol.* 2015;33(27):3029-3035.
7. Omer N, Le Deley M-C, Piperno-Neumann S, et al. Phase-II trials in osteosarcoma recurrences: A systematic review of past experience. *Eur J Cancer.* 2017;75:98-108.
8. Martin JW, Squire JA, Zielenska M. The genetics of osteosarcoma. *Sarcoma.* 2012;6.
9. Mohseny AB, Machado I, Cai Y, et al. Functional characterization of

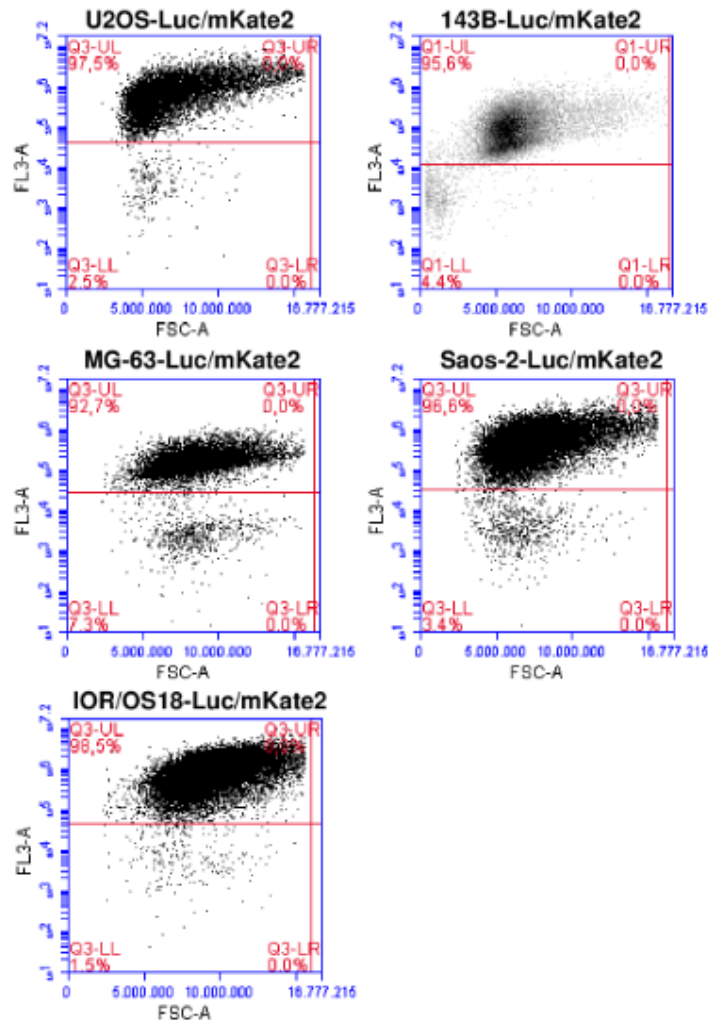
osteosarcoma cell lines provides representative models to study the human disease. *Lab Invest*. 2011;91(8):1195-1205.

10. Kunz P, Fellenberg J, Moskovszky L, et al. Osteosarcoma Microenvironment: Whole-Slide Imaging and Optimized Antigen Detection Overcome Major Limitations in Immunohistochemical Quantification. Hartl D, ed. *PLoS One*. 2014;9(3):e90727.
11. Ottaviano L, Schaefer K-L, Gajewski M, et al. Molecular characterization of commonly used cell lines for bone tumor research: A trans-European EuroBoNet effort. *Genes, Chromosom Cancer*. 2010;49(1):40-51.
12. Kresse SH, Rydbeck H, Skårn M, et al. Integrative Analysis Reveals Relationships of Genetic and Epigenetic Alterations in Osteosarcoma. *PLoS One*. 2012;7(11):e48262.
13. Garimella R, Eskew J, Bhamidi P, et al. Biological characterization of preclinical Bioluminescent Osteosarcoma Orthotopic Mouse (BOOM) model: A multi-modality approach. *J Bone Oncol*. 2013;2(1):11-21.
14. Vormoor B, Knizia HK, Batey MA, et al. Development of a Preclinical Orthotopic Xenograft Model of Ewing Sarcoma and Other Human Malignant Bone Disease Using Advanced *In Vivo* Imaging. Nurminskaya M, ed. *PLoS One*. 2014;9(1):e85128.
15. Creen V, Biteau K, Amiaud J, et al. Bone microenvironment has an influence on the histological response of osteosarcoma to chemotherapy: retrospective analysis and preclinical modeling. *Am. J. Cancer Res*. 2017;7:2333–2349
16. Miretti S, Roato I, Taulli R, et al. A Mouse Model of Pulmonary Metastasis from Spontaneous Osteosarcoma Monitored In Vivo by Luciferase Imaging. Callaerts P, ed. *PLoS One*. 2008;3(3):e1828.
17. Plessier A, LeDret L, Varlet P, et al. New avatars of diffuse intrinsic pontine gliomas (DIPG) from stereotactic biopsies performed at diagnosis. *Oncotarget*. 2017;5:52543–52559.

18. Niforou KM, Anagnostopoulos AK, Vougas K, Kittas C, Gorgoulis VG, Tsangaris GT. The proteome profile of the human osteosarcoma U2OS cell line. *Cancer Genomics Proteomics*. 5(1):63-78.
19. Puchalapalli M, Zeng X, Mu L, et al. NSG Mice Provide a Better Spontaneous Model of Breast Cancer Metastasis than Athymic (Nude) Mice. Cukierman E, ed. *PLoS One*. 2016;11(9):e0163521.
20. Uluçkan Z, Segaliny A, Botter S, Santiago JM, Mutsaers AJ. Preclinical mouse models of osteosarcoma. *Bonekey Rep*. 2015;4 :670.
21. Daudigeos-Dubus E, LE Dret L, Rouffiac V, et al. Establishment and characterization of new orthotopic and metastatic neuroblastoma models. *In Vivo*. 2014;28(4):425-434.
22. Quintana E, Shackleton M, Sabel MS, Fullen DR, Johnson TM, Morrison SJ. Efficient tumour formation by single human melanoma cells. *Nature*. 2008;456(7222):593-598.
23. Ren L, Mendoza A, Zhu J, et al. Characterization of the metastatic phenotype of a panel of established osteosarcoma cells. *Oncotarget*. 2015;6(30):29469-29481.
24. Lauvrak SU, Munthe E, Kresse SH, et al. Functional characterisation of osteosarcoma cell lines and identification of mRNAs and miRNAs associated with aggressive cancer phenotypes. *Br J Cancer*. 2013;109(8):2228-2236.
25. Buddingh EP, Kuijjer ML, Duim RA, et al. Tumor-infiltrating macrophages are associated with metastasis suppression in high-grade osteosarcoma: a rationale for treatment with macrophage-activating agents. *Clin Cancer Res*. 2011;17:2110-2119.
26. Alfranca A, Martinez-Cruzado L, Tornin J, et al. Bone microenvironment signals in osteosarcoma development. *Cell Mol Life Sci*. 2015;72(16):3097-3113.

27. Zhang Y, Mai Q, Zhang X, Xie C, Zhang Y. Microenvironment Signals and Mechanisms in the Regulation of Osteosarcoma. In: *Osteosarcoma - Biology, Behavior and Mechanisms. InTechOpen, London, UK. 2017.*
28. Mueller F, Fuchs B, Kaser-hotz B. Comparative biology of human and canine osteosarcoma. *Anticancer Res.* 2007; 27:155–164.
29. Stewart E, Federico SM, Chen X, et al. Orthotopic patient-derived xenografts of paediatric solid tumours. *Nature.* 2017;549:96-100.

Supplementary Data



Supplementary Figure.2.S1: Characterization of luciferase-transduced osteosarcoma cells. mKate2 (FL3-A) selection by flow cytometry of transduced U2OS-luc/mKate2, 143B-luc/mKate2, MG-63-luc/mKate2, Saos-2-luc/mKate2 and IOR/OS18-luc/mKate2 cells showed a rate of more than 90% positive cells.

Chapter 3:

***In vitro* and *in vivo* establishment and characterization of bioluminescent orthotopic chemo-resistant osteosarcoma models in NSG mice.**

***In vitro* and *in vivo* characterization of bioluminescent orthotopic resistant osteosarcoma models in NSG mice and resistance mechanisms**

Maria Eugenia Marques da Costa^{1,2}, Estelle Daudigeos-Dubus¹, Anne Gomez-Brouchet³, Bastien Job⁴, Antonin Marchais¹, Noemie Pata-Merci⁵, Betty Leite⁵, Conceição Santos⁶, Birgit Geoerger^{1,7}, Nathalie Gaspar^{1,7}

¹ Vectorology and Anticancer Therapies, CNRS UMR 8203, Paris-Sud University, Gustave Roussy, Paris-Saclay University, 94805 Villejuif, France

² CESAM & Department of Biology, University of Aveiro, 3810 Aveiro, Portugal

³ Department of Pathology, IUCT-Oncopole, CHU of Toulouse and University of Toulouse; Pharmacology and structural biology institut, CNRS UMR5089, 31059 Toulouse, France

⁴ US23-INSERM, Bioinformatics core facility, Gustave Roussy, 94805 Villejuif, France

⁵ AMMICA, Genomic platform, Gustave Roussy, 94805 Villejuif, France

⁶ Department of Biology, Faculty of Sciences, University of Porto, 4000 Porto, Portugal

⁷ Department of Oncology for Children and Adolescents, Gustave Roussy, 94805 Villejuif, France

Abstract

Osteosarcoma is the most common malignancy of the bones with peak incidence at adolescence. Despite current treatment strategies including chemotherapy and surgery, the long-term survival rate has reached a plateau; chemoresistance and metastatic spread remaining the major problems. Our aim was to develop and characterize *in vitro* and *in vivo* bioluminescent resistant models to usual anti-osteosarcoma chemotherapy, and analyze their behavior comparatively to their parental counterparts, as well as understand the resistance mechanisms involved. Cells were selected *in vitro* for resistance to methotrexate and doxorubicin, by continuous exposure to these drugs. Five methotrexate-resistant and one doxorubicin-resistant *in vitro* models were obtained. P-glycoprotein was the main mechanism detected in the HOS-R/DOXO. Different mechanisms of acquired resistance specific to methotrexate according to the genetic background of the cell lines were observed. Differential analysis of gene expression (RNAseq) and copy number abnormalities (aCGH) also revealed modulation of different pathways implicated in cell mobility. Two parental (HOS and Saos-2-B) and their counterpart resistant cell lines (HOS-R/MTX, HOS-R/DOXO and Saos-2-B-R/MTX) were transduced with luciferase/mKate2 and injected intratibially into NSG mice. Resistant bioluminescent orthotopic CDX models (HOS-R/MTX, HOS-R/DOXO and Saos-2-B-R/MTX) injected intratibially into NSG mice at primary site showed similar behavior compared to their parental counterpart (HOS and Saos-2-B) with HOS showing slightly difficulties to adapt initially. Resistant CDX-models retained resistance without drug pressure, showing a slower and lower metastatic spread. These models may further help on new therapies development and testing in osteosarcoma, as well as to better understand the resistance mechanisms involved, in order to improve patients survival.

Key words: osteosarcoma, *in vivo*, *in vitro*, Saos-2-B, HOS, bioluminescence, resistance, Methotrexate, Doxorubicin, *MDR1*, *DHFR*

Introduction

Osteosarcoma (OS) is the first primary malignant bone tumor that predominantly occurs during adolescence^{1,2}. Standard treatment of osteosarcoma combines neoadjuvant and post-operative chemotherapy with complete surgery of all involved sites (primary tumor and metastases when present). Osteosarcoma prognosis has not improved in almost four decades, and treatment failure is usually due to metastatic relapse after first-line chemotherapy. The risk factors of relapse during the first-line treatment are the presence of metastases at diagnosis and poor response to neoadjuvant chemotherapy^{1,3–5}. Resistance to therapy, both intrinsic (phenomenon present prior to chemotherapy administration) and acquired (phenomenon revealed after administration of chemotherapeutic agents), participate to the treatment failure leading to recurrence. Several mechanisms of chemoresistance have been described in osteosarcoma, from decreased intracellular drug accumulation mediated by RFC or PgP, drug inactivation by GSTP1, enhanced DNA repair by APE1 or ERCC, perturbations in mTOR or IGF-IR signal transduction pathways, apoptosis and autophagy-related chemoresistance, miRNA dysregulation and cancer stem cell-mediated drug resistance, as well as interaction between osteosarcoma cells and their microenvironment⁶.

The aim of this work was to develop and characterize osteosarcoma models resistant to usual chemotherapeutic agents *in vitro*, and analyze their behavior comparatively to their parental counterparts *in vitro* and *in vivo* in a bone orthotopic setting (bioluminescent cell-derived xenograft CDX-models).

Methods

Cell line culture

A panel of osteosarcoma cell lines with different genetic background were used: HOS (*TP53* mutation and homozygous loss of *CDKN2A*), 143B (HOS virally transfected with *Ki-ras* oncogene), Saos-2 (*TP53* deleted, *RB1* mutated and normal *CDKN2A*), MG-63 (homozygous deletion of *CDKN2A*, normal *RB1* and first intron rearrangements in *TP53*) and IOR/OS18 (*TP53* deletion>EX3/EX4 and *CDKN2A* homozygous loss, normal *RB1*)^{7,8}. Mycoplasma test was performed each month by PCR. The Human 143B was purchased from the American Type Culture Collection

and HOS, Saos-2, IOR/OS18 and MG-63 osteosarcoma cell lines were kindly provided in the frame of the European Consortium Innovative Therapeutics for Children with Cancer (ITCC). Testing Saos-2 issued from two different culture flasks, we observed two slightly different CGH profile (Supplementary Fig.3.S1). We carried on the experiments with both, and named the second one Saos-2-B.

The cell lines were cultured, using early passages in Dulbecco's modified Eagle medium (DMEM, GIBCO/Invitrogen, Saint Aubin, France) supplemented with 10% (v/v) fetal bovine serum (FBS, GIBCO/Invitrogen, Saint Aubin, France) at 37°C in a humidified atmosphere (5% CO₂ and 95% air).

Compounds

Doxorubicin (DOXO), Methotrexate (MTX), Cisplatin (CISP), Etoposide (ETOP), Vincristine (VCR) and Verapamil (VER) were purchased from Sigma Aldrich (St Louis, MO, USA), mafosfamide from Toronto Research Chemicals Inc (TRC) (Toronto, Canada) and cabozantinib from LC Laboratories (US, Canada). Compounds were diluted in dimethyl sulfoxide (DMSO) (Sigma Aldrich, St Louis, MO, USA) except cisplatin diluted in N,N-dimethylformamide (DMF) (Sigma Aldrich, St Louis, MO, USA) and stored at -20°C at 10mM stock solution.

***In vitro* development of chemotherapy resistant osteosarcoma cell lines.**

Early passage of osteosarcoma cell lines were seeded into T75 flasks. The different human cell lines were serially passaged in DMEM in one flask as an untreated control along with chemotherapy treated cells cultured in DMEM supplemented with 10% FBS and containing an initial concentration of 0.01 µM for DOXO or 0.07 µM for MTX. Cells were exposed continuously to the compound until 80% confluent and then passaged. The medium was changed every three days. When treated cells were able to tolerate and grow at this concentration, the compound concentration was progressively increased, along the passages, up to 1 µM of MTX for all cell lines, except MG-63 (maximum concentration used of 0.03 µM) and 1.3 µM of DOXO for HOS. After resistance confirmation of cells under drug pressure (Drug ON) was confirmed, cultures in drug-free medium for at least nine weeks (Drug OFF)

before being used for further experiments were established. The same was performed with mafosfamide.

***In vitro* doubling time, proliferation (MTS assay) and migration assay**

For doubling time determination, cellular proliferation rates were analyzed by live-cell imaging using the Incucyte system (Essens Bioscience, Birmingham, UK). Cells were seeded in a 96-well plate and placed in the Incucyte. Phase-contrast photographs (4 per well) were taken automatically every four hours for 72h.

Growth inhibition was determined using the CellTiter 96 Aqueous One Solution Cell Proliferation Assay (MTS assay) (Promega Corporation, Charbonnières, France), according to the manufacturer instructions. Parental and resistant derived-HOS and 143B cell lines were seeded at 5,000 cells/well, and parental and resistant derived-Saos-2 and Saos-2-B cell lines at 10,000 cells/well in a 96-well plate and left to settle overnight at 37 °C in DMEM with 10% FBS. The cells were treated with different drugs at concentrations ranging from 0 to 100 µM (doxorubicin, etoposide, mafosfamide and cabozantinib), or 0 to 50 µM (cisplatin) or 0 to 500 µM (MTX) or 0 to 10 µM (Vincristine). Verapamil was used at 5 µM and cabozantinib at 0.1 µM, to revert PgP function. Cell viability was determined 72 hours after treatment by MTS assay. The cell proliferation was measured at an emission wavelength of 490 nm in an automatic plate reader (Elx808; Fisher Bioblock Scientific SAS, Illkirch, France). The IC₅₀ was calculated as the drug concentration that inhibits cell growth by 50% compared with control. The resistance index (RI) was defined by the ratio of IC₅₀ resistant line/IC₅₀ parental line.

Cellular motility was assessed by *in vitro* scratch assay. All the cell lines were seeded in a 96-well ImageLock tissue culture plate (Essen BioScience 4379) at an appropriate density and incubated in a standard cell incubator for 24h. The cells were then scraped with the WoundMaker™ to create precise and reproducible wounds and treated with 0.01 µM (MTX, Doxorubicin, Cisplatin and etoposide) or 0.2 µM (Mafosfamide), IC₅₀ and 10xIC₅₀. The 96 well plate was placed into the IncuCyte™ system (Essens Bioscience, Birmingham, UK) and two images per well were taken automatically every 3 h for 48 h. The data analyses were performed with

Graphpad Prism® Software version 5.00 (Graphpad Software Inc, La Jolla, CA, USA).

Transfection and cell transduction with luc/mkate2 (transgene) *in vitro*

The procedures were performed in sterile and safety conditions as described before⁹.

***In vivo* parental and resistant bioluminescent CDX models**

Animal experiments were approved by the CEEA26, CEEA PdL N°6 Ethics Committee and the Ministry of Agriculture (approval number: APAFIS#1648-2015090713516480) and performed under the conditions established by the European Community (Directive 2010/63/UE).

Orthotopic bioluminescent cell derived xenograft (CDX) models were established in 7 week-old immunodeficient NSG mice by intratibial injection, as previously described^{9,10}. Two parental cell lines (HOS-Luc/mKate2 and Saos-2-B-Luc/mKate2) and their counterparts resistant to either MTX (HOS-Luc/mKate2/MTX and Saos-2-B-Luc/mKate2/MTX) or DOXO (HOS-Luc/mKate2/DOXO) were used. The NSG mice were purchased at Gustave Roussy (Villejuif, France). Intratibial injection was performed as previously described⁹ under a sterile atmosphere. Briefly, 1.5×10^6 cells were injected in 5-10µl Matrigel (Corning, Wiesbaden, Germany) solution at 4 mg/ml into anesthetized (3% isoflurane) NSG mice. A 0.5 cm skin incision was performed and cells were injected into the tibia intramedullary cavity, skin was sutured right after. Buprenorphine at 0.3 mg/kg was applied in addition to the general anesthesia.

The mice were monitored clinically every week for general symptoms (weight and tumor size by bioluminescence and CT scan). They were euthanized at the onset of general symptoms (e.g. weight loss, difficulty to walk). At the sacrifice day, a sample from one *in vivo* primary tumor of resistant cell lines was cultured.

***In vivo* and *ex vivo* imaging, CT scan and bioluminescence and histology**

In vivo and *ex vivo* images were acquired using an IVIS SpectrumCT (Perkin Elmer, Courtaboeuf, France) as previously described⁹. Briefly, NSG mice were injected

intraperitoneally with 150 mg/kg of D-luciferin (Beetle luciferin, Promega, Charbonnières, France) and under anesthesia (3% isoflurane) body imaged for primary tumor detection and for metastatic spread was performed. After sacrifice, *ex vivo* anatomical parts imaging was also performed (legs, lungs, and spleen) immersed in 150 µg/ml of D-luciferin and imaged individually.

Anatomical parts were fixed in a 4% paraformaldehyde, and embedded in paraffin. Tissues were stained with hematoxylin-eosin-safranin (HES) for morphology. Paraffin sections were processed after heat-induced antigen retrieval using a mouse anti-firefly luciferase monoclonal antibody (1:200, ThermoFisher Scientific, Waltham, MA, USA). The cytoplasmic signal was revealed with the Klear mouse kit (GBI labs). Slides were examined using light microscopy (Zeiss, Marly-Le-Roy, France). Single representative whole tumor tissue section from each animal was digitized using a slide scanner NanoZoomer 2.0-HT (C9600-13, Hamamatsu Photonics). Histology was reviewed by a human bone expert pathologist.

Acid nucleic extraction

Human osteosarcoma cell lines samples (parental, drug ON and drug OFF), were frozen in liquid nitrogen until the moment of extraction. DNA and RNA were isolated using AllPrep DNA/RNA mini kit (Qiagen, Germany) according manufacturer's instructions.

Oligonucleotide aCGH assay

In all experiments, sex-matched normal DNA from a pooled human female or male (Promega, Madison, WI, USA) was used as a reference. Oligonucleotide aCGH processing was performed as detailed in the manufacturer's protocol (version 7.5; <http://www.agilent.com>). Equal amounts (500 ng) of tumor and normal DNAs were fragmented with AluI and RsaI (Fermentas, Euromedex, France). The fragmented DNAs were labelled with cyanine Cy3-deoxyuridine triphosphate (dUTP) or Cy5-dUTP. Hybridization was carried out on SurePrint G3 Human CGH Microarray 4x180K (Agilent Technologies, Santa Clara, CA, USA) arrays for 24 h at 65°C in a rotating oven (Robbins Scientific, Mountain View, CA) at 20 rpm. The hybridization was followed by appropriate washing steps. Scanning of glass microarrays was

performed with an Agilent G2505C DNA Microarray scanner at 100% PMT with 3 μm resolution at 20°C in low ozone concentration environment. Data were extracted from scanned TIFF images using the Feature Extraction software (v11.5.1.1, Agilent), along with protocol CGH_1105_Oct12. All further data manipulation were performed under the R statistical environment in v3.4 (<http://cran.r-project.org>). Raw intensities were normalized according to their dye composition (Cy3 fitted over Cy5). Data were transformed to $\log_2(\text{Test/Ref})$ and normalized according to their local GC content through a lowess regression. Resulting profiles were segmented with the CBS algorithm¹¹ implemented in the DNACopy package (v1.42) using default parameters. Profiles were centered using the most centered out of the three most populated peaks of the smoothed $\log_2(\text{Test/Ref})$ distribution density. Aberration levels were called by setting a $\log_2(\text{Test/Ref})$ threshold automatically adapted to the internal noise for each profile, considered as one-fourth of the median value of the absolute differences between consecutive $\log_2(\text{Test/Ref})$ measures along the genome. Segmented, called profiles were then aggregated and hierarchically clustered using the Pearson distance and Ward aggregation method. Profiles comparisons were performed, for each pair, first by performing a linear regression of the profile with the lowest dynamics (measured as its interquartile range) to the profile with the highest one; the probe-to-probe direct difference of the $\log_2(\text{Test/Ref})$ of the two profiles was then computed, and the differential profile was segmented and called as described previously. Genomic regions called as different in the pair of profiles were annotated using the UCSC annotation tables (cytoBandIdeo, cpgIslandExt, wgRna, refGene, dgvMerged), corresponding to the hg19 genome build.

RNA sequencing

RNA sequencing analysis was performed as previously described¹². RNA sequencing libraries were prepared with TruSeq Stranded mRNA kit following recommendations: the key steps consist of PolyA mRNA capture with oligo dT beads 1 μg total RNA, fragmentation to approximately 400 bp, DNA double strand synthesis, and ligation of Illumina adaptors amplification of the library by PCR for sequencing. Libraries sequencing was performed using Illumina sequencers

(NextSeq 500 or HiSeq 2000/2500/4000) in 75 bp paired-end mode. Quality of stranded pair-ended RNA-seq libraries was evaluated with fastqc. Reads were mapped with Salmon v0.8.1¹² using GRCh37 ENSEMBL mRNA dataset as reference sequences. Differential mRNA expression was measured with DESeq2 R package from raw read count table¹³.

Differential mRNA expression lists were compared using Venn diagrams produced by Venny 2.1.0 (<http://bioinfogp.cnb.csic.es/tools/venny/>). Toppfun website was used for functional enrichment analysis (<https://toppgene.cchmc.org/enrichment.jsp>).

Reverse Transcription-quantitative PCR (RT-qPCR)

The Parental and Resistant cells were collected in 450 µl of RLT solution + β-mercaptoethanol (10% final concentration). Total RNA was isolated using the Trizol reagent (ThermoFisher Scientific, Waltham, MA, USA) and reverse transcribed. *TOPO2A*, *MDR1* and *MRP1* amplification was monitored with StepOnePlus PCR System (AB Applied Biosystems, Villebon-sur-Yvette, France) using Maxima SYBR Green/ROX qPCR (ThermoFisher Scientific, Waltham, MA, USA) according to manufacturer's instructions. The primers used are described in Supplementary Table.3.SI. Samples were run in triplicate relative abundance of each target was normalized using glyceraldehyde-3-phosphate dehydrogenase (*GAPDH*) expression levels. Fold changes for transcripts normalized using the $2^{-\Delta\Delta Ct}$ formula¹⁴.

Results

Development of *In vitro* osteosarcoma lines resistance

Acquired resistance to MTX developed in 5 lines within 2-3 months, up to 14xIC₅₀ (1 µM) for HOS, Saos-2, Saos-2-B, 25 xIC₅₀ (1 µM) for 143B and 5xIC₅₀ (0.03 µM) for MG-63 (more sensitive to MTX), after 8-9 months exposure (Fig.3.1A). IC₅₀ of parental and resistant line are given in Supplementary Table.3.SII. No further resistance was obtained in primary resistant IOR/OS18 cell line. No morphologic, growth rate or migration differences was seen between the acquired-MTX-resistant lines and their parental counterparts, under basal condition without drug (Supplementary Fig.3.S2A/B/C). Under continuous drug pressure (Drug ON), all

lines had high RI to MTX > 40. Without MTX treatment (Drug OFF), MG-63-R/MTX RI normalized in two weeks (RI=2), HOS-R/MTX RI decreased from 100 to 40 in 9 weeks, and RI remained stable up to 9 weeks for the other cell lines.

Acquired resistance to doxorubicin developed only in HOS, after a longer exposure time (3-4 months). HOS-R/DOXO was resistant up to 5xIC₅₀ (1.3 μ M) (Fig.3.1A). No morphological difference between parental/resistant cell lines was seen. HOS-R/DOXO grew and migrated more slowly than its parental line (doubling time=45h and 25h respectively) (Supplementary-Fig.3.S2A/B/C). HOS-R/DOXO Drug ON had a high RI=212 which decreased to 87 in the absence of doxorubicin pressure (Drug OFF) for 9 weeks.

Despite continuous exposure to mafosfamide up to 2 months, none of the lines developed resistance. IC₅₀ of the parental lines for mafosfamide were higher (7-27 μ M) than those for methotrexate and doxorubicin (data not shown).

Cross-resistance to other chemotherapeutic agents

RI to other chemotherapeutic agents and to the multi-tyrosine kinase inhibitor cabozantinib were similar on drug ON and drug OFF cells, except for R/MTX MG-63. Only results from the drug ON resistant cell lines are shown in Fig.3.1B.

No cross-resistance was observed with any compound tested in the MTX-resistance lines drug ON (Fig.3.1B), as for drug OFF condition, except in MG-63-R/MTX which had increased RI (between 5-10) for MAF, CISP and ETOP, only in drug OFF condition (data not shown).

In HOS-R/DOXO, cross-resistance with etoposide oriented toward a multi-drug resistance phenomenon, such as *PgP* (MDR1=ABCB1) protein, confirmed by cross-resistance with vincristine (another *PgP* substrate). In HOS-R/DOXO, verapamil, a *PgP* inhibitor, partially reverted DOXO and VCR resistance (Fig.3.1C) but not ETOP or MTX cross-resistance (data not shown). The weaker *PgP* inhibitor cabozantinib did not modify the RI of any drug tested (data not shown). Increased MDR1 mRNA (RT-qPCR) and protein (WB) level (Fig.3.1D) and decreased TOPO2A protein level (WB) were confirmed lower in the HOS-R/DOXO cell line comparatively to the parental cell line (Fig.3.1E).

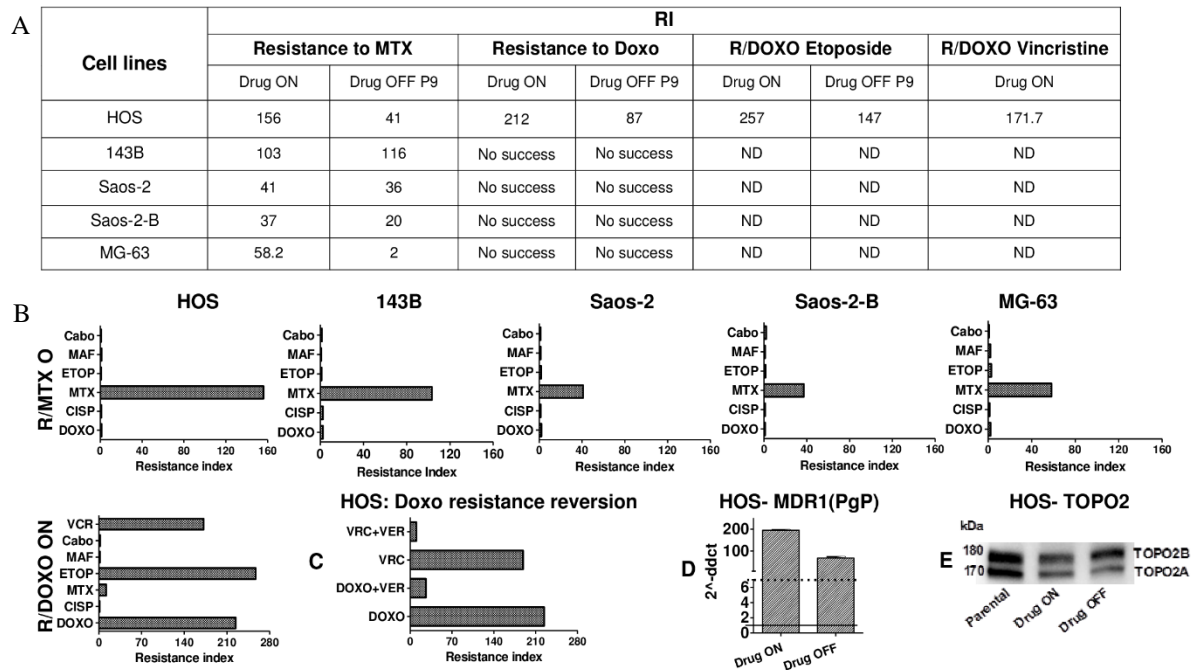


Figure 3.1: Acquired *in vitro* resistance to methotrexate and doxorubicin in osteosarcoma cell lines and cross-resistance to other chemotherapeutic agents used in osteosarcoma. RI values were obtained through the Ratio IC₅₀ Resistant / IC₅₀ Parental. A - Resistance Index (RI) values of the resistant cell lines to MTX and to DOXO Drug ON and Drug OFF as well the RI of the resistant cell lines to DOXO treated with Etoposide and Vincristine (VCR). Resistance selection was performed for IOR/OS18, however was not possible to obtain a resistant cell line. B- RI presented for resistant cell lines to MTX and to DOXO Drug ON treated with doxorubicin, methotrexate, etoposide, cisplatin, mafosfamide, cabozantinib and vincristine. C- RI of HOS-R/DOXO treated with vincristine or doxorubicin alone or in combination with Verapamil (VER - PgP inhibitors). D- MDR1 (PgP) expression in HOS-R/DOXO drug ON and drug OFF obtained by RT-qPCR. E- Topoisomerase IIa (TOPO2A) expression in HOS parental, HOS-R/DOXO drug ON and drug OFF obtained by Western blot. ND-Not done.

Copy number and gene expression differential analysis between resistant and parental lines

Differential analysis of aCGH and RNA sequencing revealed that copy number abnormalities (CNA; Fig.3.2A) and gene expression (GE; Fig.3.2B) profiles of the resistant lines were more closely related to their parental counterparts than with any other line.

Common acquired CNA were seen in MTX-resistant lines issued from similar genetic background (HOS/143B and Saos-2/Saos-2-B, respectively). MTX-resistant HOS-R/MTX and 143B-R/MTX acquired gains on chromosomes 5q (5:71,484,019-96,791,800; containing *DHFR*), 9q, and 12p; acquired losses on chromosome 21q (containing *SLC19A1* located on chr21: 46,934,628-46,962,385), 2q (3 regions, including one with small variation containing *UGT1A*), 20q; and had no CNA in region initially gained in the parental counterpart line (chromosome 7p, 15q, 18p and 20p) (Fig.3.2A and supplementary Fig.3.S1). For 143-R/MTX line, two different losses in *SCL19A1=RFC* gene suggested a break in the gene. MTX-resistant Saos-2-R/MTX and Saos-2-B-R/MTX acquired common CNA with less amplitude but different from those seen in HOS-R/MTX and 143B-R/MTX. *MTHFR* locus (chr1:564,423-17,221,943) was slightly gained, while *DHFR* locus was not modified. *SCL19A1=RFC* locus was lost in Saos-2-R/MTX (Diff.l2r=-0,335) and not modified in Saos-2-B-R/MTX. In MG-63-R/MTX a gain in *DHFR*-containing region, without modification on *SCL19A1=RFC*, *MTHFR* and *UGT1A* regions.

Fourteen genes were differentially expressed in GE analysis (Fig.3.2C) between all resistant line drug OFF versus parental lines. Nine gene had a known function and seven have been previously involved in MTX metabolism and sensitivity (*SCL19A1=RFC*; *XYLT1*, xylosyltransferase enzyme catalyzes transfer of UDP-xylose to serine residues of an acceptor protein substrate)¹⁶, osteosarcoma predisposition (*COL18A1*)¹⁷, osteosarcoma metastatic potential (*ANKRD1*)¹⁸, osteosarcoma oncogenesis (*RTN1*)¹⁹, bone metabolism (*BMP6*, secreted ligand of the TGF-beta), and extracellular matrix (*ADAMTSL1*), and two other (*FOXA2*, *AFF3*). All MTX-resistant-lines had acquired decreased mRNA *SCL19A1=RFC* expression, irrespective of MTX pressure (Drug ON and OFF, except for the HOS-R/MTX drug OFF which had increase *SCL19A1=RFC* expression compared to drug

ON) (Fig.3.2D), and irrespective of the CNA changes observed. *RFC* mutations know to inactivate (Leu291Pro) or decrease (Ser46Asn, Ser4Pro and Gly259Trp) *RFC* activity and implicated in MTX-resistance, were not found in our lines by RNAseq analysis. *DHFR* mRNA expression levels showed few changes, except in HOS-R/MTX and 143B-R/MTX drug OFF where mRNA expression was increased mainly in MTX-resistant cells drug OFF (Fig.3.2D). Protein levels of DHFR (WB) increased in all the MTX resistant cell lines drug ON compared to parental counterpart, especially in MG-63, 143-B and HOS (Fig.3.2E). DHFR protein level decreased in drug OFF condition to the parental levels, except for HOS-R/MTX and 143B-R/MTX which had a gain in the *DHFR* region and where protein levels remained higher than in parentals. *MTHFR* mRNA expression did not changed. Between other genes with mRNA variation, CAN variations are seen only in *COL18A1* in HOS and 143B with two levels of loss suggesting a break in the gene. The acquired CNA in the unique doxorubicin resistant line HOS-R/DOXO regions were enriched in genes down-regulated in ME-A cells (breast cancer) undergoing apoptosis in response to doxorubicin (MSigDB C2: CGP Curated Gene Sets, v6.0) and in genes implicated in cisplatin resistance of human Ovarian Li09 (GeneSigDB). The main regions gained were on chromosomes 7:86,259,619-88,276,590 (Diff.l2r +4.7369) containing *ABCB1*=MDR1=PgP and *ABCB4*, and on chromosomes 11:102,449,766-103,152,951 (Diff.l2r +3.1626) containing several matrix metalloproteinases (MMPs). Several other regions with acquired CNA contained multiple multidrug resistance genes (on chromosomes 1, 2, 4, 6, 7, 10, 11, 16, 17, 21 and X), including *ABCC1*. Low *ABCC1* (MRP1) mRNA levels observed by RT-qPCR showed that MRP1 mechanism maybe is not link to the doxorubicin resistance in our HOS-R/DOXO cell line (data not shown). All gained regions in HOS-R/DOXO were enriched in genes involved in cell adhesion (GO:0007156 and GO:0098742), Cadherin and Wnt pathways. The lost regions in HOS-R/DOXO were enriched in genes involved in the immunity (type I interferon receptor binding, GO:0005132 and CXCR chemokine receptor binding, GO:0045236).

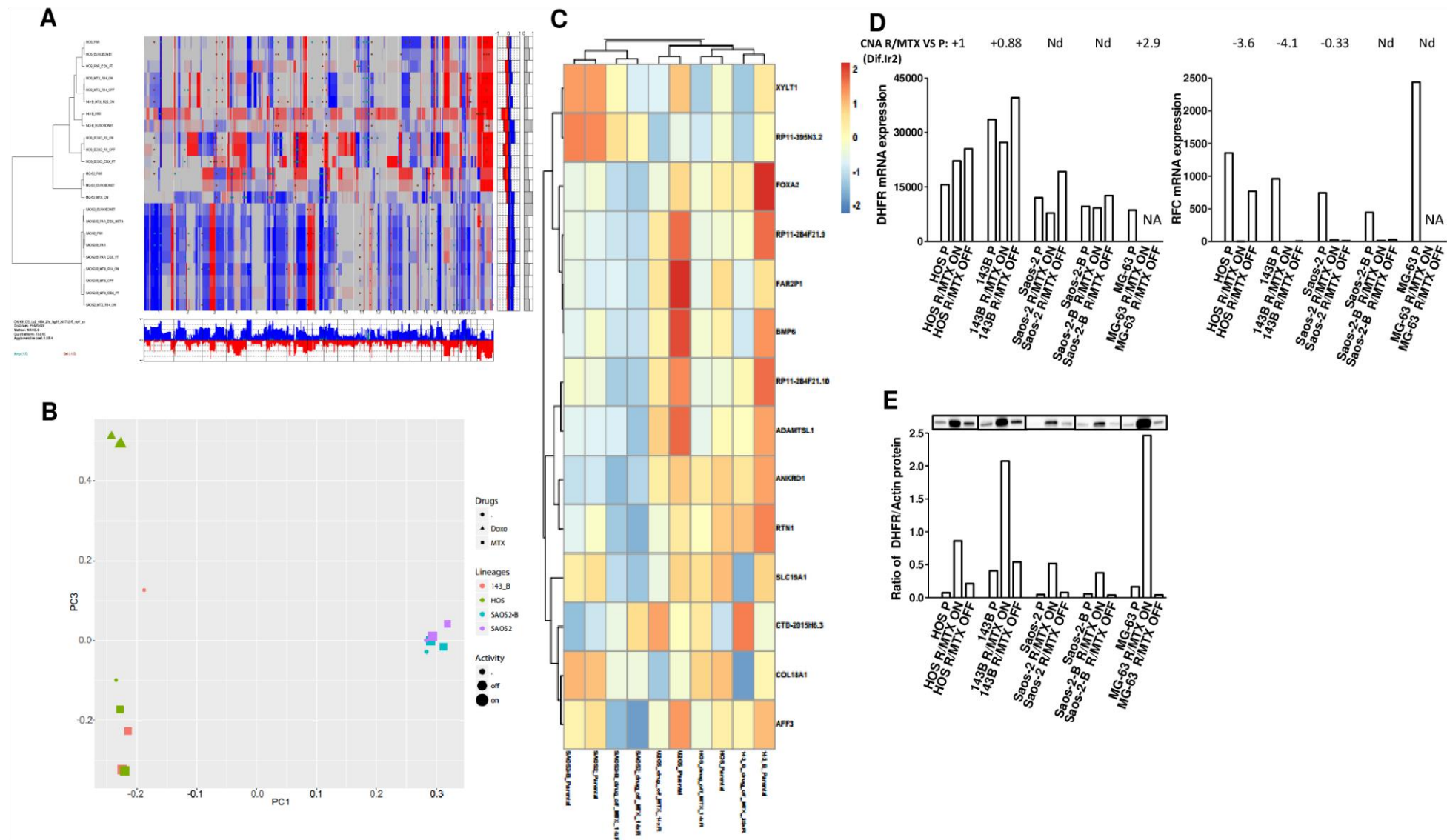


Figure 3.2: (previous page) Differential analysis of aCGH and RNA sequencing of the resistant and parental cell lines as well as DHFR and RFC expression. A- copy number abnormalities (CNA); B - gene expression (GE - PCA); C- differentially expressed in GE analysis; D- DHFR and RFC mRNA expression and CNA values; E- DHFR expression at protein level obtained by Western-blot. Nd- CAN not different in resistant and parental cell lines.

***In vivo* bioluminescent orthotopic parental and resistant CDX models of HOS and Saos-2-B**

The parental and resistant osteosarcoma cell lines were successfully transduced with a rate above 90% of Luc/mKate2 positive cells after selection by flow cytometry (Supplementary Fig.3.S3), then injected in an orthotopic setting (intratibial). Primary tumor uptake/growth and the metastatic behavior of parental and resistant models were followed using IVIS SpectrumCT system. *In vivo* and *ex vivo* bioluminescence, CT scan images and histology (HES and luciferase staining), confirmed that the imaging changes correspond to the injected human osteosarcoma cells (Supplementary Table.3.SIII). The different models revealed tumor-bearing tibia bone structure abnormalities similar to those observed in the human osteosarcoma disease. *In vivo* metastases were not detected by CT scan due to its resolution. HES staining confirmed the osteosarcoma nature of primary tumors and metastasis. We then compared the *in vivo* behavior between the parental and resistant models.

***In vivo* primary tumor characteristics of the resistant orthotopic cell-derived bioluminescent osteosarcoma xenograft models**

Bone engraftment rates of resistant and their respective parental counterpart were similar, except for the HOS-R/DOXO-CDX that had a lower engraftment rate (Fig.3.3A). HOS-resistant lines adaptation to the *in vivo* bone environment was more difficult than for the parental, with an initial decrease in *in vivo* bioluminescent detection (up to day 27), then followed by faster growth than the HOS-Parental-CDX (Fig.3.3B). Saos-2-B-R/MTX-CDX behaved as its parental counterpart for primary tumor growth. The resistant models retained the primary tumor-induced bone abnormalities of their parental counterpart in CT scan (Fig.3.4). The slow growing

osteolytic HOS-CDX-models were confined to bone, while the fast growing Saos-2-B-CDX-models induced aggressive osseous and extraosseous mass with osteocondensation deforming the leg. HES reveal the osteoblastic nature of all models with some fibroblastic component (Fig.3.4) with no morphological differences between parental and resistant CDX.

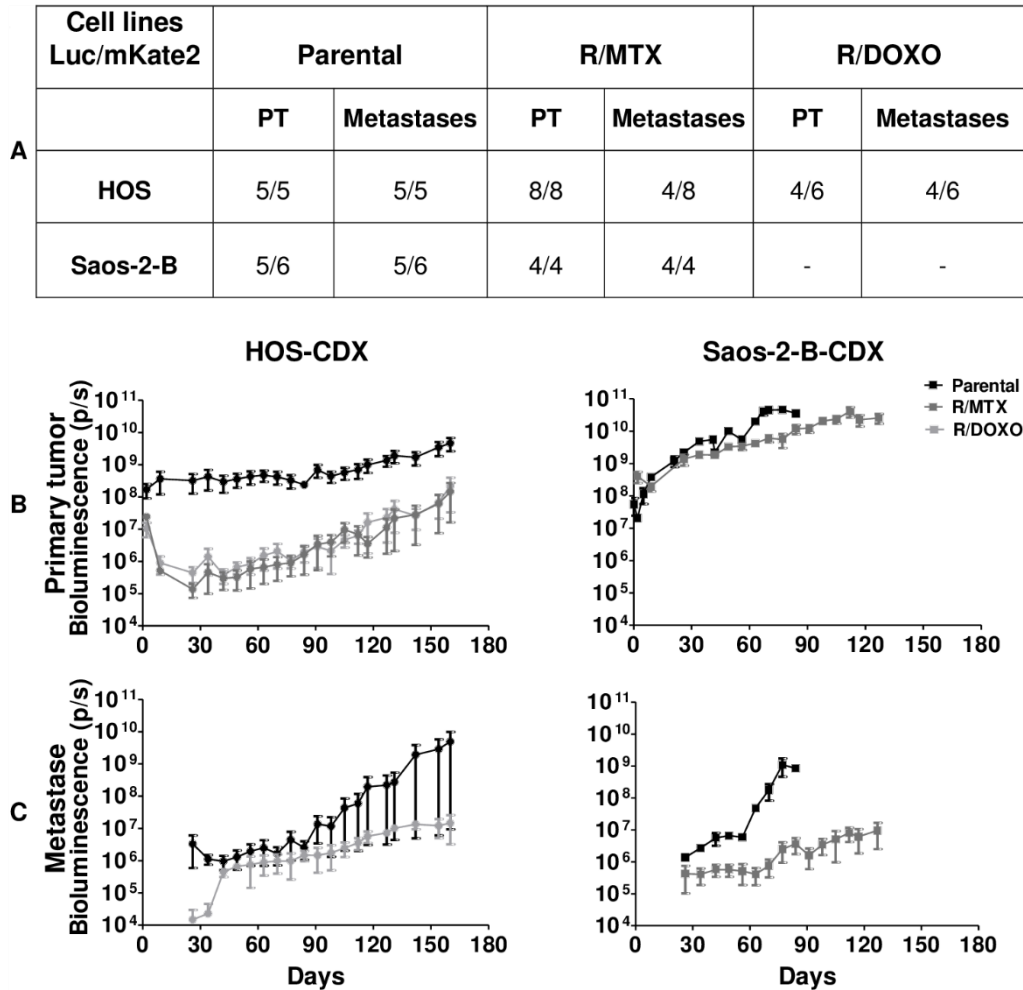


Figure 3.3: *In vivo* growth and metastatic behavior of the resistant orthotopic bioluminescent osteosarcoma cell line derived xenografts compared to their parental counterpart. *In vivo* tumor growth and metastatic potential of HOS-parental-CDX, Saos-2-B-parental-CDX, HOS-R/MTX-CDX, Saos-2-B-R/MTX-CDX and HOS-R/DOXO-CDX orthotopic bioluminescent models. A- Primary tumor growth engraftment and metastatic rate according to osteosarcoma cell line (Parental and Resistant). B- Primary tumor *in vivo* bioluminescence detection overtime. C- Metastases *in vivo* bioluminescence detection overtime.

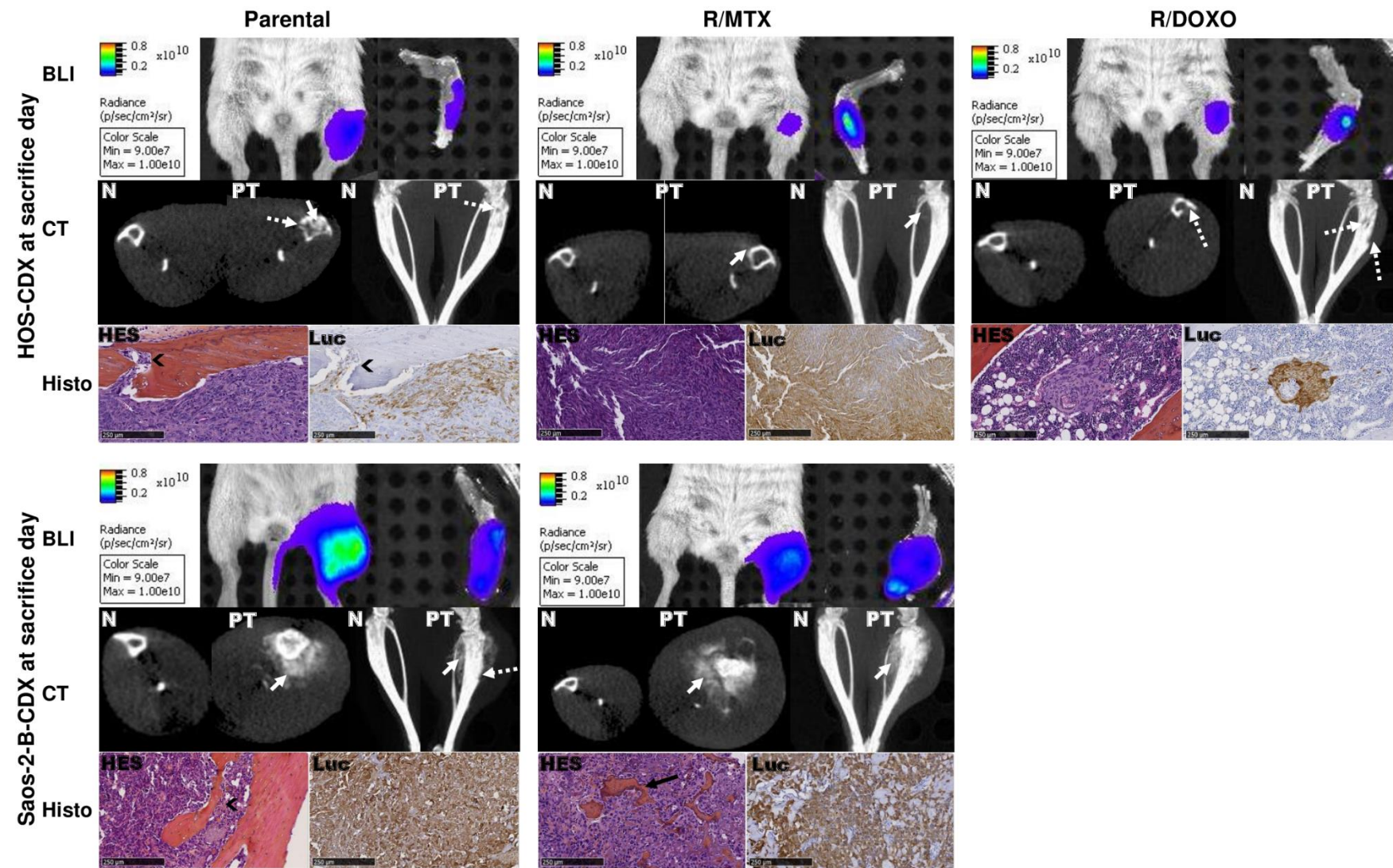


Figure 3.4: (previous page) *In vivo* primary tumor characteristics of the bioluminescent parental and resistant orthotopic cell-derived osteosarcoma xenograft models in NSG mice by intratibial injection. Orthotopic osteosarcoma bioluminescent models in NSG mice at sacrifice time: HOS-CDX (top panel), Saos-2-B-CDX (bottom panel); Both parental-CDX (left panel), both R/MTX-CDX (middle panel) and HOS-R/DOXO-CDX (right panel). *In vivo* bioluminescence imaging (BLI) by IVIS SpectrumCT system of the primary tumor (left leg) compared to the control leg (right leg). *In vivo* CT scan imaging (CT) by IVIS SpectrumCT system of the normal leg (N) and Primary tumor (PT), showing osteocondensation (plain white arrow) and osteolysis (dotted white arrow), changes were first noted 63, 91 and 77 days after injection for HOS-parental-CDX, HOS-R/MTX-CDX, HOS-R/DOXO-CDX and at day 41 and 49 days after injection for Saos-2-B-parental-CDX and Saos-2-R/MTX-CDX, respectively. Histology (Histo) using Hematoxylin Eosin Saffron (HES) and luciferase staining of the primary tumor and normal bone at 7.45x magnification, showing osteoid matrix (big black arrow) and infiltration by the tumor cells in the bone (small black arrow).

***In vivo* metastatic behavior of the resistant orthotopic cell-derived bioluminescent osteosarcoma models**

Metastases were detected by *in vivo* bioluminescence in all CDX models 30 days after injection, except for HOS-R/MTX-CDX where no metastases were detectable (Fig.3.3C). Metastases in parental-CDX models grew faster than in resistant-CDX models, without correlation with the primary tumor growth rate and size (Fig.3.3C). At mice sacrificed time (day 84 and 127 for parental and Saos-2-B-resistant-CDX, respectively, and day 160 for all HOS models), combined *ex vivo* bioluminescence and histology confirmed lung metastases in all models (Fig.3.5), although detectable only by *ex vivo* bioluminescence in HOS-R/MTX-CDX (Fig.3.5). Lung metastases were bigger, more frequent and numerous in the Saos-2-B-parental-CDX than in HOS-parental-CDX models, and in parental-CDX models compared to their resistant-CDX counterparts. Unique bone metastases on the opposite leg (not injected) and unusual spleen metastases were detected in all models except in HOS-R/MTX-CDX. HES did not detect morphological differences between parental and resistant CDX.

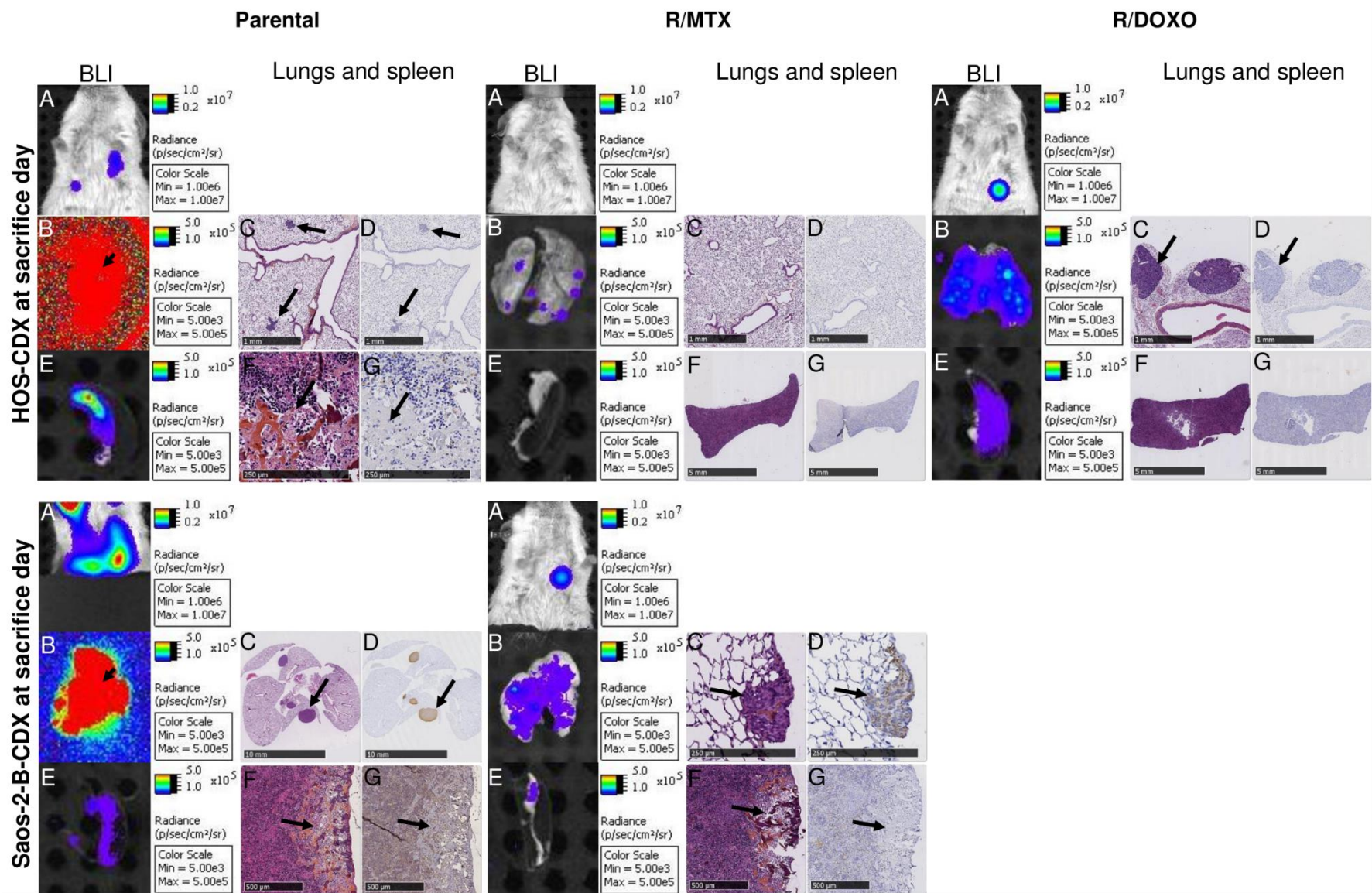


Figure 3.5: (previous page) *In vivo* metastatic behavior of the resistant orthotopic cell-derived xenografts bioluminescent osteosarcoma models comparatively to their parental counterpart in NSG mice by intratibial injection. Orthotopic osteosarcoma bioluminescent models in NSG mice at sacrifice time: HOS-CDX (top panel), Saos-2-B-CDX (bottom panel); Both parental-CDX (left panel), both R/MTX-CDX (middle panel) and HOS-R/DOXO-CDX (right panel). *In vivo* (A) and ex vivo bioluminescence of lung (B) and spleen (E) metastases (BLI). Lung Hematoxylin Eosin Saffron (HES) (C) and luciferase staining (D) at 1.5x magnification for all HOS-CDX and 0.21 and 10.8x magnification for Saos-2-B-parental-CDX and Saos-2-B-R/MTX-CDX, respectively. Spleen HES (F) and luciferase staining (G) at 10.8 and 0.36x magnification for HOS-parental-CDX and both Resistant-CDX, respectively, and 3x for all the Saos-2-B-CDX models. Plain arrows showed metastases.

***In vivo* resistance mechanisms**

PgP and MRP1 mRNA expression levels in the parental-CDX *in vivo* samples were increased compared to the levels observed *in vitro* in parental cell line they are issued of. PgP was higher in the Saos-2-B-CDX parental model (especially in the metastases comparatively to the primary tumor) and MRP1 higher in the parental HOS-CDX model. TOPO2A mRNA expression levels were decreased in both CDX models compared to the in vitro cells (metastases Saos-2-B showed slightly lower expression than primary tumor) (Fig.3.6A). PgP protein in IHC was detected in HOS-R/DOXO-CDX (Fig.3.6B) but not in the parental and HOS-R/MTX-CDX (data not shown) primary tumors.

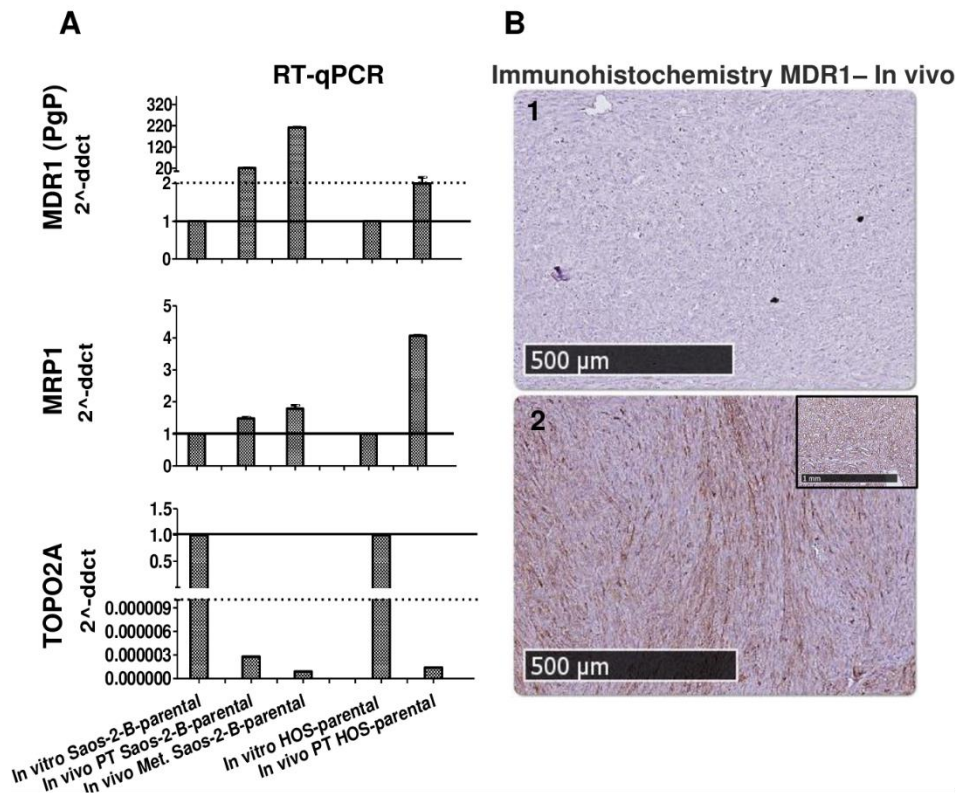


Figure.3.6: Resistance mechanism observed in the *in vivo* CDX models. A- MDR1 (PgP), MRP1 and TOPO2A expression in *in vivo* PT (Saos-2-B-parental and HOS-parental CDX modes) and in Metastases (Saos-2-B-parental-CDX model) normalized with the respectively *in vitro* parental cell line performed by RT-qPCR. B- MDR1 (PgP) expressed in the positive control (normal human kidney - image surrounded with black lines) and in HOS Parental (B1) and in HOS-R/DOXO (B2) CDX models in the PT tissue obtained by immunohistochemistry. PT- primary tumor, Met- metastases

***In vitro* behavior of the *in vivo* orthotopic cell-derived bioluminescent osteosarcoma models**

After sacrifice, cell derived from primary tumors of each resistant-CDX models were cultured *in vitro* and the drug sensitivity analyzed. All the resistant-CDX grew *in vitro* and remained drug resistance, with RI similar (Saos-2-B-R/MTX-CDX-cells; RI=37 and 34), decreased (HOS-R/DOXO-CDX-cells RI=212 and 42), or increased (HOS-R/MTX-CDX-cells; RI 156 and >2000), before and after *in vivo* injection, respectively (Fig.3.7).

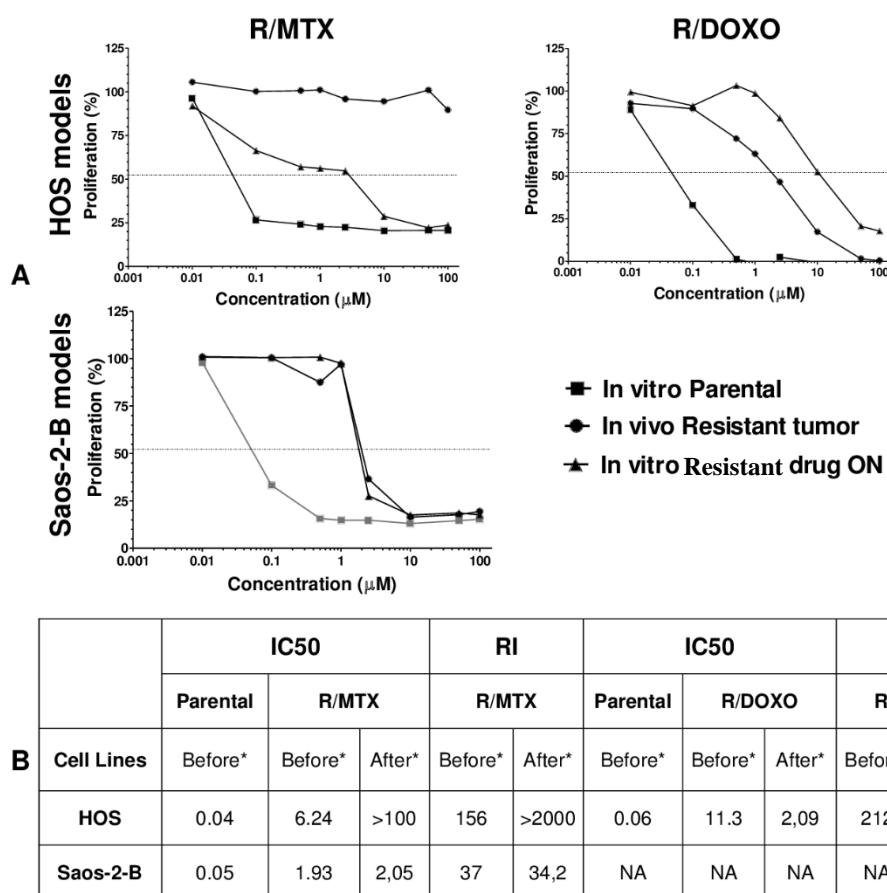


Figure.3.7: Resistance phenotype of the orthotopic resistant osteosarcoma CDX models cultured *in vitro* after mice sacrifice (HOS-R/MTX-CDX-cells, HOS-R/DOXO-CDX-cells and Saos-2-B-R/MTX-CDX-cells), comparatively to the respective parental and resistant drug ON cell line *in vitro*. A- Proliferation of each model treated with the respectively drug to which they are resistant: R/MTX – treated with MTX; R/DOXO – treated with doxorubicin. B – IC50 and RI of each model. Parental and Resistant drug ON before introduction in the mice and resistant drug ON cell line after injection in NSG mice and cultured *in vitro* after mice sacrifice. * Before or after injection of the cell lines in NSG mice. NA – Not available

Discussion

We developed *in vitro* osteosarcoma models resistant either to doxorubicin (HOS) or MTX (HOS, 143B, MG-63, 2 closely related Saos-2/Saos-2-B lines), by continuous *in vitro* exposure to these chemotherapeutic agents, adding new models to those described in the literature^{2,20–23}.

Acquired *in vitro* resistance establishment was influenced by initial sensitivity to the drugs, and other potential factors²⁴. In primary resistance lines, no further acquired resistance could be obtained (IOR/OS18 resistant to all drugs, mafosfamide high IC50 in all lines). In primary sensitive cells, MTX induced high resistance levels in all lines while doxorubicin resistance was more difficult to obtain and occurred in one line.

Modifications induced by *in vitro* acquired resistance affect both GE and CNA, in a drug and cell line dependent manner²⁴, with different mechanisms of resistance. As previously observed, doxorubicin-resistant line showed up-regulation of the multidrug drug resistant protein PgP by ABCB1 gain²⁵. However, PgP up-regulation in HOS-R/DOXO might not explain the whole resistant phenotype, several multiple multidrug resistance genes in CNA gained regions are candidates, as other genes implicated in the apoptotic response to doxorubicin. Mechanisms of acquired-MTX-resistance involved down-regulation of SCL19A1 mRNA coding for the ubiquitous transporter for folates (RFC)²⁶ and increased DHFR protein expression²⁶, with variation depending on the genetic background of osteosarcoma cells²⁰. Mechanism of resistance persisted despite drug removal, although at lower level for HOS-R/MTX, but not for MG-63-R/MTX where the resistance was lost after two weeks without drug. This resistant phenotype paralleled the mRNA level of SLC19A1, irrespective of the CNA variation observed. DHFR protein increased was dependent on the presence of the MTX in culture with involvement of post-transcriptional regulation as mRNA levels were up-regulated in the resistant lines drug OFF, and irrespective of the gain of DHFR region (present in HOS, 143B and MG-63, but not in SaOS-2 or Saos-2-B), The link between RB1 expression and MTX-resistance mechanisms previously reported with increased DHFR by gene amplification in RB1-positive osteosarcoma cell lines and RFC expression decrease without DHFR involvement in *RB1*-negative lines²⁰, does not totally applied to our models.

The incidence and mechanism of resistance acquired to these drugs differently affect other treatments used. As expected, the multi-drug resistant phenotype of HOS-R/DOXO decreased *in vitro* sensitivity of other anti-osteosarcoma drugs substrate of PgP (Etoposide, vincristine)²⁷. But other induced-changes in our

doxorubicin-resistant line might affect other drug sensitivity not necessarily linked to PgP. Indeed, MTX sensitivity was decreased as previously observed in other models²⁰ and associated with RFC expression down-regulation. Cisplatin sensitivity was not impacted²⁵ in the continuous shot exposure drug assay (72 hours). However, CNA analysis revealed an enrichment in genes involved in cisplatin resistance, which questioned the impact of concomitant long term administration of both drugs as used in patient first-line treatment^{5,28}. The impact on the clinical efficacy of ABCB1/ABCC1 inhibitor was shown to revert *in vitro* resistance in other doxorubicin-resistant osteosarcoma lines²⁷, will also have to be followed, on a multidrug treatment context. Cabozantinib was shown to inhibit PgP activity in hepatoblastoma cells²⁹, but did not revert resistance in our HOS-R/DOXO cell line. With our highly MTX-resistant lines (RI > 40), no cross-resistance was found with the other tested drugs. However, cross-resistance with doxorubicin and ifosfamide, (also with epirubicine, theprubicin and paclitaxel) but not with cisplatin, has been observed in low and intermediate MTX-resistant Saos-2 lines (RI of 4.87 and 12.73, respectively) with low RFC expression³⁰. The significance for the patients is unclear and probably more complexity is added by other potential cellular/molecular programs modified on acquired resistant lines, not directly linked to the mechanism of action and metabolism of one drug. Indeed, several more general, cellular and biological pathways were modulated in the resistant lines, implicated in cell adhesion, extra cellular matrix and immunity, which cannot fully be access *in vitro* but might modify the resistant-cell behavior *in vivo*.

The bone microenvironment is known to have an important role in osteosarcoma progression³¹, has been shown to influence drug sensitivity in osteosarcoma syngeneic models³² and might influence resistance phenotype²⁴. We developed *in vivo* orthotopic bioluminescent parental and resistant CDX models, with the same experimental procedure used for our previous parental-CDX models in NSG mice⁹. The different *in vivo* primary tumor bone behavior (slow growing osteolytic HOS-CDX, fast growing osteocondensed Saos-2-B-CDX), metastatic potential (faster metastatic spread in Saos-2-B-CDX) and morphology⁹ were retained by the resistant lines. However, these resistant lines showed clear *in vivo* behavior modifications. HOS-R/DOXO had lower engraftment rate. HOS-resistant-CDX had

initial adaptation difficulties to the bone microenvironment then their growth rates were faster than in parental line. Most importantly all resistant-CDX presented different metastatic behaviors, with a slower and lower lung metastatic spread than in parental lines. Similar behavior has been observed with other *in vivo* models of metastatic spread by direct intra-venous injections of doxorubicin-resistant osteosarcoma U2OS and Saos-2 variants (MDR1 overexpression by gene amplification) in athymic nude mice, only when resistant-cells injected straight after treated medium culture, and not when cultured in medium free of drug for a week before injection²⁵.

In our CDX-models, the resistant lines at mice sacrificed retained their resistant phenotype. Times intervals between cell injection and detection of primary tumor growth and metastatic spread are still compatible with drug testing *in vivo*.

These resistant-CDX models might be useful to further test new drug in osteosarcoma models and might complement other osteosarcoma models. However, they do not fully reflect the heterogeneity and complexity of osteosarcoma human tumor and does not give access to the immune system, as developed in immunocompromised mice. Patient derived xenograft models from relapsed samples might bring complementary knowledge on human osteosarcoma resistance to drug, while syngeneic (mice or dog) or humanized osteosarcoma models might partially give access to the immunity role in osteosarcoma resistance to treatment.

Acknowledgments

We thank the Platform of Preclinical Evaluation for providing immunocompromised mice and animal care, Olivia Bawa for performing the histology slides, Irene Villa for having scanned the histology slides and Alec Guyomard for some genetic samples analysis. To Noémie Assoun for help on some DNA/RNA extraction, Valerie Roufiac for help on IVIS spectrumCT system function, Carole Lecinse for critical reading of the manuscript and to the Portuguese Foundation for Science and Technology (FCT, <http://www.fct.pt/>) through the PhD fellowship to Maria Eugénia Marques da Costa (SFRH/BD/89137/2012).

References

1. Yang X, Yang P, Shen J, et al. Prevention of multidrug resistance (MDR) in osteosarcoma by NSC23925. *Br J Cancer*. 2014;110(12):2896-2904.
2. Wang J, Li G. Mechanisms of methotrexate resistance in osteosarcoma cell lines and strategies for overcoming this resistance. *Oncol Lett*. 2015.
3. Posthumadeboer. Mechanisms of Resistance Molecular involvement Drug Target Drug References. *Oncol Discov*. 2013.
4. Duan Z, Gao Y, Shen J, et al. miR-15b modulates multidrug resistance in human osteosarcoma *in vitro* and *in vivo*. *Mol Oncol*. 2017;11(2):151-166.
5. Bielack SS, Smeland S, Whelan JS, et al. Methotrexate, Doxorubicin, and Cisplatin (MAP) Plus Maintenance Pegylated Interferon Alfa-2b Versus MAP Alone in Patients With Resectable High-Grade Osteosarcoma and Good Histologic Response to Preoperative MAP: First Results of the EURAMOS-1 Good Response Randomized Controlled Trial. *J Clin Oncol*. 2015;33(20):2279-2287.
6. He H, Ni J, Huang J. Molecular mechanisms of chemoresistance in osteosarcoma (Review). *Oncol Lett*. 2014;7(5):1352-1362.
7. Ottaviano L, Schaefer K-L, Gajewski M, et al. Molecular characterization of commonly used cell lines for bone tumor research: A trans-European EuroBoNet effort. *Genes, Chromosom Cancer*. 2010;49(1):40-51.
8. Lauvrak SU, Munthe E, Kresse SH, et al. Functional characterisation of osteosarcoma cell lines and identification of mRNAs and miRNAs associated with aggressive cancer phenotypes. *Br J Cancer*. 2013;109(8):2228-2236.
9. Marques da Costa ME, Daudigeos-Dubus E, Gomez-Brouchet A et al. Establishment and characterization of *In vivo* orthotopic bioluminescent xenograft models from human osteosarcoma cell lines in Swiss nude and NSG mice. *Cancer Med*. 2018;7(3):665-676.

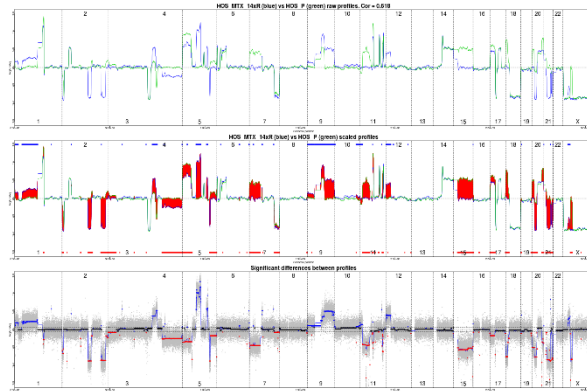
10. Uluçkan Ö, Bakiri L, Wagner EF. Characterization of Mouse Model-Derived Osteosarcoma (OS) Cells *In Vitro* and *In Vivo*. In: Humana Press, New York, NY; 2015:297-305.
11. Olshen AB, Venkatraman ES, Lucito R, Wigler M. Circular binary segmentation for the analysis of array-based DNA copy number data. *Biostatistics*. 2004;5(4):557-572.
12. Harttrampf AC, Lacroix L, Deloger M, et al. Molecular Screening for Cancer Treatment Optimization (MOSCATO-01) in Pediatric Patients: A Single-Institutional Prospective Molecular Stratification Trial. *Clin Cancer Res*. 2017;15;23(20):6101-6112.
13. Patro R, Duggal G, Love MI, Irizarry RA, Kingsford C. Salmon provides fast and bias-aware quantification of transcript expression. *Nat Methods*. 2017;14(4):417-419.
14. Love MI, Huber W, Anders S. Moderated estimation of fold change and dispersion for RNA-seq data with DESeq2. *Genome Biol*. 2014;15(12):550.
15. Tsubaki M, Satou T, Itoh T, et al. Overexpression of MDR1 and survivin, and decreased Bim expression mediate multidrug-resistance in multiple myeloma cells. *Leuk Res*. 2012;36(10):1315-1322.
16. Yang X-R, Xiong Y, Duan H, Gong R-R. Identification of genes associated with methotrexate resistance in methotrexate-resistant osteosarcoma cell lines. *J Orthop Surg Res*. 2015;10:136.
17. Guo Z, Zhang T, Wu J, Wang H, Liu X, Tian L. Genetic polymorphisms in COL18A1 influence the development of osteosarcoma. *Int J Clin Exp Pathol*. 2015;8(9):11531-11536.
18. Gvozdenovic A, Boro A, Meier D, et al. Targeting $\alpha\beta 3$ and $\alpha\beta 5$ integrins inhibits pulmonary metastasis in an intratibial xenograft osteosarcoma mouse model. *Oncotarget*. 2016;7(34):55141-55154.

19. Both J, Krijgsman O, Bras J, et al. Focal chromosomal copy number aberrations identify CMTM8 and GPR177 as new candidate driver genes in osteosarcoma. *PLoS One*. 2014;9(12):e115835.
20. Serra M, Reverter-Branchat G, Maurici D, et al. Analysis of dihydrofolate reductase and reduced folate carrier gene status in relation to methotrexate resistance in osteosarcoma cells. *Ann Oncol*. 2004;15(1):151-160.
21. Hattinger CM, Stoico G, Michelacci F, et al. Mechanisms of gene amplification and evidence of coamplification in drug-resistant human osteosarcoma cell lines. *Genes, Chromosom Cancer*. 2009;48(4):289-309.
22. Selga E, Oleaga C, Ramírez S, de Almagro MC, Noé V, Ciudad CJ. Networking of differentially expressed genes in human cancer cells resistant to methotrexate. *Genome Med*. 2009;1(9):83.
23. Yang J, Guo W, Wang L, et al. Cisplatin-resistant osteosarcoma cells possess cancer stem cell properties in a mouse model. *Oncol Lett*. 2016;12(4):2599-2605.
24. Zahreddine H, Borden KLB, Wu JH. Mechanisms and insights into drug resistance in cancer. 2013;313(9):8-1.
25. Serra M, Scotlandi K, Manara MC, et al. Establishment and characterization of multidrug-resistant human osteosarcoma cell lines. *Anticancer Res*. 1993;13(2):323-329.
26. Guo W, Healey JH, Meyers PA, et al. Mechanisms of Methotrexate Resistance in Osteosarcoma. *Clin Cancer Res*. 1999:621-627.
27. Fanelli M, Hattinger CM, Vella S, et al. Targeting ABCB1 and ABCC1 with their Specific Inhibitor CBT-1® can Overcome Drug Resistance in Osteosarcoma. *Curr Cancer Drug Targets*. 2016;16(3):261-274.
28. Piperno-Neumann S, Le Deley M-C, Rédini F, et al. Zoledronate in combination with chemotherapy and surgery to treat osteosarcoma (OS2006):

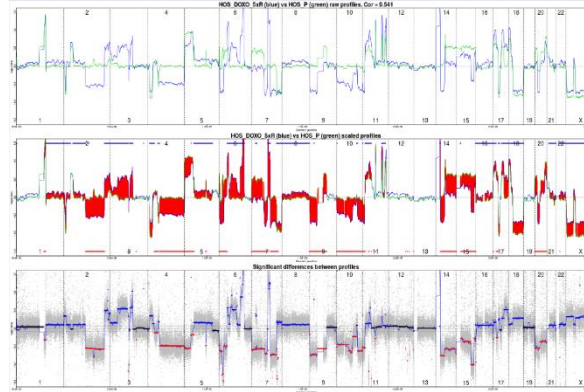
- a randomised, multicentre, open-label, phase 3 trial. *Lancet Oncol.* 2016;17(8):1070-1080.
29. Xiang Q, Chen W, Ren M, et al. Cabozantinib suppresses tumor growth and metastasis in hepatocellular carcinoma by a dual blockade of VEGFR2 and MET. *Clin Cancer Res.* 2014;20(11):2959-2970.
 30. Wang J, Li G. Relationship between RFC gene expression and intracellular drug concentration in methotrexate-resistant osteosarcoma cells. *funpecrp.com.br Genet Mol Res Mol Res.* 2014;13(133):5313-5321.
 31. Zhang Y, Mai Q, Zhang X, Xie C, Zhang Y. Microenvironment Signals and Mechanisms in the Regulation of Osteosarcoma. In: *Osteosarcoma - Biology, Behavior and Mechanisms. InTechOpen, London, UK.* 2017.
 32. Creen V, Biteau K, Amiaud J, et al. Bone microenvironment has an influence on the histological response of osteosarcoma to chemotherapy: retrospective analysis and preclinical modeling. *Am J Cancer Res.* 2017;1;7(11):2333-2349.

Supplementary data

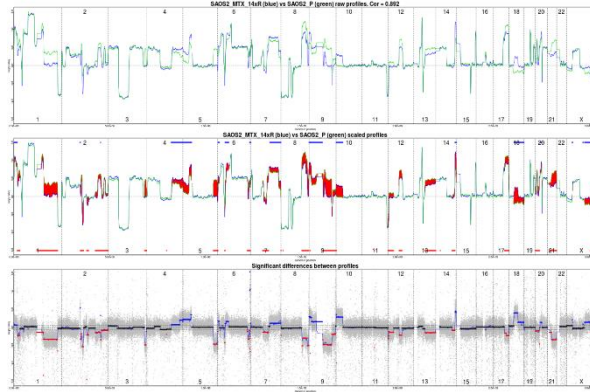
HOS vs HOS-R/MTX



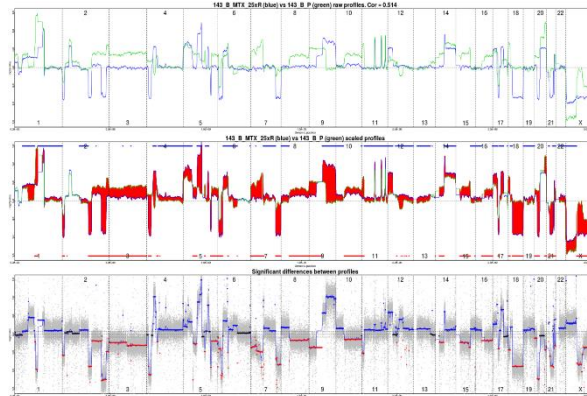
HOS vs HOS-R/DOXO



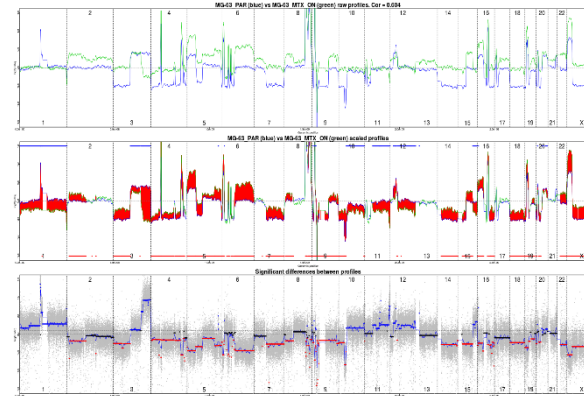
Saos-2 vs Saos-2-R/MTX



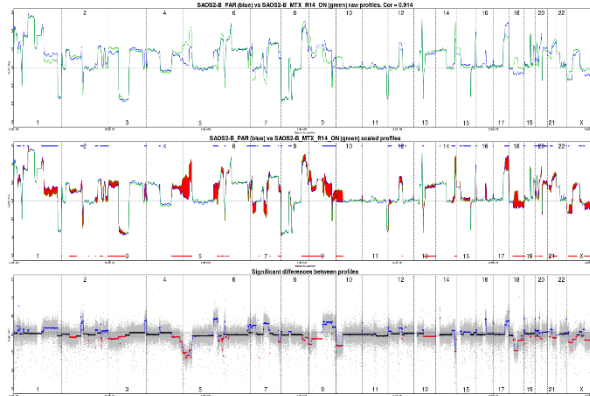
143B vs 143B-R/MTX



MG-63 vs MG-63-R/MTX



Saos-2-B vs Saos-2-B-R/MTX



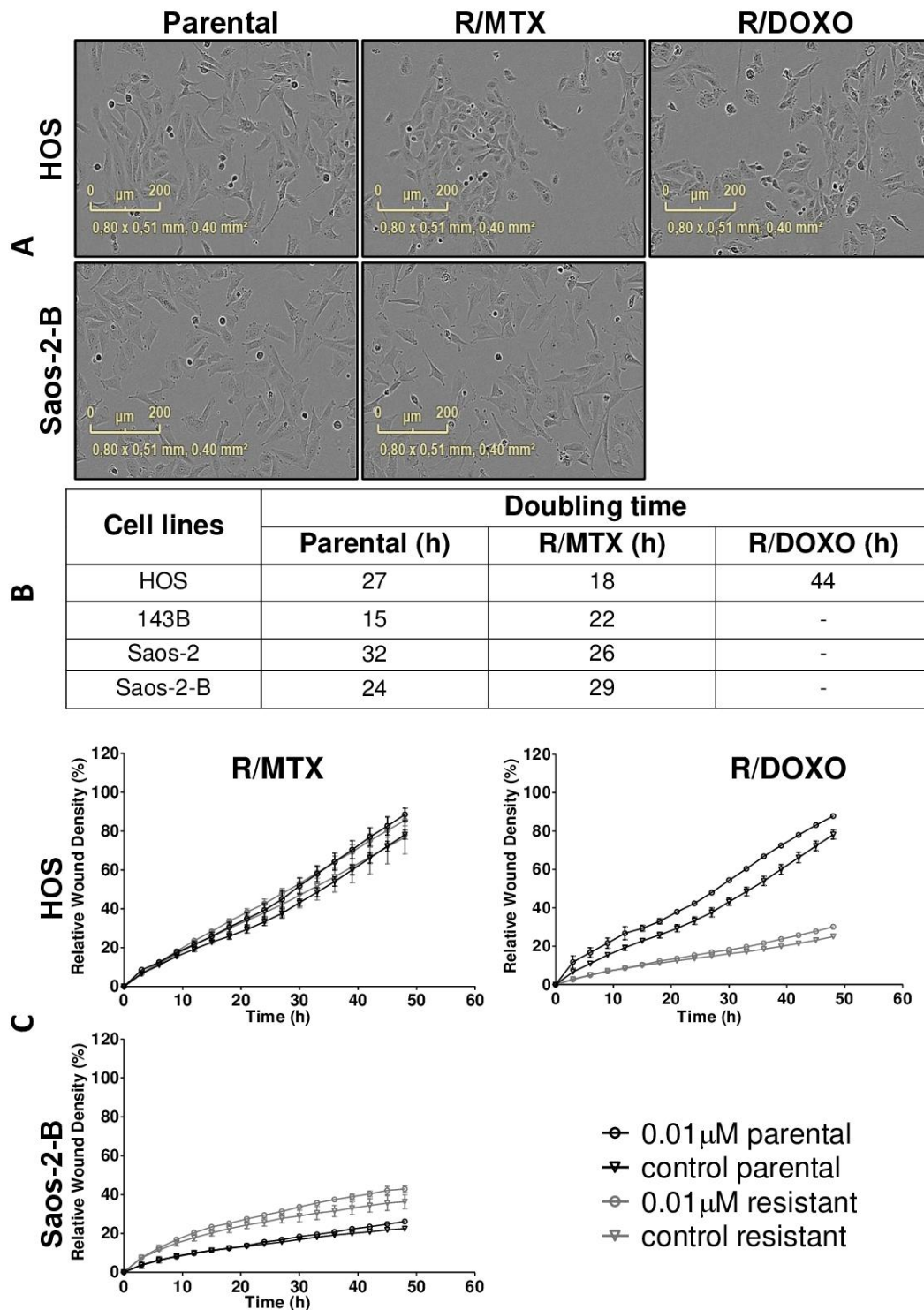
Supplementary Figure.3.S1: CGH differential analysis of parental and resistant cell lines.

Supplementary Table.3.SI: Primers were used to amplify topoisomerase IIa (*TOPO2A*), multidrug resistance protein 1 (*MDR1*) or P-glycoprotein 1 (*PgP*), multidrug resistance associated protein 1 (*MRP1*) and Glyceraldehyde 3-phosphate dehydrogenase (*GAPDH* – used as control) cDNAs by quantitative real-time PCR.

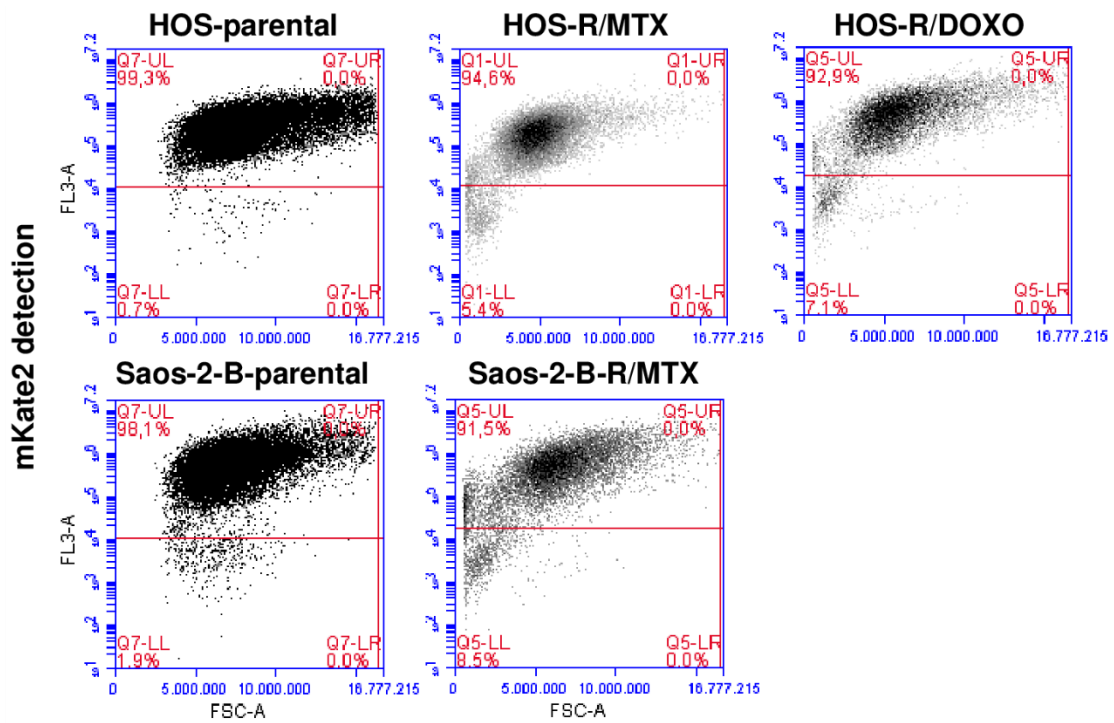
Gene	forward primer	reverse primer
<i>MDR1</i>	5'-TGGAGGAAGACATGACCAGG-3'	5'-CAAGACCTCTTCAGCTACTGC-3'
<i>MRP1</i>	5'-TCTACCTCCTGTGGCTGAATCTG-3'	5'-CCGATTGTCTTTGCTCTTCATG-3'
<i>TOP2A</i>	5'-TTGAAGACGCTTCGTTATGGG-3'	5'-CCATCACAACCTGGCCCTCTC-3'
<i>GAPDH</i>	5' ATCCCATCACCATCTTCCAG-3'	5' CCATCACGCCACAGTTTCC-3'

Supplementary Table.3.SII: Acquired *in vitro* resistance to MTX and DOXO. IC₅₀ values of the Parental and resistant cell lines to MTX and to DOXO Drug ON and Drug OFF and of DOXO Resistant cell line treated with etoposide (R/DOXO). IC₅₀ values were calculated using Prisma version5 using cell proliferation data after 72h of treatment.

	IC50								
	Resistance to MTX			Resistance to Doxo			R/DOXO Etoposide		
	Parental	Drug ON	Drug OFF P9	Parental	Drug ON	Drug OFF P9	Parental	Drug ON	Drug OFF P9
HOS	0.04	6.24	1.64	0.06	11.3	4.36	0.7	180	90.5
HOS-143B	0.04	4.13	4.64	-	-	-	ND	ND	ND
Saos-2	0.05	2.05	1.78	-	-	-	ND	ND	ND
Saos-2-B	0.05	1.93	1.51	-	-	-	-	-	-
MG-63	0.05	2.91	0.1	-	-	-	ND	ND	ND



Supplementary Figure.3.S2: *In vitro* characteristics of HOS and Saos-2-B parental and cell lines resistant to MTX and DOXO. A- Morphology; B- Doubling time; C -Migration potential with (0.01 μ M) and without (control) treatment. MTX resistant Cell lines were treated with MTX and the DOXO resistant cell line were treated with doxorubicin (DOXO). Parental cell lines were treated with MTX and DOXO.



Supplementary Figure.3.S3: Characterization of luciferase-transfected osteosarcoma cells. Data shown for the two osteosarcoma parental cell lines (HOS-parental and Saos-2-B-parental) and for the respectively methotrexate and doxorubicin resistant cell lines (HOS-R/MTX, HOS-R/DOXO and Saos-2-B-R/MTX) after FACS selection showing a rate of more than 90% of luciferase positive cells.

Supplementary Table.3.SIII: Morphological and histological characteristics of all osteosarcoma bioluminescent orthotopic CDX: HOS-parental-CDX, HOS-R/MTX-CDX, HOS-R/DOXO-CDX, Saos-2-B-parental-CDX and Saos-2-B-R/MTX-CDX. BLI- *In vivo* and *ex vivo* bioluminescence; CT-Computed Tomography; Histo-Histology; FB-fibroblastic subtype; OB-Osteoblastic subtype; HG-High-Grade osteosarcoma; NA-Not Available; ND-Not done; + -Positive detection; - -Negative detection; Met-Metastases.

Cell line Luc/mKate 2	Resistance	Primary tumor				Metastases					
		Histo	BLI	CT		Lung		Bone		Spleen	
		Sub-type		Calcification	Osteolysis	Histo	BLI	Histo	BLI	Histo	BLI
HOS	Parental	HG FB+OB	++	+	++	++	++	-	-	+	+
		HG FB+OB	++	+	++	++	++	-	+	-	-
		HG FB+OB	++	+	+	-	+	-	-	-	-
		HG FB+OB	++	+	+	-	+	-	-	-	-
		HG FB+OB	++	+	+	-	+	-	-	-	-
	R/MTX	HG FB+OB	+	+	+	-	+	-	-	-	-
		-	+	-	-	-	-	-	-	-	-
		HG FB+OB	+	+	NA	-	+	-	-	-	-
		-	+	NA	NA	-	-	-	-	-	-
		-	+	NA	NA	-	+	-	-	-	-
		HG FB+OB	+	+	+	-	-	-	-	-	-
		-	+	+	+	-	-	-	-	-	-
		+	+	-	+	-	+	-	-	-	-
	R/DOXO	HG FB+OB	+	-	+	-	+	-	-	-	-
		HG FB+OB	+	-	+++	+	+	-	+	-	+
		HG FB+OB	+	-	+	-	+	-	-	-	-
		-	+	-	-	-	-	-	-	-	-
Saos-2-B	Parental	HG OB	+++	++++	+	-	++	-	ND	+	+
		HG FB+OB	+++	++++	+	+++	++++ (Visible)	-	ND	-	+
		HG OB	+++	++++	+	+	++++ (Visible)	-	ND	+	+
		HG OB	+++	++++	+	+++	++++ (Visible)	+	+	-	+
		HG OB	+++	++++	+	+	+++	+	+	-	+
	R/MTX	HG FB+OB	+++	++++	+	+	++	-	-	-	-
		HG OB	+++	+++	+	-	+	-	-	+	+
		HG FB+OB	+++	+++	+	-	+	+	+	+	+
		HG FB+OB	+++	++++	+	+	+	-	-	-	-

Chapter 4:

Establishment and characterization of *in vivo* orthotopic osteosarcoma patient-derived xenograft (PDX) models

Establishment and characterization of new *in vivo* orthotopic osteosarcoma patient-derived xenograft models

Maria Eugenia Marques da Costa^{1,2}, Noémie Assoun¹, Windy Rondof¹, Anne Gomez-Brouchet³, Jean-Yves Scoazec⁴, Tiphaine Adam-de-Baumais¹, Marlène Pasquet⁵, Conceição Santos⁶, Birgit Geoerger^{1,7}, Estelle Daudigeos-Dubus^{1*},
Nathalie Gaspar^{1,7*}

¹ Vectorology and Anticancer Therapies, CNRS UMR 8203, Paris-Sud University, Gustave Roussy, Paris-Saclay University, 94 805 Villejuif, France

² CESAM & Department of Biology, University of Aveiro, 3810 Aveiro, Portugal

³ Department of Pathology, IUCT-Oncopole, CHU of Toulouse and University of Toulouse; Pharmacology and structural biology institut, CNRS UMR5089, 31059 Toulouse, France

⁴ Department of medical Biology and pathology, Gustave Roussy, 94 805 Villejuif, France

⁵Department of pediatric hemato-oncology, CHU of Toulouse, 31059 Toulouse, France

⁶ Department of Biology, Faculty of Sciences, University of Porto, Rua do Campo Alegre, 4000 Porto, Portugal

⁷ Department of Oncology for Children and Adolescents, Gustave Roussy, 94805 Villejuif, France

*Both author have contributed equally to the last author position

Abstract

Osteosarcoma is a rare bone tumor of the adolescent and young adults in which resistance to chemotherapy and metastatic spread constitute the main prognostic factors. Despite multiple efforts to improve osteosarcoma treatment in the last four decades, survival has not improved and metastatic relapse, mainly in the lungs, constitutes the main cause of treatment failure. New drug identification and validation requires pre-clinical models that capture the diversity, heterogeneity of the patients' tumors and mimic at best the human resistant disease. Therefore, we established and characterized patient-derived xenograft (PDX) osteosarcoma models in NSG mice, in a subcutaneous and an orthotopic bone (paratibial) setting, derived from human osteosarcoma biopsy samples of patients with refractory or relapse disease after at least one line of chemotherapy. From 3 sample patients one subcutaneous and one orthotopic PDX-model were obtained to each one (3 subcutaneous and 3 orthotopic PDX-models). Morphological and molecular characterization using histology, whole exome and RNA sequencing revealed a high consistency between the models and their primary tumor at relapse from they are issued but also with the tumor at diagnosis of the patient. Secondary *in vitro* cell cultures issued from these 3 subcutaneous PDX models confirmed high resistance to chemotherapy, especially to methotrexate. Sensitivity testing to the multi-tyrosine kinase inhibitors cabozantinib, pazopanib and regorafenib *in vitro* showed high sensitivity to the prior two agents but resistance to regorafenib. Sensitivity to multi-tyrosine kinase inhibitor will be further tested *in vivo* and compared to the clinical response observed in the patient.

Key words: osteosarcoma, *In vivo*, Patient Derived Xenograft (PDX), paratibial, subcutaneous, resistance

Introduction

Osteosarcoma (OS) is a rare disease of adolescents and young adults with no outcome improvement in the last 40 years¹. Patients suffering from this highly malignant bone cancer^{2,3}, especially those with metastatic disease at diagnosis, those with poor histological response to first line neoadjuvant chemotherapy and those who relapse at lung metastatic site, have a very dismal prognosis⁴⁻⁶. The last decade of multiple clinical phase II trials in relapse/refractory osteosarcomas have not translated in improved outcome⁷. Factors that contribute to this situation are the complexity of osteosarcoma genetics and epigenetics⁸, the importance of bone and immune microenvironment in the disease^{2,9}, and the lack of suitable models representative of the diversity, complexity and heterogeneity of osteosarcomas, as well as of the chemo-resistant and metastatic behaviors, that could help for pre-clinical testing of innovative effective therapies and for the identification of predictive biomarkers of efficacy^{2,10}.

Several *in vivo* cell-derived xenografts (CDX) in murine sub-cutaneous models and more rarely orthotopic CDX-models of human osteosarcoma were developed and characterized¹⁰⁻¹³. Most of these CDX derived from primary tumor samples at diagnosis and more rarely from metastatic or recurrent diseases^{8,11}. Few were developed specifically for their metastatic potential¹⁴. Although they have provided important information in the understanding of osteosarcoma biology, these CDX-models which derived from cell lines that might have been in *in vitro* culture for a long time, were not fully representative of the osteosarcoma heterogeneity^{15,16}. In the last years, patient-derived xenograft (PDX) models have been developed to better mimic the biology and heterogeneity of human tumors¹⁵. However, few PDX models have yet been described for osteosarcoma, partly due the low engraftment rate and the relatively long time required for tumor establishment of this models^{17,18}. Different programs are ongoing to established PDX models from different adult and pediatric tumor types, in Unites States (MAST protocol, NCT01050296)¹⁹ and Europe (MAPPYACTS trial, NCT02613962; ITCC-P4 within the IMI2 program). Very recently, 15 osteosarcoma orthotopic PDX models were published from either diagnostic (n=8) or recurrence samples (n=7, including 2 local relapses) (MAST protocol, NCT01050296)¹⁹ with no drug evaluation.

We will present here the establishment and characterization of new subcutaneous and orthotopic, paratibial osteosarcoma PDX models in NOD-SCID- γ c-/- (NSG) mice, issued from relapsed osteosarcoma samples of patients accrued in the MAPPYACTS trial (NCT02613962, Molecular Profiling for Pediatric and Young Adult Cancer Treatment Stratification) at Gustave Roussy Institute (Villejuif, France) and some drug testing results.

Methods

Translational research context

MAPPYACTS clinical trial (NCT02613962, Molecular Profiling for Pediatric and Young Adult Cancer Treatment Stratification) is a prospective, multicentric, clinical proof-of-concept study to stratify targeted therapies adapted to molecular profiling of relapsed and refractory pediatric tumors^{20,21}. Ancillary studies included the development and characterization of experimental patient derived xenograft (PDX) models and primary cell lines.

All models presented here have been developed from patients with refractory/relapsed osteosarcoma accrued at Gustave Roussy.

Human refractory/relapsed osteosarcoma tumor sample collection

Briefly, following informed consent, tumor samples were collected by surgical resection or CT or ultrasound-guided intentional tumor biopsy, with one piece immediately frozen for the clinical analysis and a fresh tumor sample obtained at the same time, immediately placed in transport media (DMEM media used with 1% antibiotics), conserved at 4°C for a maximum of 24 h or immediately transferred to the research laboratory at room temperature or soft frozen in FBS containing 10% DMSO. In patients, blood samples were collected at the same time as tumor samples and were submitted to FICOLL gradient separation, to extract constitutional DNA.

The clinical part included both Whole Exome Sequencing (WES) and RNA Sequencing (RNAseq) on patients' tumor tissues. Data interpretation of molecular

genetic alterations detected by WES and RNAseq and treatment recommendation were done within a multidisciplinary therapeutic molecular biology tumor board. For the development of preclinical models, the samples were immediately processed at their arrival at Gustave Roussy sites. The different procedures are described below.

Frozen tumor sample at diagnosis issued from the patients with successful PDX models were collected and analyzed with the same technics (WES, RNAseq).

Development of *In vivo* Orthotopic human osteosarcoma PDX models

Experiments were validated by the CEEA26, CEEA PdL N°6, Ethic committee (approval number: 2015032614359689 V7) and carried out under conditions established by the European Community (Directive 2010/63/UE). Animals were purchased at Gustave Roussy (Villejuif, France) and maintained in the respective animal facilities following standard animal regulation, health and care, and ethical controls.

Osteosarcoma PDXs were established from relapsed osteosarcoma patients by sample implantation in immunocompromised NOD.Cg-Prkdc^{scid} Il2rg^{tm1Wjl}/SzJ (NSG) mice or in Nude mice. Under anesthesia with isoflurane (3% isoflurane, 1.5l/min air), tumor samples were implanted either subcutaneously (~5 mm³) by performing a skin incision on the back and implanting the tumor sample in the flanks under the skin²³ and/or on orthotopic position, paratibially (~2 mm³) between muscle and bone tibia after a 0.5 cm skin incision and a gentle activation of the periosteum (periosteum denudation)¹⁰. For the first patients, implantation was also performed into the left kidney capsule (tumor sample of 2-5 mm³; engraftment confirmed with an Aplio XG ultrasound equipped with a probe of high frequency wide band, 7-14 MHz; LTP 1202; Toshiba), to offer a vascularized hypoxic microenvironment to the tumor²⁴.

Subcutaneous and paratibial xenografts were detected by palpation, tumor gross apparition (caliper measurements), as well as bone structure alterations by CT scan imaging for paratibial model. Surgery and CT scan imaging were performed under anesthesia with 3% (v/v) isoflurane. To avoid bone pain, an analgesic (buprenorphine at 0.3 mg/kg) was applied in addition to the general anesthesia or

when symptoms appeared. Clinical status, tumor uptake and tumor growth were evaluated 1-3 times a week. The experiments lasted until tumors reached specific endpoints detailed in the ethical projects like significant weight loss or difficulty to walk. Tumor doubling time (T_d) was determined in an exponential growth phase between 200 and 400 mm³, for the subcutaneous models²³.

If tumor growth was not detected 6 months after implantation, the mice were sacrificed, and considered as an engraftment failure. When tumor grew, the mice were sacrificed when tumor volume reach around 600 mm³ in the kidney capsule implantation, 1500 mm³ subcutaneously or when clinical signals (eg difficulties to move) started to appear in paratibial models. Then, for each further passage, the PDX tumor was divided in different pieces, one for new mice implantation subcutaneously and/or paratibially, one for soft congelation (frozen in FBS, +1% (v/v) DMSO), one for dry congelation (frozen in nitrogen) and one prepared for histology.

***In vivo* CT scan imaging**

IVIS SpectrumCT (Perkin Elmer, Courtaboeuf, France) was used for images acquirement. This system allows the primary tumor and metastases detection by X-ray tomography co-registered with optical images. The lower section of the body (area of the lower legs) was imaged for primary tumor detection and the chest to detect metastatic spread, especially to the lung.

Histology

Organs were fixed in 4% (v/v) paraformaldehyde, and embedded in paraffin. Tissues were stained with hematoxylin-eosin-safranin (HES) for morphology. Slides were examined using light microscopy (Zeiss, Marly-Le-Roy, France) and a single representative whole-tumor tissue section from each animal was digitized using a slide scanner NanoZoomer 2.0-HT (C9600-13, Hamamatsu Photonics). Histology was reviewed by a human bone expert pathologist.

***In vitro* primary and secondary cell culture**

Osteosarcoma cells from human osteosarcoma relapsed samples were cultured *in vitro* directly from the patient's tumor sample (primary cultures) or from osteosarcoma PDX samples of our new growing models after passage 2 (secondary cultures). For both types of culture, each tumor sample was cut in several small pieces using a scalpel and then dissociated mechanically with a 22G needle in medium to prevent the tumor from drying out. The tumor preparation was resuspended in Dulbecco's modified Eagle medium (DMEM, GIBCO/Invitrogen, Saint Aubin, France) supplemented with 20% (v/v) fetal bovine serum (FBS, GIBCO/Invitrogen, Saint Aubin, France), plated in T75 flasks and incubated at 37°C in a humidified atmosphere (5% CO₂ and 95% air). All the procedures were performed under sterile conditions. Mycoplasma test was performed each month by PCR.

Compounds

The compounds used (doxorubicin, methotrexate, cisplatin, etoposide), were purchased from Sigma Aldrich (St Louis, MO, USA), from Toronto Research Chemicals Inc (TRC - Toronto, Canada) (mafosfamide) and from LC Laboratories (US, Canada) (regorafenib, pazopanib, cabozantinib). All the compounds were diluted in dimethyl sulfoxide (DMSO) (Sigma Aldrich, St Louis, MO, USA) except cisplatin diluted in N,N-dimethylformamide (DMF) (Sigma Aldrich, St Louis, MO, USA) and stored at -20°C at 10 mM stock solution.

Treatment (MTS assay)

Growth inhibition was determined using the CellTiter 96 Aqueous One Solution Cell Proliferation Assay (MTS assay) (Promega Corporation, Charbonnieres, France), according to the manufacturer instructions and as performed before¹⁰.

Cells issued from our PDX models were seeded *in vitro* in DMEM supplemented with 20% (v/v) FBS at 7000 cells/well in a 96-well plate and incubated at 37°C under overnight. The cells were treated with different drugs at concentrations ranging from 0 to 100 µM (doxorubicin, MTX, etoposide, mafosfamide, cabozantinib, regorafenib and pazopanib), or 0 to 50 µM (cisplatin). Seventy-two hours after, cell viability was

determined by adding 20 µl of MTS solution to each well. After 1-5h of incubation (cell line metabolism dependent) at 37°C cell proliferation was measured at an emission wavelength of 490 nm in an automatic plate reader (Elx808; Fisher Bioblock Scientific SAS, Illkirch, France). The IC50 was calculated as the drug concentration that inhibits cell growth by 50% compared with control.

Molecular characterization of human samples and *in vivo* PDX-models (WES and RNAseq)

Human samples and osteosarcoma PDX samples, either subcutaneous or paratibial, were frozen in liquid nitrogen until the moment of extraction. Tumor DNA and RNA, and germline DNA were isolated using AllPrep DNA/RNA micro kit (Qiagen, Germany) according manufacturer's instructions.

Whole Exome (WES) and RNA sequencing analysis was performed as previously described²². Whole exome sequencing (WES) was performed from 500 ng of sample (tumor, using Agilent SureSelect V5 (50Mb) or Clinical Research Exome (54Mb) kit. The mutational load obtained using WES, was calculated by dividing the number of somatic non-synonymous mutations by the number of bases having a depth greater than or equal to 4 in the tumor BAM file. RNA sequencing libraries were prepared with TruSeq Stranded mRNA kit following recommendations: the key steps consist of PolyA mRNA capture with oligo dT beads 1 µg total RNA, fragmentation to approximately 400 bp, DNA double strand synthesis, and ligation of Illumina adaptors amplification of the library by PCR for sequencing. Libraries sequencing was performed using Illumina sequencers (NextSeq 500 or HiSeq 2000/2500/4000) in 75 bp paired-end mode in both techniques and data sequencing were processed by bioinformatics analyses. For the optimized detection of potential fusion transcripts by RNAseq an in-house designed metacaller approach was used.

Molecular comparison of human samples and *in vivo* PDX-models (WES and RNAseq)

All molecular analysis results, from WES or RNAseq of the PDX samples will be reviewed and compared to the patient tumor analysis, both at the relapse corresponding to the PDX and at diagnosis. Molecular comparison is ongoing.

Statistical analysis

The data were shown as the mean \pm standard error of mean (SEM) using Graphpad Prism® Software version 5.00 (Graphpad Software Inc, La Jolla, CA, USA).

Results

Seventeen tumor/blood samples were collected from 16 patients with refractory/relapsed osteosarcoma accrued in MAPPAYACT trials and analyzed at Gustave Roussy (Fig.4.1). Fourteen of these samples issued from 13 patients were implanted in mice. One patient (#32) had two biopsies at different relapse as the first sample was not contributive for molecular analysis (lung nodule then lymph node). From the 14 patients, 4 fresh tumor samples were cultures in vitro (primary cultures). Secondary cultures (using PDX cells) from the 3 established PDX models were also performed.

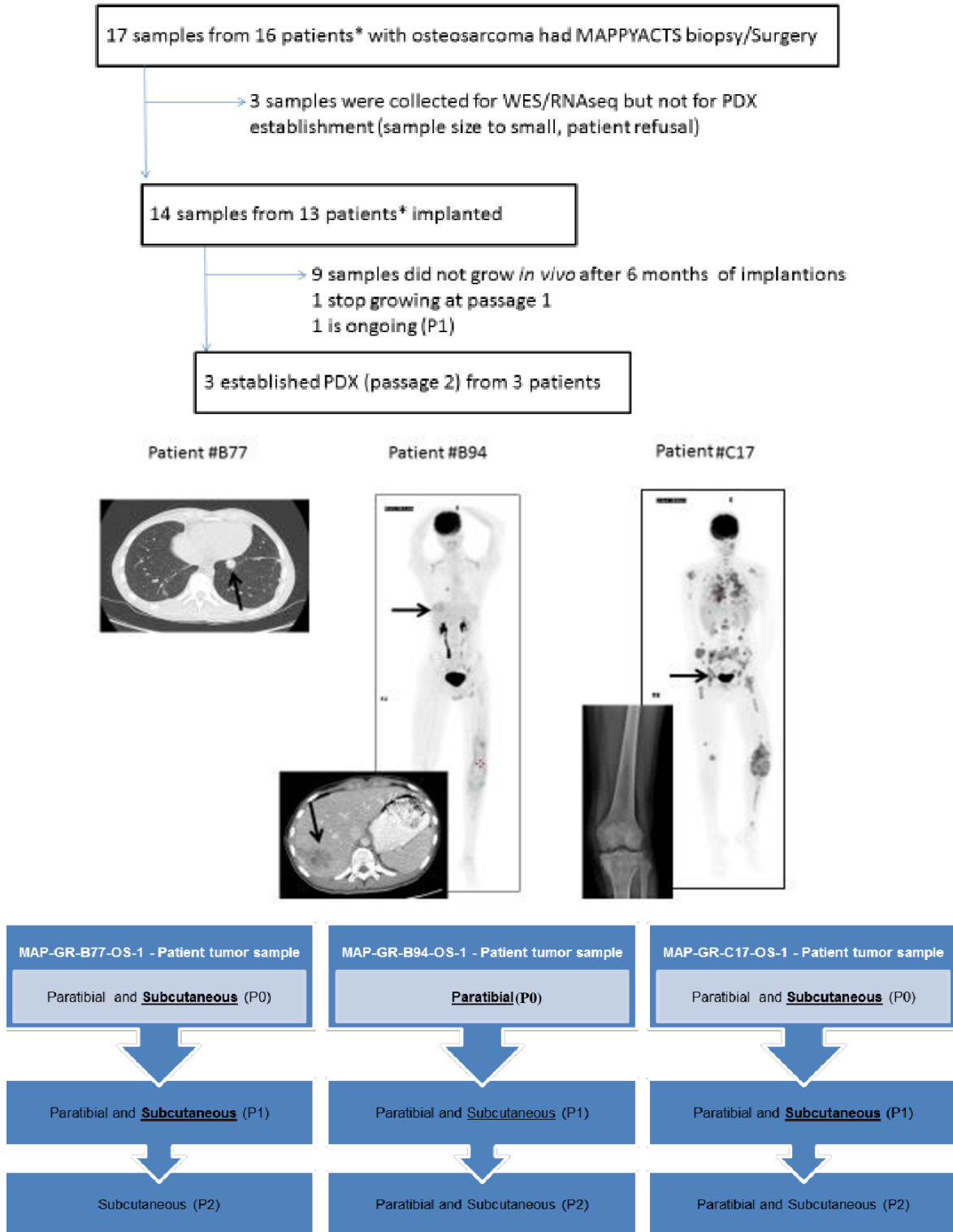


Figure 4.1: Patient and sample flow chart. *Patient (#32) had two different samples collected and implanted at different progression time.

Osteosarcoma PDX *in vivo* establishment

A small fragment of 14 relapsed osteosarcoma samples were implanted directly from the patients in different body localizations of NSG mice (Table.4.I): in the kidney capsule (n=5), subcutaneously (n=8) and/or in paratibial (n=11). Only one of the 5 first samples implanted (#A32-2) grew in the kidney capsule no further than P1 and this technique was stopped. Tumor engraftment at P0 was observed in 2/14 patients (#B77, #C17), at both subcutaneous and paratibial sites (#B77, #C17), in one paratibial site (#C94, no subcutaneous implantation performed) (Fig.4.1). The last sample #C04 with tumor engraftment at both site was frozen in FBS+1% DMSO and stored at -80°C (frozen in a coolbox that allows a temperature decrease of 1°C/min) before subcutaneous and paratibial implantation. The median delay for tumor detection from implantation was of 2.6 months in both implantation sites (1.6-4.2 months and 1.0-4.2 for subcutaneous and paratibial, respectively) (Table.4.I). Only three of these models were able to reach at least passage 2 (P2) in both localizations (MAP-GR-B77-OS-1, MAP-GR-C17-OS-1 and MAP-GR-B94-OS-1) leading to a PDX-establishment rate of 3/8 subcutaneously and 3/11 paratibially. All 3 subcutaneous models have a tumor take rate of 100% and 50, 40 and 80% for the orthotopic models MAP-GR-B77-OS-1, MAP-GR-C17-OS-1 and MAP-GR-B94-OS-1 respectively. In the implantation of the first growing MAP-GR-B77-OS-1 subcutaneous model in nude mice, it was however observed a much slower tumor development than in NSG mice (Supplementary Fig.4.S1). For the following procedures, nude mice were not used.

Table.4.I (next page): Patients characteristics and PDX development. M-male, F-female, PHR- poor histological response, GHR- good histological response, OS2006-first line treatment of osteosarcoma in France⁴ which can combine different chemotherapies: M-EI - methotrexate-etoposide-ifosfamide, AP- doxorubicin-platinum, API-AI - doxorubicin-platinum-ifosfamide, EI - etoposide-ifosfamide, OS2TTP-second line treatment of relapsed osteosarcoma in France (NCT00978471) randomizing HD- high-dose-thiotepa, GEMOX-gemcitabin-oxaliplatin, VP16-Carbo- etoposide-carboplatin, EDX-endoxan-cyclophosphamide, CR- complete response, PR- partial response, SD- stable disease, PD- progressive disease, ?- disease not yet evaluated under therapy, PD- progressive disease, R- relapse, Met- metastatic, Px- *in vivo* passage n°x.

	Patient characteristics and treatment								Characteristic at time of implantation				SC PDX*		Paratibial PDX	
PDX id	Gender	Histology osteosarcoma	Age at diagnosis	Metastatic at diagnosis	First line histological response (%) viable tumor	Treatments prior MAPPYACTS biopsy/surgery	Whole exome sequencing (WES) somatic alterations	Treatments after MAPPYACTS biopsy/surgery (response /outcome)	Age	Disease status	Primary or metastatic disease	Tumor sample implanted	Initial uptake delay (months)	PDX Stage	Initial uptake delay (months)	PDX Stage
MAP-GR-A07-OS-1	M	Osteoblastic	7.4	lung	PHR 25%*	1-OS2006: M-EI, AP 2-GD, EI, HD-Thio	EGFR somatic mutation p.R23G*57 TSC2 germline mutation p. V221M + LOH	EDX/Rapamune (PD) Pembrolizumab (PD) Sorafenib (PD) Denozumab (PD, Dead)	9.5	PD / R N°2	Met	Lung biopsy	Not done		Not done	
MAP-GR-A32-OS-1	M	Chondroblastic	16.5	lung	PHR 30%*	1- OS2006: M-EI, AP 2- GEMOX 3- VP16-carbo 4- MEK3475-051-04 Pembrolizumab	NA	EDX/Rapamune (PD)	18.0	PD	Met	Lung biopsy	Did not grow		Not done	
MAP-GR-A32-OS-2	M	Chondroblastic	16.5	lung	PHR 30%*	Same as above 5-EDX/Rapamune	no	Denozumab (PD) Pazopanib (SD)	18.0	PD	Met	Lymph node biopsy	Did not grow		Did not grow	
MAP-GR-A56-OS-1	F	Osteosarcoma	11.2	Lung, tibia	GHR 0%*	1- OS2006: M-EI, AP	no target	Lenvatinib (NE) myelodysplasia	11.7	R	Met	Lung surgical resection	Did not grow		Did not grow	
MAP-GR-A78-OS-1	M	Telangectatic	11.8	-	GHR 2%	1-OS2006: M-EI	FGF14: amplification 0.93 Mb (10 copies) TP53: deletion 1.6 Mb (1.1 copies)+ gain 2.05 Mb (3.4 copies)+ TP53/TTC19 fusion CDK4 : amplification 0.56 Mb (9.6 copies)	OS2TTP: AP	13.5	R N°1	PT	Femur biopsy	Not done		Did not grow	
MAP-GR-A80-OS-1	M	10% osteoblastic 60% chondroblastic 30% fibroblastic	19.3	-	GHR 6%	1- OS2006 : M-EI	PDGFRA amplification 1.4Mb (8.5 copies) TP53: heterozygous somatic pathogenic mutation p.XXXX+10 ATRX heterozygous somatic pathogenic mutation p.L1189* CDKN2A/2B heterozygous deletion 0.7 Mb (1.2 copies)	OS2TTP: AP, HD-EDX WEE1inh/Carbo MEK15394 (PD) Denosumab	19.7	R N°1	Met	Lung Surgical resection	Did not grow		Did not grow	
MAP-GR-A95-OS-2	F	with giant cell	11.2	-	PHR 45%*	1- OS2006 M-EI, AP	CDK4 amolification 0.2 Mb (4.8Mb)	Lenvatinib (PR-PD) Cabozantinib (?)	12.1	PD/R N°2	Met	Lung surgical resection	Did not grow		Not done	
MAP-GR-B40-OS-1	M	Osteoblastic	16.9	-	PHR 25%*	1- OS2006: M-EI, AP, Zometa 2- OS2TPP: EI, HD-thio 3- EDX/rapamune	TET2: pathogenic somatic mutation p.R1095* IRF7 pathogenic somatic mutation p.R860*	Pazopanib (SD-PD) Olaparib/irinotecan	21.9	R N°2	Met	Lung biopsy	Did not grow		Not done	
MAP-GR-B77-OS-1	M	Osteoblastic	14.4	-	PHR 60%*	1- OS2006: M-EI, AP 2- OS2TPP: EI	TP53 somatic mutation p.C135Y CDKN2A/2B heterozygous deletion ATRX focal loss of one copy	HD-Thio (PD) Lenvatinib (SD)	16.9	R N°2	Met	Lung surgical resection	1,6	>P2	1	>P2
MAP-GR-B94-OS-1	M	Telangiectasic	16.2	Lung	GHR 0%*	1- OS2006: M-EI 2- API-AI	TP53 p.S241A somatic homozygous mutation pathogenic RB1 c.1695+1G>T somatic homozygous mutation IGF1R focal amplification (>40 copies)	AP (PD) Pazopanib	17.3	PD/R N°2	Met	Liver biopsy	P1 From P0 PT	>P2	4.2	>P2
MAP-GR-C04-OS-1*	F	Fibroblastic	13.8	-	PHR 28%*	1- API-AI 2- EI	PDGFA amplification (5 copies) CDKN2A/2B homozygous deletion VEGFA amplification (5 copies) TP53-P14KB fusion CCND3 amplification (5 copies)	Lenvatinib (SD; PD) Pazopanib (PD)	15.3	R N°1	PT	Biopsy	3,6	P2 since 06-12-17	-	P2 since 06-12-17
MAP-GR-C17-OS-1	F	Osteosarcoma	16.0	Osteosarcomatosis, Lung, bone, skin lymph node	NA	1- API-AI	RB1 somatic mutation p.Tyr321Ter IGF1R focal amplification(13 copies)	EI (PD-Dead)	16.5	R N°1	Met	Lymph node biopsy	2.3	>P2	NA	>P2
MAP-GR-C22-OS-1	M	Fibroblastic	16.8	Lung	GHR 8?	1- OS2006: M-EI, API, AP	NA	Surgery, Cryotherapy only	18.7	R N°3	Met	Lung biopsy	Did not grow		Did not grow	
MAP-GR-C61-OS-1	M	Chondroblastic & chondromyxoid	11.0	-	GHR 1,5%*	1- OS2006: M-EI 2- AP	NA	Pazopanib	12.9	PD /R N°1	Met	Biopsy	-	ongoing since 7 7-17	-	ongoing since 7-7-17

Osteosarcoma PDX *in vivo* local growth rate and behavior

In subcutaneous models, the time between implantation and the start of tumor growth detection depends on the initial tumor sample (shorter for MAP-GR-B77-OS-1 than MAP-GR-C17-OS-1) and the passage number (longer at passage P0 than at P2) (Fig.4.2). Once primary tumor growth had started then the tumor growth rate appeared similar between samples and passages. At passage P2, SC-PDX growth started from days 7, 13 and 18 for MAP-GR-B77-OS-1, MAP-GR-C17-OS-1 and MAP-GR-B94-OS-1 respectively, and reached a size around 900 mm³ at days 30 (MAP-GR-B77-OS-1) and 40 (MAP-GR-C17-OS-1 and MAP-GR-B94-OS-1) after implantation. The doubling time of subcutaneous tumors for passage 0 was 5.6, 8 and 17 days for MAP-GR-B77-OS-1, MAP-GR-C17-OS-1 and MAP-GR-C04-OS-1 and 4.6, 9 and 10 days for passage 2 for MAP-GR-B77-OS-1, MAP-GR-C17-OS-1 and MAP-GR-B94-OS-1, respectively (Fig.4.2). Primary tumor growth evaluation was more difficult with paratibial-PDX models due to the localization.

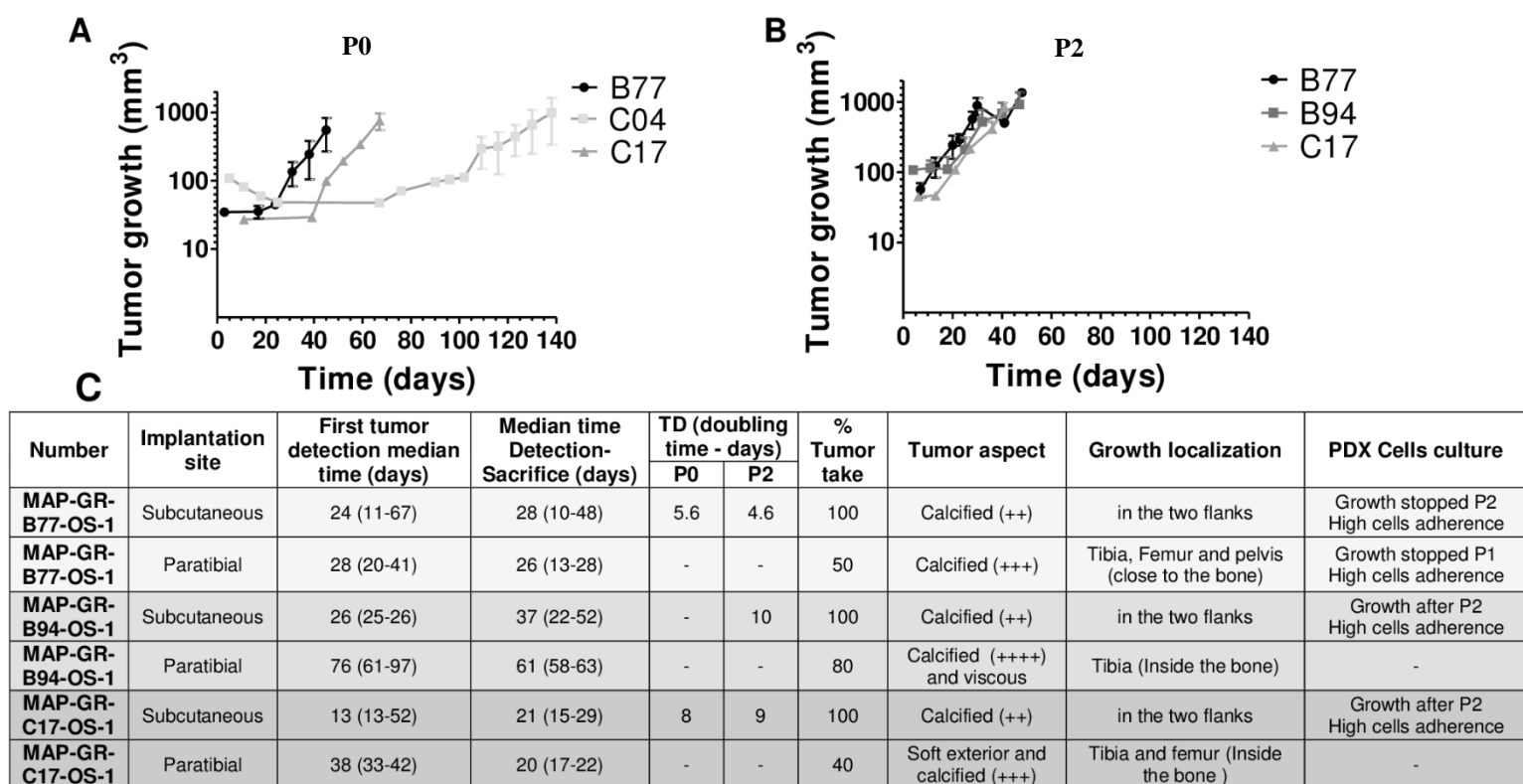


Figure 4.2: Tumor engraftment, *in vivo* growth and morphologic characteristics of the 3 subcutaneous and paratibial PDX models in NSG mice: Tumor growth of subcutaneous models in passage 0 (A) for MAP-GR-B77-OS-1 (B77), MAP-GR-C17-OS-1 (C17) and MAP-GR-C04-OS-1 (C04) (MAP-GR-B94-OS-1 was not implanted at passage 0 in subcutaneous site) and passage 2 (B) for MAP-GR-B77-OS-1, MAP-GR-B94-OS-1 (B94) and MAP-GR-C17-OS-1 (MAP-GR-C04-OS-1 has not reached the passage 2 for the moment) and tumor characteristics for different passages and at sacrifice day for subcutaneous and paratibial models (C). *subcutaneous MAP-GR-C04-OS-1 grow from patient frozen sample.

CT scan performed on the sacrifice day of the different passages detected intra-tumor calcification in all models (paratibial and subcutaneous), although more pronounced in paratibial than in subcutaneous models (Fig.4.3). In paratibial models the observed abnormalities were similar to those presented by patients, with aggressive bone lesions, detection of aberrant new bone formation extending within the extra-osseous mass (osteocondensation), and some osteolysis (bone destruction). MAP-GR-B77-OS-1 developed on the tibia, however, tumor extra-osseous growth was observed on the femur/pelvis. The three models (MAP-GR-B77-OS-1, MAP-GR-C17-OS-1 and MAP-GR-B94-OS-1) showed more osteocondensation than osteolysis. MAP-GR-C17-OS-1 developed in the tibia with femur extension while MAP-GR-B94-OS-1 originated only in the tibia. MAP-GR-B94-OS-1 was the model with more osteocondensation inside and outside the bone (Fig.4.3).

HES staining confirmed the osteosarcoma nature of the primary tumors from both subcutaneous and paratibial PDX models. In both cases, proliferation consisted of osteoblastic cells (MAP-GR-B77-OS-1 and MAP-GR-B94-OS-1) with atypia and mitosis. Osteoid production was present with necrosis and cystic alterations. MAP-GR-C17-OS-1 showed also a mix of osteoblastic and chondroblastic subtype. All the models showed pleomorphic cells and also anaplastic cells on the MAP-GR-B77-OS-1 (Fig.4.3 and Table.4.II).

Osteosarcoma PDX in vivo metastatic potential

No clinical signs or CT-scan abnormality at day of animal sacrifice permitted to detect metastasis. Metastases were detected only by histology at sacrifice time in 2 paratibial PDX models. Metastases were detected for paratibial models in the lungs in MAP-GR-C17-OS-1, in the bone in MAP-GR-B94-OS-1, and in the spleen in the both models. No metastases were observed in the liver. No metastases were detected in subcutaneous models (Table.4.II)

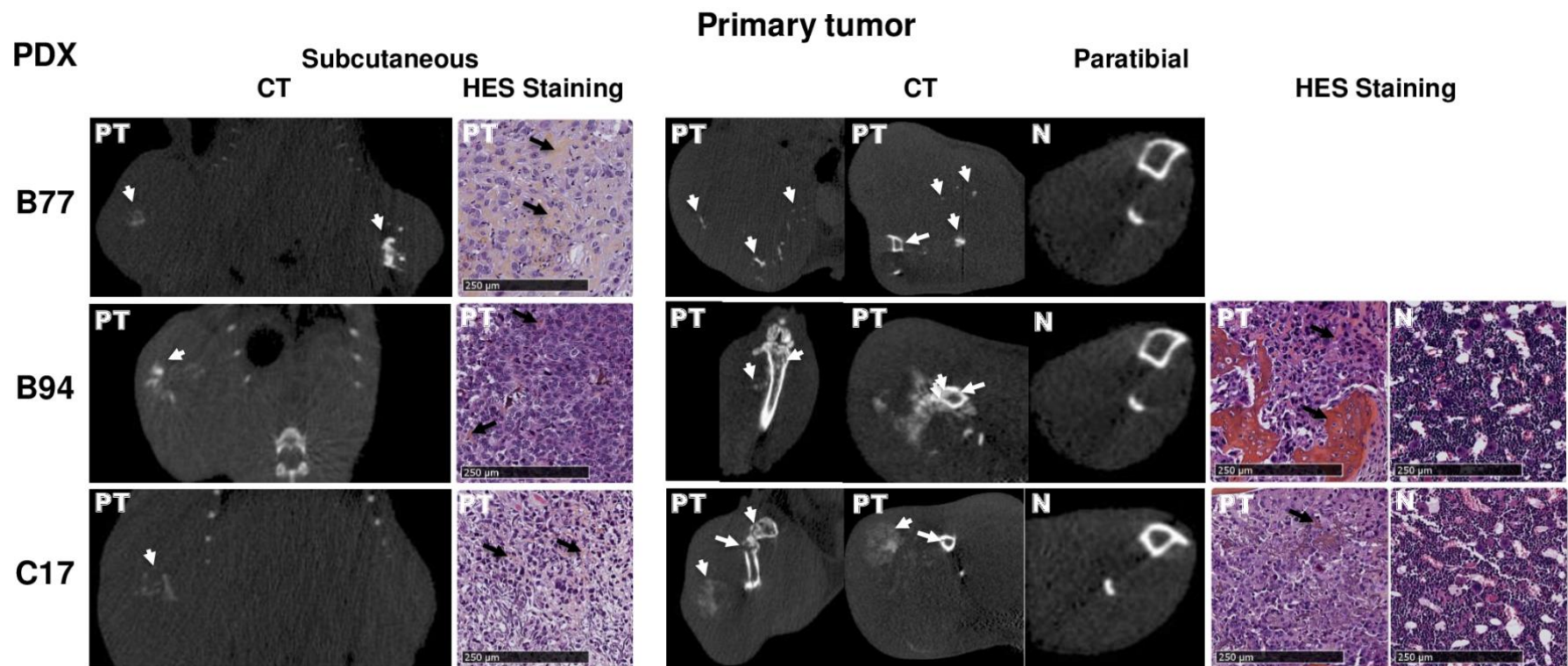


Figure 4.3: Radiological and morphological primary tumor PDX characteristics by two different types of implantation (subcutaneous and paratibial). The small white arrows show osteocondensation, the biggest white arrows show osteolysis and the black arrows osteoid matrix (orange color). B77- MAP-GR-B77-OS-1; B94 - MAP-GR-B94-OS-1; C17- MAP-GR-C17-OS-1; PT- Primary tumor; N – Normal tissue

Table.4.II: Radiological and morphological characteristics of the primary tumor and metastases for the MAP-GR-B77-OS-1, MAP-GR-B94-OS-1, MAP-GR-C17-OS-1 PDX established by two different types of implantation (subcutaneous and paratibial). Histo – Histology; HG – High-grade; OB – Osteoblastic subtype; CB – Chondroblastic subtype; NA – Not applicable; ND – Not done.

PDX	Implantation type	Primary tumor						Metastases			
		Histo- HES				CT		Histo- HES			
		Sub-type	Osteoid Matrix	Cells morphology	Necrosis	Calcification	Osteolysis	Lung	Bone	Spleen	Liver
MAP-GR-B77-OS-1	Subcutaneous	HG OB	Yes (+)	Pleomorphic and anaplastic	+	++	-	-	NA	-	-
	Paratibial	HG OB	Yes (++)	pleomorphic	+	++	+	-	-	ND	ND
MAP-GR-B94-OS-1	Subcutaneous	HG OB	Yes (+)	pleomorphic	+	++	-	-	NA	-	-
	Paratibial	HG OB	Yes (+++)	pleomorphic	+	++++	++	-	+	+	-
MAP-GR-C17-OS-1	Subcutaneous	HG OB+CB	Yes (+) (osteoid and chondroblastic)	pleomorphic	++	++	-	-	NA	-	-
	Paratibial	HG OB+CB	Yes (++) (osteoid and chondroblastic)	pleomorphic	++	+++	++	+	-	+	-

Patient's Characteristics

Characteristics of these 13 patients with samples implanted in mice are described in Table.4.I. Samples were issued from 10 males and 4 females with a median age of 16.5 years (range 9.5-21.9) at time of biopsy/surgery. At diagnosis, disease was localized with good histological response (n=3), localized with poor histological response (n=4), metastatic with good histological response (n=3), metastatic with poor histological response (n=3). They received before biopsy/surgery in the frame of MAPPYACTS, one (n=5), two (n=4), three (n=1) or five (n=1) lines of treatment, with the five chemotherapeutic agents know to be efficient in phase-II trials (methotrexate, doxorubicin, cisplatin, ifosfamide and etoposide), except two patients that did not received methotrexate. In addition, one patient received zoledronic acid, two rapamune, and one pembrolizumab, before biopsy/surgery.

The three patients from who PDX samples were obtained (#B77, #C17 and, #B94) presented very aggressive disease at diagnosis.

MAP-GR-B77-OS-1 PDX models were issued from a 14-year-old boy. At diagnosis he presented with a localized osteoblastic osteosarcoma of the femur. Poor histological response (60% of residual viable cells) was observed after M-EI chemotherapy according to OS2006/sarcome09 trial²⁵, post-operative treatment continues with AP. A first pulmonary relapse occurred at 18 months (M18) from the initial diagnosis treated by EI. The second lung metastatic relapse occurred at 12 months of the first relapse and 6 months from the end of second line treatment. The cumulative dose of chemotherapy before MAPPYACTS inclusion was for methotrexate 96 g/m², doxorubicin, 350 mg/m², cisplatinum 600 mg/m², ifosfamide 72 g/m², and etoposide 1800 mg/m². The surgical resection of the lung metastasis at second relapse (M30 from diagnosis) was used for MAPPYACT molecular analysis and PDX establishment. He then received high-dose thiotepa, as consolidation treatment of this third complete remission. A third pulmonary progression occurred four months after the previous one (M34 from diagnosis). The disease was stabilized after four months of lenvatinib he underwent complete surgical excision and the patient was still alive at 42 months from initial diagnosis. Potential targetable molecular abnormalities were *TP53* somatic mutation p.C135Y and homozygous deletion of *CDKN2A/2B*.

MAP-GR-B94-OS-1 PDX model was issued from a 16 year-old boy. At diagnosis he presented a telangiectatic osteosarcoma of the femur with an initial local vessel invasion and lung metastasis. Local and lung metastatic progression occurred during preoperative chemotherapy by M-EI (after cycle 1, week 7). The chemotherapy was switched for API-AI (2 cycles) leading to partial response at both local and metastatic site. Surgery of the primary tumor and lung metastasectomy showed no residual viable cell after these neoadjuvant chemotherapies. Several infectious complications delayed the post-surgery chemotherapy which continued with EI (4 cycles). A new local and metastatic progression (lung, liver and bone) occurred under treatment at 11 months from diagnosis (M11). The cumulative dose of chemotherapy before MAPPYACTS inclusion were for methotrexate 36g/m², doxorubicin 240 mg/m², cisplatin 300 mg/m², ifosfamide 84 g/m², and etoposide 1800 mg/m². A liver metastasis of the second relapse (M11 of diagnosis) was biopsied for MAPPYACTS molecular analysis and PDX establishment. The patient had several surgeries of the metastases and for prosthesis infection, then received one cycle of AP and progressed (M15 from diagnosis). After 3 months of pazopanib a partial remission of the disease and a left asymptomatic pneumothorax were observed, then the disease progressed at 6 months of treatment. The patient is still alive at 22 months from the initial diagnosis, with a recurrent disease and a persistent asymptomatic pneumothorax. Potential targetable molecular abnormalities were somatic homozygous mutations in *TP53* (p.S241A) and *RB1* (c.1695+1G>T), and an *IGF1R* focal amplification (>40 copies). He also presented a germline ATM mutation p.D1637G.

MAP-GR-C17-OS-1 PDX models were issued from a 16 year-old girl. At diagnosis, she had a rare presentation of osteosarcomatosis with a very large femoro-tibial mass associated with multiple bone, lung, lymph node, muscular and subcutaneous localizations. The treatment by API-AI achieved metabolic good partial response with minimal tumor volume shrinkage at all sites. Local and metastatic progression occurred under treatment after 4 API-AI cycles (M5 from diagnosis). The cumulative dose of chemotherapy before MAPPYACTS inclusion were for doxorubicin, 360 mg/m², cisplatin 400 mg/m², and ifosfamide 60 g/m². A right inguinal lymph node metastasis at first progression was biopsied for MAPPYACTS molecular analysis

and PDX establishment (M5 from diagnosis). One cure of EI was started but treatment was stopped due to very rapid disease progression and massive alteration of performance status. The patient died of progressive disease 4 months later (M9 from diagnosis). Potential targetable molecular abnormalities were *RB1* somatic mutation p.Tyr321Ter and *IGF1R* focal amplification (13 copies).

Resistance/sensitivity to drugs of the different models ***Osteosarcoma primary and secondary in vitro cultures***

When tumor material was sufficient, *in vitro* primary tumor cell cultures directly derived from the patient tumor were tried (MAP-GR-A56-OS-1, MAP-GR-A80-OS-1, MAP-GR-B77-OS-1 and MAP-GR-A095-OS-2). MAP-GR-A80-OS-1 and MAP-GR-A095-OS-2 grew until passage 7 and 5, respectively, but no drug testing was performed due to fibroblasts contamination.

Secondary cultures issued from the 3 PDX samples (*in vivo* passages) were grown *in vitro*. All models showed slow cell growth and high adherence, leading to difficulties on trypsinization (Fig.4.2). MAP-GR-B77-OS-1 reached passage 2 after 1 month in culture and cell growth after passage 2 stopped, while MAP-GR-C17-OS-1 and MAP-GR-B94-OS-1 reached passage 2 after 2/3 weeks and grew after passage 2 (Fig.4.2). Drug testing in these cells confirmed high levels of resistance to usual chemotherapeutic agents used in osteosarcoma, especially for MTX with $IC_{50} > 100 \mu M$ (Table.4.III), much higher than the IC_{50} s of our previously described MTX-resistant osteosarcoma cell line models²⁶.

As two patients received multi-tyrosine kinase inhibitor with either stable (#B77, lenvatinib) or partial response (#B94 pazopanib), we tested three of them *in vitro* (cabozantinib, regorafenib and pazopanib). Sensitivity to these drugs were different for a same patient. High resistance levels were observed with regorafenib ($IC_{50} > 100 \mu M$). The cells derived from the PDX of the patient #B94 who had partial response to pazopanib had an IC_{50} of $46.7 \mu M$ and a 20 times greater sensitivity to cabozantinib (Table.4.III).

Table.4.III: IC50 of different cell lines (parental and cell lines selected to be resistant) in comparison with the PDX-cells (MAP-GR-B77-OS-1, MAP-GR-B94-OS-1 and MAP-GR-C17-OS-1) cultured and treated *in vitro*. The treatment was performed with: MTX, doxorubicin, etoposide, cisplatin, mafosfamide, cabozantinib, regorafenib and pazopanib.

Cells		IC50 (µM)							
		MTX	DOXO	ETOP	CISP	MAF	Cabo	Rego	Pazo
HOS	Parental	0.04	0.05	0.7	4.80	12.7	6.5	ND	ND
	R/MTX	6.24	0.07	0.67	5.38	16.8	5.76	ND	ND
	R/DOXO	0.48	10.6	180	3	14.30	13.6	ND	ND
HOS-143B	Parental	0.04	0.04	0.68	1.68	14.3	14.6	ND	ND
	R/MTX	4.13	0.10	0.90	3.96	12.7	23	ND	ND
Saos-2	Parental	0.05	0.05	2.97	4.28	17.6	18	ND	ND
	R/MTX	2.05	0.10	5.21	6.44	23.90	23.9	ND	ND
Saos-2-B	Parental	0.05	0.06	2.80	5.20	20.30	7,58	ND	ND
	R/MTX	1.93	0.06	3.76	5.96	21	15,30	ND	ND
MG-63	Parental	0.05	0.1	2	2.48	13.30	8.5	ND	ND
	R/MTX	2,91	0.24	9.81	3.38	26.20	6	ND	ND
U2OS	Parental	0.05	0.1	4.4	10	33	ND	ND	ND
IOR/OS18	Parental	1.3	0.18	5.86	4.62	27.13	ND	ND	ND
MAP-B77	-	>100	0.18	76.3	22.6	57.6	ND	ND	ND
MAP-B94	-	>100	0.7	14.5	2.63	50	2.69	>100	46.7
MAP-C17	-	>100	0.19	17.5	6.09	13.2	20.6	>100	14.8

Discussion

We established three new subcutaneous and orthotopic (paratibial denudated) osteosarcoma PDX models derived from refractory/relapse human samples in NSG female mice.

The engraftment rate was of 30% with a median interval of 2.6 months, lower but quicker than the recent published series of 15 orthotopic osteosarcomas with another method (both mechanic and enzymatic dissociation, intercondylar femur cell injection in NSG female mice, engraftment rate of 48% with a median interval from implantation of 3.75 months, range 1.5-9)¹⁹.

Both subcutaneous and paratibial PDX models mimic the human disease in terms of histology (osteoid formation) and in term of imaging for the orthotopic models with aggressive local bone tumor-induced abnormalities. Some of these models also

mimic the human disease in terms of spontaneous metastatic spread, especially when they developed in an orthotopic setting. The metastatic potential of the orthotopic PDX models were not described in Stewart et al¹⁹. Although molecular comparison (WES and RNAseq) between PDX (subcutaneous and paratibial) models and the corresponding patients tumor at relapse and diagnosis they are issued from are ongoing. Several comparisons will be performed to approach: first, the representativeness of the PDX models compared to the human relapse samples they are issued of; second, the similarities or differences between both subcutaneous and orthotopic PDX models; and finally, the clonal evolution and mechanism of resistance acquired between diagnostic and relapse samples of each patient with a PDX. General analyses will explore copy number abnormalities, mutations, fusions, and gene expression profiles, more specific analysis might include exploration of the known mechanisms of resistance to the several drugs either received by the patient before the MAPPYACTS biopsy (e.g RFC, DHFR for MTX, PgP for doxorubicin, etc) or used in patient after the MAPPYACTS biopsy (e.g. sumscan for MTKI) or in the PDX models.

We expect that the molecular characteristic of the human relapse disease will be retained by the PDX models, as in a panel of 15 different PDX issued from pediatric tumor recently published, the 15 osteosarcoma PDX models had the best clonal preservation¹⁹.

The primary growth properties of our PDX models when established (\geq passage P2) had also the advantage to be compatible with the timelines for drug testing at both sites. *In vivo* drug testing has not yet been done, and ethical authorization process is ongoing.

In the meantime, we derived secondary *in vitro* cell culture from the subcutaneous PDX models that confirmed the high level of resistance to chemotherapeutic agents previously used in the patients, especially to methotrexate and including in one patient that did not receive it (#C17). We also observed differential sensitivity to different multi-tyrosine kinase inhibitors currently in clinical trial or not, with no sensitivity to regorafenib and inter-patient and intra-patient variability in term of sensitivity to cabozantinib and pazopanib. IC50 of cabozantinib was in the same range of those observed with human hepatoma cell lines²⁷. Cabozantinib reverses

multidrug resistance hepatoma cell lines resistant to doxorubicin by modulating the function of P-glycoprotein²⁷, but not in our previous HOS-DOXO-resistant cell line model.

Several compounds will be also tested *in vivo* such as the multityrosine kinase inhibitor cabozantinib and other molecules or combination according to the molecular abnormalities detected in patient and PDX samples (e.g. *TP53* mutation and Wee1 inhibitor + carboplatin or other chemo or BRCAness phenotype and PARP inhibitor + irinotecan). No drug testing has been published yet on osteosarcoma PDX models¹⁹.

Conclusion

The establishment of osteosarcoma subcutaneous and orthotopic (paratibial denudated) PDX models derived from refractory/relapse human samples in NSG has been achieved. It was also demonstrated the advantages of these subcutaneous (rapid growth, easy detection) and orthotopic (interrelation of the tumor with the bone microenvironment) osteosarcoma PDX (preserved tumor heterogeneity) models in terms of drug testing. However, their development in immunocompromised mice (NSG) will not allow to access the immune microenvironment role in drug sensitivity/resistance. Several teams are now working in humanized PDX models.

Acknowledgments

We thank the Preclinical Evaluation Platform for providing immunocompromised mice and animal care, the Imaging and Cytometry Platform for help on CT scan imaging especially Valerie Rouffiac, Olivia Bawa for the histology slides preparation, Irene Villa for performing the histology slides scans, Brenda Mallon for samples shipment and collection, Carole Lecinse for manuscript editing and to the Portuguese Foundation for Science and Technology (FCT, <http://www.fct.pt/>) through the PhD fellowship to Maria Eugénia Marques da Costa (SFRH/BD/89137/2012).

References

1. Isakoff MS, Bielack SS, Meltzer P, Gorlick R. Osteosarcoma: Current Treatment and a Collaborative Pathway to Success. *J Clin Oncol*. 2015;33(27):3029-3035.
2. Zhang Y, Mai Q, Zhang X, Xie C, Zhang Y. Microenvironment Signals and Mechanisms in the Regulation of Osteosarcoma. In: *Osteosarcoma - Biology, Behavior and Mechanisms*. InTechOpen, London, UK. 2017.
3. Guijarro M V, Ghivizzani SC, Parker Gibbs C, Blanco Aparicio C. Animal models in osteosarcoma. *Front Oncol*. 2014; 4: 189.
4. Piperno-Neumann S, Le Deley M-C, Rédini F, et al. Zoledronate in combination with chemotherapy and surgery to treat osteosarcoma (OS2006): a randomised, multicentre, open-label, phase 3 trial. *Lancet Oncol*. 2016;17(8):1070-1080.
5. Bielack SS, Smeland S, Whelan JS, et al. Methotrexate, Doxorubicin, and Cisplatin (MAP) Plus Maintenance Pegylated Interferon Alfa-2b Versus MAP Alone in Patients With Resectable High-Grade Osteosarcoma and Good Histologic Response to Preoperative MAP: First Results of the EURAMOS-1 Good Response Randomized Controlled Trial. *J Clin Oncol*. 2015;33(20):2279-2287.
6. Kempf-Bielack B, Bielack SS, Jürgens H, et al. Osteosarcoma relapse after combined modality therapy: An analysis of unselected patients in the Cooperative Osteosarcoma Study Group (COSS). *J Clin Oncol*. 2005;23(3):559-568.
7. Omer N, Le Deley M-C, Piperno-Neumann S, et al. Phase-II trials in osteosarcoma recurrences: A systematic review of past experience. *Eur J Cancer*. 2017;75:98-108.
8. Kresse SH, Rydbeck H, Skårn M, et al. Integrative Analysis Reveals Relationships of Genetic and Epigenetic Alterations in Osteosarcoma. *PLoS*

One. 2012;7(11).

9. Heymann M-F, Heymann D. Immune Environment and Osteosarcoma. In: *Osteosarcoma - Biology, Behavior and Mechanisms*. InTechOpen, London, UK. 2017.
10. Marques da Costa ME, Daudigeos-Dubus E, Gomez-Brouchet A et al. Establishment and characterization of *In vivo* orthotopic bioluminescent xenograft models from human osteosarcoma cell lines in Swiss nude and NSG mice. *Cancer Med*. 2018;7(3):665-676.
11. Mohseny AB, Machado I, Cai Y, et al. Functional characterization of osteosarcoma cell lines provides representative models to study the human disease. *Lab Investig*. 2011;91(8):1195-1205.
12. Garimella R, Eskew J, Bhamidi P, et al. Biological characterization of preclinical Bioluminescent Osteosarcoma Orthotopic Mouse (BOOM) model: A multi-modality approach. *J Bone Oncol*. 2013;2(1):11-21.
13. Creen V, Biteau K, Amiaud J, et al. Bone microenvironment has an influence on the histological response of osteosarcoma to chemotherapy: retrospective analysis and preclinical modeling. *Am J Cancer Res*. 2017;1;7(11):2333-2349
14. Ren L, Mendoza A, Zhu J, et al. Characterization of the metastatic phenotype of a panel of established osteosarcoma cells. *Oncotarget*. 2015;6(30):29469-29481.
15. Inoue T, Terada N, Kobayashi T, Ogawa O. Patient-derived xenografts as *in vivo* models for research in urological malignancies. *Nat Rev Urol*. 2017; 14(5):267-283
16. Holen I, Speirs V, Morrissey B, Blyth K. In vivo models in breast cancer research: progress, challenges and future directions. *Dis Model Mech*. 2017;10(4):359-371.
17. Blattmann C, Thiemann M, Stenzinger A, et al. Establishment of a patient-

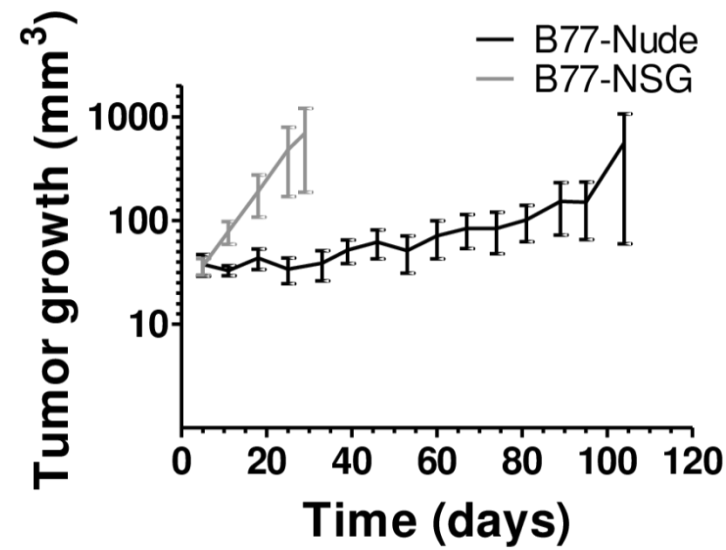
- derived orthotopic osteosarcoma mouse model. *J Transl Med*. 2015;13:136.
18. Guilhamon P, Butcher LM, Presneau N, et al. Assessment of patient-derived tumour xenografts (PDXs) as a discovery tool for cancer epigenomics. *Genome Medicine*. 2014;6:116.
 19. Stewart E, Federico SM, Chen X, et al. Orthotopic patient-derived xenografts of paediatric solid tumours. *Nat Publ Gr*. 2017;549.
 20. <https://clinicaltrials.gov/ct2/show/NCT02613962>.
 21. Georger, Birgit; Schleiermacher, Gudrun; Pierron, Gaelle; Lacroix L et al. Abstract CT004: European pediatric precision medicine program in recurrent tumors: first results from MAPPYACTS molecular profiling trial towards AcSe-ESMART proof-of-concept study. *Cancer Res*. 2017;77(13 Supplement):CT004-CT004.
 22. Harttrampf AC, Lacroix L, Deloger M, et al. Molecular Screening for Cancer Treatment Optimization (MOSCATO-01) in Pediatric Patients: A Single-Institutional Prospective Molecular Stratification Trial. *Clin Cancer Res*. 2017;15;23(20):6101-6112.
 23. Rössler J, Monnet Y, Farace F, et al. The selective VEGFR1-3 inhibitor axitinib (AG-013736) shows antitumor activity in human neuroblastoma xenografts. *Int J Cancer*. 2011;128(11):2748-2758.
 24. Pavía-Jiménez A, Tcheuyap VT, Brugarolas J. Establishing a human renal cell carcinoma tumorgraft platform for preclinical drug testing. *Nat Protoc*. 2014;9(8):1848-1859.
 25. Gaspar N, Occean B-V, Pacquement H, et al. Results of methotrexate-etoposide-ifosfamide based regimen (M-EI) in osteosarcoma patients included in the French OS2006/sarcome-09 study. *Eur J Cancer*. 2018;88:57-66.
 26. Marques da Costa ME, Daudigeos-Dubus E, Gomez-Brouchet A et al. *In vitro*

and *in vivo* establishment and characterization of bioluminescent orthotopic chemo-resistant osteosarcoma models in NSG mice. 2018. *In press*

27. Xiang Q, Chen W, Ren M, et al. Cabozantinib suppresses tumor growth and metastasis in hepatocellular carcinoma by a dual blockade of VEGFR2 and MET. *Clin Cancer Res.* 2014;20(11):2959-2970.

Supplementary data

A



B

Number	Strain type	First tumor detection median time (days)	Median time Detection-Sacrifice (days)	Tumor aspect	Growth localization
MAP-GR-B77-OS-1	Nude	67	32,5	calcified	in the two flanks
MAP-GR-B77-OS-1	NSG	11	18	calcified	in the two flanks

Supplementary Figure.4.S1: Tumor growth characteristics by subcutaneous implantation in Nude and NSG mice for MAP-GR-B77-OS-1. A– Tumor growth in Nude versus NSG with the time; B – Tumor development characteristics

Chapter 5:

Discussion and Conclusions

Osteosarcoma remains a disease which requires new treatments to improve disease outcome¹⁻⁴. The main challenges are the metastatic spread of the disease and its resistance to currently used chemotherapeutic agents, which will ultimately lead to death. Developing better and diverse preclinical models is crucial to take into account the complex genetic/epigenetic background, the heterogeneity of these tumors and the importance of the bone and immune microenvironment.

The work performed during my thesis led to an essential contribution in developing new and diverse osteosarcoma pre-clinical models with metastatic potential and chemoresistance phenotype, to understand the mechanisms of resistance, and to finally use this panel of models to test new drugs in osteosarcoma and better predict the clinical behavior of the drugs in the patients.

Osteosarcoma is the second highest cause of cancer related death in children and adolescents, affecting mainly the long bones⁵. It's a very complex bone disease, where cells of origin, genetic/epigenetic alterations, osseous and immune microenvironment and others parameters play an important role in tumorigenesis. Treatment has improved with the chemotherapy implementation, unfortunately, in metastatic or recurrent patients, 5-year survival rates are reduced to only 20%. Metastases at diagnosis and resistance to chemotherapy are two prognostic factor of high risk of relapse in this disease¹⁻⁴ (Fig.5.1). All these points show the importance of developing models, especially in an orthotopic setting, that allow understand better this disease (eg. resistance mechanism) as well as to test new drugs that leads to an increase of the patients' survival.

In this work, we used osteosarcoma cells from different sources (previously established cell lines and human relapse tumor samples) to access different degrees of sensitivity/resistance and different mechanisms of resistance to chemotherapy, and different metastatic potential.

In vitro, a panel of previously established cell lines with different genetic background were modified by continuous exposure to different drugs, with high importance in osteosarcoma treatment (methotrexate and doxorubicin), to induce resistance, allowing exploration of the mechanism of acquired resistance (decrease RFC expression and/or increased DHFR expression in methotrexate resistant cells and increased PgP in doxorubicin resistant cells, with cross-resistance to etoposide)^{3,6}.

We also used one previously established cell line issued from an already metastatic tumor at diagnosis, the IOR/OS18, that present spontaneous higher degree of resistance to the five anti-osteosarcoma drug tested (methotrexate, doxorubicin, etoposide, mafosfamide, cisplatinum). Two parental cell lines (HOS and Saos-2-B) were implanted *in vivo* in an orthotopic bone setting and posteriorly *in vitro* culture (cells derived from CDX models) showing increased level of resistance. The *in vivo* growth increased the level of resistance of these cells with a mechanism to be further explored. The cells that presented the highest degree of resistance to all five drugs were in vitro secondary cell culture of cells issued from our PDX models (PDX were established from human osteosarcoma samples of relapsed/refractory disease).

To mimic at best the human disease which initiate in a bone microenvironment and spontaneously spread mainly to the lungs, we established different *in vivo* orthotopic models, either issued from established cell lines (CDX models) or from human relapsed tumor samples (PDX models) (Fig.5.1). We determined that Saos-2-B cell line injected intratibially in NSG mice allowed higher engraftment rate, primary tumor growth/bone abnormalities and metastatic spread than paratibial injection or Nude mice. We developed another intra-osseous CDX from a cell line with a different genetic background (HOS), showing a very different *in vivo* behavior. Saos-2-B-CDX were fast growing tumors with important extra-osseous masses and both osteolysis and osteocondensation, while HOS-CDX resulted in local disease with mainly bone destruction and no extra-osseous mass. Both models showed spontaneous metastases in the lung and rarely in the bone, more notorious in Saos-2-B-CDX model than in HOS. However, unusual metastases in the spleen were also observed, as described in others osteosarcoma CDX models in immunocompromised mice (lymph node, kidney, ovary etc)^{7,8}. The resistant counterpart cell lines induced *in vitro* were also injected in the same conditions in NSG mice (Saos-2-B-R/MTX-CDX, HOS-R/MTX-CDX and HOS-R/DOXO-CDX). Although the primary tumors behavior was not changed by the *in vitro* drug selection, their metastatic potential was clearly impaired (less and slower metastatic spread) compared to their parental counterpart. The main advantage of these CDX

models was their bioluminescent properties, which allowed to follow *in vivo* primary tumor growth and lung metastases spreading in real-time. The disadvantage of CDX models consisted of the nature of the cells used. Indeed, CDX models derived from *in vitro* cell lines which might have been in culture for long time, allowing genomic alterations (eg. adaptation to *in vitro* environment), and the lack of representativeness of the real osteosarcoma tumor heterogeneity⁹.

To overcome this last difficulty, we developed three PDX models derived from patient tumor samples collected from metastatic site of relapse refractory disease. As our CDX, our PDX models mimic human osteosarcoma behavior *in vivo*. Morphologically, CDX resemble osteosarcoma but comparatively, PDX model morphology was closer to the human disease they were derived from. Lung metastases were not detectable in subcutaneous PDX models, but only in orthotopic PDX models, confirming that orthotopic settings better reflected the human osteosarcoma behaviors than the subcutaneous settings. Osteosarcoma PDX models allow the patient's tumor heterogeneity preservation and the tumor cells growth in relation with their own stroma, better representing the tumor behavior observed in the patients¹⁰. A recent publication described 15 intra-osseous PDX osteosarcoma models which retain the molecular and cellular features of the patient tumors, the epigenetic landscape of their developmental origins and clonal preservation¹⁰. On other hand the assays on PDX models are currently ongoing and results will be further explored. The absence of bioluminescence renders *in vivo* follow up of tumor growth more difficult in the PDX orthotopic models, although easier when the tumor was implanted subcutaneously than in an orthotopic setting. However, the implantation site of the PDX models might differentially impact drug sensitivity, as described in an *in vivo* syngeneic osteosarcoma model¹¹. The low patient material availability and the low engraftment rate make these models difficult to obtain. The IMI2-P4 consortium is working on increased availability of these PDX models and we are participating to this effort through our work on the PDX ancillary study of the MAPPYACTS trial. However, the use of immuno-compromised mice strain (NSG mice) to favor engraftment, do not allow access the role of the immune context in tumor development, metastatic spread and sensitivity/resistance to

treatments, which is also important in osteosarcoma⁵. The advantages and inconvenient of the models are described in Table 5.I.

Globally, we have constituted a large panel of different *in vitro* and *in vivo* orthotopic (CDX, PDX) osteosarcoma models with various sensitivity/resistance to chemotherapy and metastatic potential that might prove to be useful for new drug testing. We have tested the effect of cabozantinib in all the *in vitro* models and showed that even in very chemoresistant models, cabozantinib efficacy can be observed. *In vivo* testing is awaited, and the results of the Phase-II trial in osteosarcoma will be available next year (NCT02243605)¹².

These models will be used to test several other drugs or combinations. The timelines of primary tumor growth and metastatic spread in both CDX and PDX models being compatible with the timelines of drug testing. Prioritization will be done based on the targetable molecular abnormalities of these different models (e.g. *TP53* mutation and Wee1 inhibitor), on the literature (BRCAness genetic signatures and PARP inhibitors combination with chemotherapy)^{13,14} or upcoming new knowledge. Indeed, we are currently analyzing the OS2006 cohort of primary tumor biopsy sample at diagnosis and the MAPPYACTS osteosarcoma cohort at relapse, for both at DNA (CGH, WES) and RNA level (RNA seq), from which new target could be issued. Humanized mice will also developed for complementary information related to immune system influence in the osteosarcoma development.

Table 5.I: Several preclinical models used and/or developed in this work and their advantages and inconvenients. R/DOXO – Resistant to doxorubicin; R/MTX – Resistant to methotrexate; SC – subcutaneous; CDX – cell-derived xenografts; PDX – patient-derived xenografts

Preclinical models	Available models	Resistant phenotype	Metastatic potential	Advantages	Inconvenient
<i>In vitro</i>					
Established cell lines					
Cell lines derived from sample at diagnosis	Primary tumor	Non			Non resistant
	Metastases (IOR/OS18)	yes (multi-drug)	not accessible <i>in vitro</i> (approach by migration/invasion assays)	Quick drug testing	
Resistant cell lines by continuous <i>in vitro</i> drug exposure	5 to MTX	yes to MTX		Mechanistic questions	
	HOS-R/DOXO	yes to doxo/etoposide			low levels of resistance and to few drugs
Secondary culture derive from xenografts in NSG mice					
Secondary cultures of cells derived from the parental CDX		increased resistance level			
Secondary cultures of cells derived from the PDX		very high degree of resistance to multiple drugs		multi drug phenotype	Slow growing, very adherent to flask
<i>In vivo</i> in NSG Mice					
CDX					
Orthotopic parental CDX	HOS, SaOS-2-B		SaOS-2-B > HOS	Bone microenvironment	Lack tumor heterogeneity
Orthotopic resistant CDX	R/MTX HOS and SaOS-2-B	yes	parental > resistant	bioluminescence detection of primary tumors and metastases	No access to immune contexture
	HOS-R/DOXO	yes	parental > resistant		
PDX					
Paratibial PDX issued from relapsed human osteosarcoma	#B77; #B94, #C17	yes		Bone microenvironment	Difficult to follow in vivo
Sub cutaneous PDX issued from relapsed human osteosarcoma	#B77; #B94, #C17	yes	paratibial > sc	Tumor heterogeneity	No access to immune contexture
				Easier drug testing Follow up	

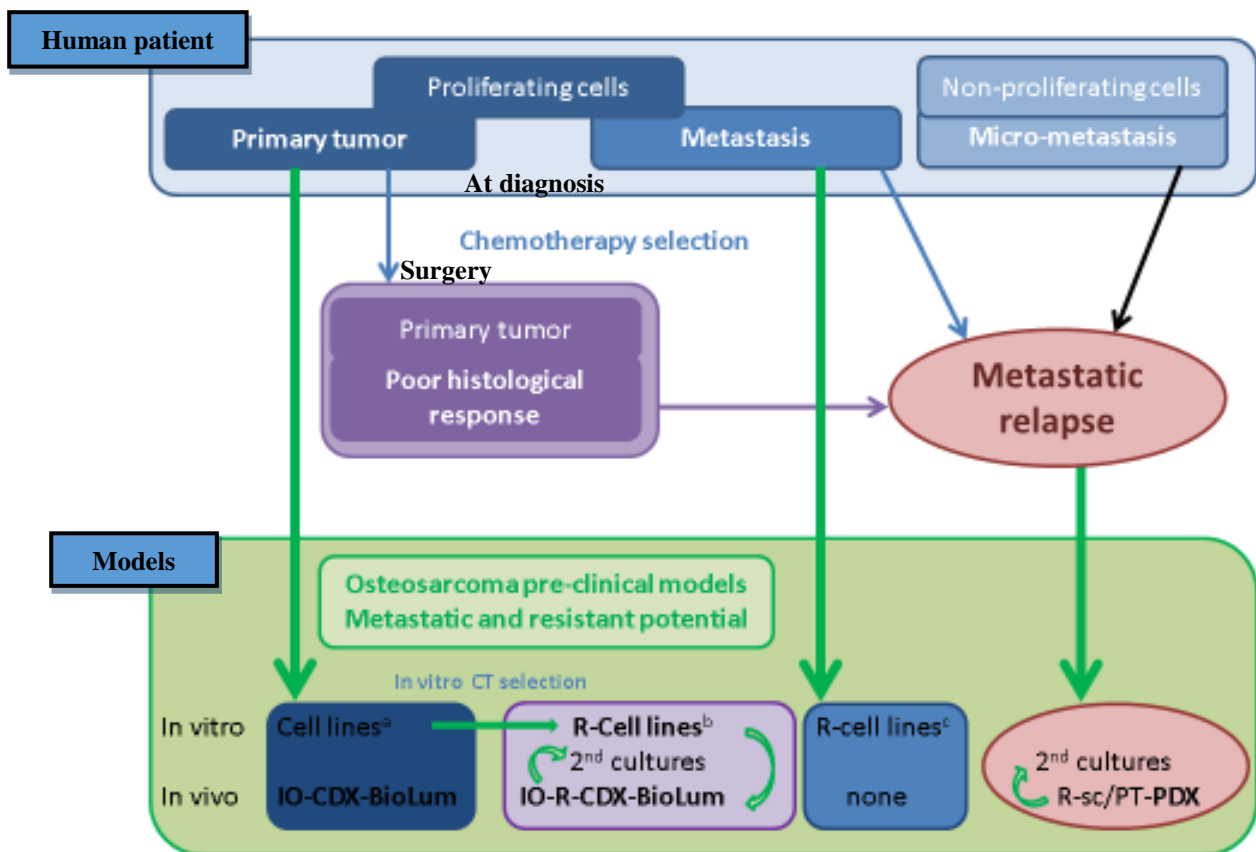


Figure 5.1: Tumor development in human patients and the different *in vitro* and *in vivo* models developed in this thesis. At diagnosis, patients with osteosarcoma present as primary tumors with or without visible metastases or undetectable micro-metastasis. Relapses, usually metastatic, arise from either primary tumor or metastatic tumor, after chemotherapy pressure selection or not (non-proliferating micrometastases not sensitive to chemotherapy). *In vitro* and *in vivo* models have been derived from these different human disease states. Established *in vitro* cell lines were usually derived from sensitive primary tumors (a), more rarely from resistant metastatic samples (e.g. IOR/OS18 derived from metastases with intrinsic resistance) (c), or were rendered resistant by *in vitro* exposure to chemotherapy to a single agent Methotrexate or doxorubicin (b). CDX models were derived from these established cell lines. PDX models were directly derived from human samples at relapse. CT=chemotherapy.

References

1. Bielack SS, Smeland S, Whelan JS, et al. Methotrexate, Doxorubicin, and Cisplatin (MAP) Plus Maintenance Pegylated Interferon Alfa-2b Versus MAP Alone in Patients With Resectable High-Grade Osteosarcoma and Good Histologic Response to Preoperative MAP: First Results of the EURAMOS-1 Good Response Randomized Controlled Trial. *J Clin Oncol*. 2015;33(20):2279-2287.
2. Posthumadeboer. Mechanisms of Resistance Molecular involvement Drug Target Drug References. *Oncol Discov*. 2013.
3. Yang X, Yang P, Shen J, et al. Prevention of multidrug resistance (MDR) in osteosarcoma by NSC23925. *Br J Cancer*. 2014;110(12):2896-2904.
4. Duan Z, Gao Y, Shen J, et al. miR-15b modulates multidrug resistance in human osteosarcoma in vitro and in vivo. *Mol Oncol*. 2017;11(2):151-166.
5. Zhang Y, Mai Q, Zhang X, Xie C, Zhang Y. Microenvironment Signals and Mechanisms in the Regulation of Osteosarcoma. In: *Osteosarcoma - Biology, Behavior and Mechanisms*. InTechOpen, London, UK. 2017.
6. Guo W, Healey JH, Meyers PA, et al. Mechanisms of Methotrexate Resistance in Osteosarcoma Mechanisms of Methotrexate Resistance in Osteosarcoma 1. 1999:621-627.
7. Garimella R, Eskew J, Bhamidi P, et al. Biological characterization of preclinical Bioluminescent Osteosarcoma Orthotopic Mouse (BOOM) model: A multi-modality approach. *J Bone Oncol*. 2013;2(1):11-21.
8. Ren L, Mendoza A, Zhu J, et al. Characterization of the metastatic phenotype of a panel of established osteosarcoma cells. *Oncotarget*. 2015;6(30):29469-29481.

9. Mohseny AB, Machado I, Cai Y, et al. Functional characterization of osteosarcoma cell lines provides representative models to study the human disease. *Lab Invest*. 2011;91(8):1195-1205.
10. Stewart E, Federico SM, Chen X, et al. Orthotopic patient-derived xenografts of paediatric solid tumours. *Nat Publ Gr*. 2017;549.
11. Creen V, Biteau K, Amiaud J, et al. Bone microenvironment has an influence on the histological response of osteosarcoma to chemotherapy: retrospective analysis and preclinical modeling. *Am J Cancer Res*. 2017;1;7(11):2333-2349
12. <https://clinicaltrials.gov/ct2/show/study/NCT02243605>
13. Kovac M, Blattmann C, Ribi S, et al. Exome sequencing of osteosarcoma reveals mutation signatures reminiscent of BRCA deficiency. *Nat Commun*. 2015;6:8940.
14. Engert F, Kovac M, Baumhoer D, Nathrath M, Fulda S. Osteosarcoma cells with genetic signatures of BRCAness are susceptible to the PARP inhibitor talazoparib alone or in combination with chemotherapeutics. *Oncotarget*. 2017;8(30):48794-48806.